



UNIVERSITY
OF TRENTO - Italy

Department of Physics

DOTTORATO DI RICERCA IN FISICA
XIV CYCLE

An Electrospray Ionization Mass
Spectrometric Study on Reactivity of
Resveratrol Induced by Metal Ions

Vajir Fakirsab Tamboli

Supervisors:
Prof. Ines Mancini
Prof. Paolo Tosi

Academic Year 2011-2012

To My Parents
Fakirsab and Shahjadbi

Abstract

Resveratrol is a polyphenolic compound produced by various plants and present in dietary sources such as red wine. In recent years, its beneficial effects for human health, including protection from heart diseases and cancer prevention, have attracted increasing interest. Resveratrol acts both as an antioxidant and a prooxidant agent when works *in vivo* with Cu(II) ions occurring naturally in living organisms. The aim of this work is to study the gas phase reactivity of resveratrol in presence of copper and iron ions, in order to more insights on the role of copper in the proposed biological mechanism. By electrospray ionization (ESI) mass spectrometry we have produced and detected some resveratrol-copper complexes by using a resveratrol/CuSO₄ solution in acetonitrile/water, and their most stable structures have been calculated at the B3LYP/6-311G(d) level of theory. The formation of dehydrodimer product was also detected in ESI-MS/MS experiments and its structure assigned with evidences for isomeric compounds from copper and iron reactions with resveratrol. Density Functional Theory (DFT) calculations have been carried out to elucidate reaction mechanisms. Finally, the crucial role of the *para*-OH group in resveratrol structure has been demonstrated by investigating reactions with copper sulfate of synthetic analogues, bearing different number and position of OH groups.

Keywords: Resveratrol, ESI-Mass spectrometry, DFT calculations, Metal complexes, Synthetic analogues

Contents

1	The molecule under investigation: Resveratrol	1
1.1	Structure and biological activities	1
1.2	Antioxidant and prooxidant properties	2
1.3	Mass spectrometric analysis of resveratrol	5
2	Mass spectrometry	7
2.1	Principles	7
2.2	Ionization Source	10
2.2.1	Atmospheric Pressure Chemical Ionization (APCI)	11
2.2.2	Electrospray Ionization (ESI)	13
2.3	Mass Analyzers	16
2.3.1	Quadrupole Analyzer	17
2.3.2	Quadrupole Ion Trap Analyzer	19
2.3.3	Fourier transform ion cyclotron resonance analyzer	22
2.4	Detector	23
3	Experimental	25
3.1	Chemicals and Materials	25
3.2	Instrumentation	25
3.2.1	Mass Spectrometry	25
3.2.2	Nuclear Magnetic Resonance	26
3.2.3	Ultraviolet–Visible Spectroscopy	27
3.3	MS analysis of resveratrol-metal complexes	28
3.4	Synthesis and structural characterization of resveratrol analogues	28
3.4.1	Dihydro-resveratrol	28
3.4.2	(<i>Z</i>)-Isomer of resveratrol	29
3.4.3	4,4'-Dihydroxy-(<i>E</i>)-stilbene	30

CONTENTS

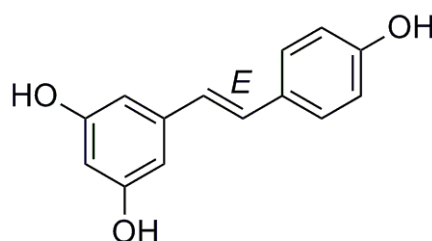
3.4.4	4-Hydroxy-(<i>E</i>)-stilbene, 3,4-dihydroxy-(<i>E</i>)-stilbene, and 3,5-dihydroxy-(<i>E</i>)-stilbene	31
3.5	Synthesis and structural characterization of dehydrodimers	33
3.5.1	From resveratrol under different conditions	33
3.5.2	From 4-HS in the presence of copper(II)sulfate	36
3.5.3	From 3,4-DHS in the presence of copper(II)sulfate	37
3.6	Density functional theory calculations	38
4	Results and discussion	39
4.1	Resveratrol-copper complexes	39
4.1.1	Mass spectrometric analysis	39
4.1.2	Density functional theory calculations	46
4.1.3	Infrared multiple photon dissociation spectroscopy	49
4.2	Resveratrol dehydrodimer in the presence of Cu(II) ions	50
4.2.1	MS analysis under different instrumental conditions	57
4.2.2	Time dependent formation	58
4.2.3	In the presence of laccase enzyme	62
4.3	Resveratrol dehydrodimer in the presence of Fe(III) ions	63
4.3.1	Metal ion induced selectivity	69
4.4	Theoretical investigation of dehydrodimer formation	70
4.5	MS analysis for synthetic analogues of resveratrol	76
4.5.1	(<i>Z</i>)-Isomer of resveratrol	77
4.5.2	4-Hydroxy-(<i>E</i>)-stilbene	77
4.5.3	4,4'-Dihydroxy-(<i>E</i>)-stilbene	81
4.5.4	3,4-Dihydroxy-(<i>E</i>)-stilbene	82
4.5.5	3,5-Dihydroxy-(<i>E</i>)-stilbene	84
5	Conclusions	87
	References	97

Chapter 1

The molecule under investigation: Resveratrol

1.1 Structure and biological activities

Resveratrol ($= (E)$ -5-[2-(4-hydroxyphenyl) ethenyl] benzene-1,3-diol], Figure 1.1) is a natural phenolic compound present in a broad variety of human food and plant species including mulberries, peanuts, grapes, grapevines, legumes and red wine. It has been first isolated from the roots of white hellebore lily *Veratrum grandiflorum* in 1940 [1] and richest source is in the weed *Polygonum cuspidatum*, root extracts of which are used in traditional Japanese and Chinese folk-medicines [2, 3]. This compound is attracting increasing attention due to its activity against many diseases, including heart diseases and cancer, and because of its low *in vivo* toxicity. It was reported that resveratrol is responsible for the anti-inflammatory, anti-mutagenic and anti-carcinogenesis properties attributable to red wine [4, 5].



Resveratrol

Figure 1.1 – Chemical structure of resveratrol.

Interest in resveratrol starts in 1992 from the observation that a low incidence

of cardiovascular diseases may coexist with intake of a high-fat diet, a phenomenon known as the “French paradox” [6,7]. It is believed that in certain parts of France, the death rate caused by coronary artery diseases is lower despite relatively high fat consumption in the human diet. This fact is associated with the consumption of red wine which contains resveratrol (1.5-3.0 mg/L of red wine), [8]. Hence, regular consumption of red wine have been shown to reduce risks of chronic disease such as atherosclerosis, inflammation and cardiovascular disease. In addition interesting effects of this compound on the lifespan of yeasts and flies, implicating its potential as an anti-aging agent in treating age-related human diseases [9,10], have been suggested. A summary of health benefits of resveratrol is shown in figure 1.2. It represents an example of the benefits given by nutraceuticals.

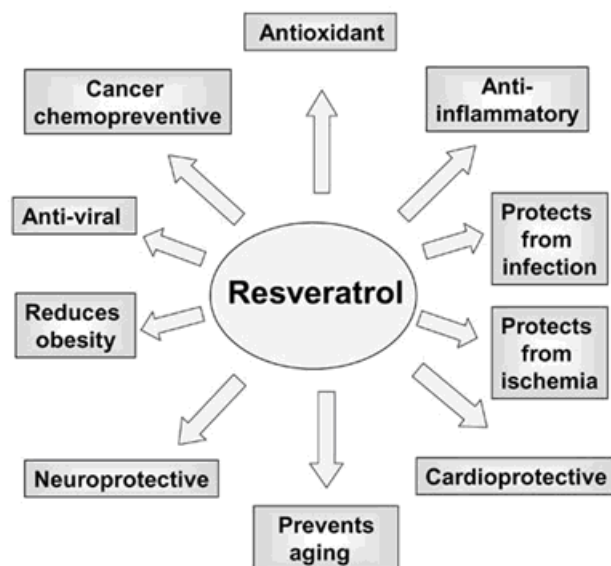


Figure 1.2 – Health benefits of resveratrol [11].

Scientific interest in resveratrol has continually increased in the last few years as evident by 4375 published studies reported in PubMed and more than 13,000 in Chemical Abstracts databases (Figure 1.3).

1.2 Antioxidant and prooxidant properties

Biological properties of resveratrol are linked to its potential of acting either as an antioxidant or a prooxidant agent [13]. Similar to most polyphenols [14], resveratrol has intrinsic antioxidant activity due to the direct quenching of reactive oxygen/nitrogen

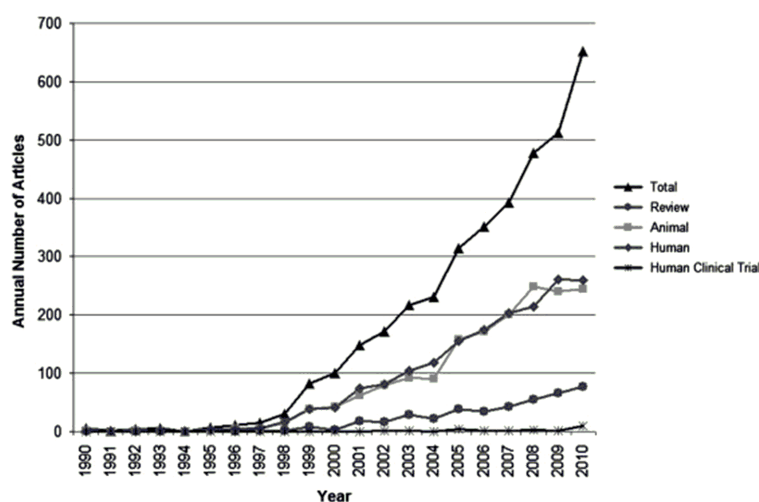


Figure 1.3 – Annual count of resveratrol articles indexed on PubMed. The results include articles with the term “resveratrol” in found in the title, abstract, or keywords [12].

species (ROS/RON). Biological systems control oxidative stress *via* a variety of antioxidative mechanisms that restrict the reactivity of oxidation catalysts and free radicals [15]. The antioxidant activity might explain the role of resveratrol in cancer chemoprevention, due to scavenging of free radicals involved in the peroxidation of membranes and oxidative damage of DNA [4]. Thus understanding the resveratrol chemistry may have relevant implications for more effective approaches to cancer prevention, as well as for the design and development of new antitumoral agents.

Resveratrol has a potent antioxidant effect because of its ability to promote the activities of a variety of antioxidative enzymes that could make major contributions to its biological role. This resveratrol property is related to the presence of hydroxyl groups in its molecular structure which can scavenge free radicals produced *in vivo*. The most favorable mechanism for radical scavenging is through hydrogen atom donation [16]. Theoretical studies on the antioxidant action have shown that hydrogen abstraction from the OH group in *para* position is more favored than from *meta* positions, leading to the formation of the phenoxide radical **2** (Figure 1.4) [17–20]. This reactive species undergoes a coupling reaction, followed by an intramolecular nucleophilic attack, to produce the dehydrodimer **3** [21] (Figure 1.4).

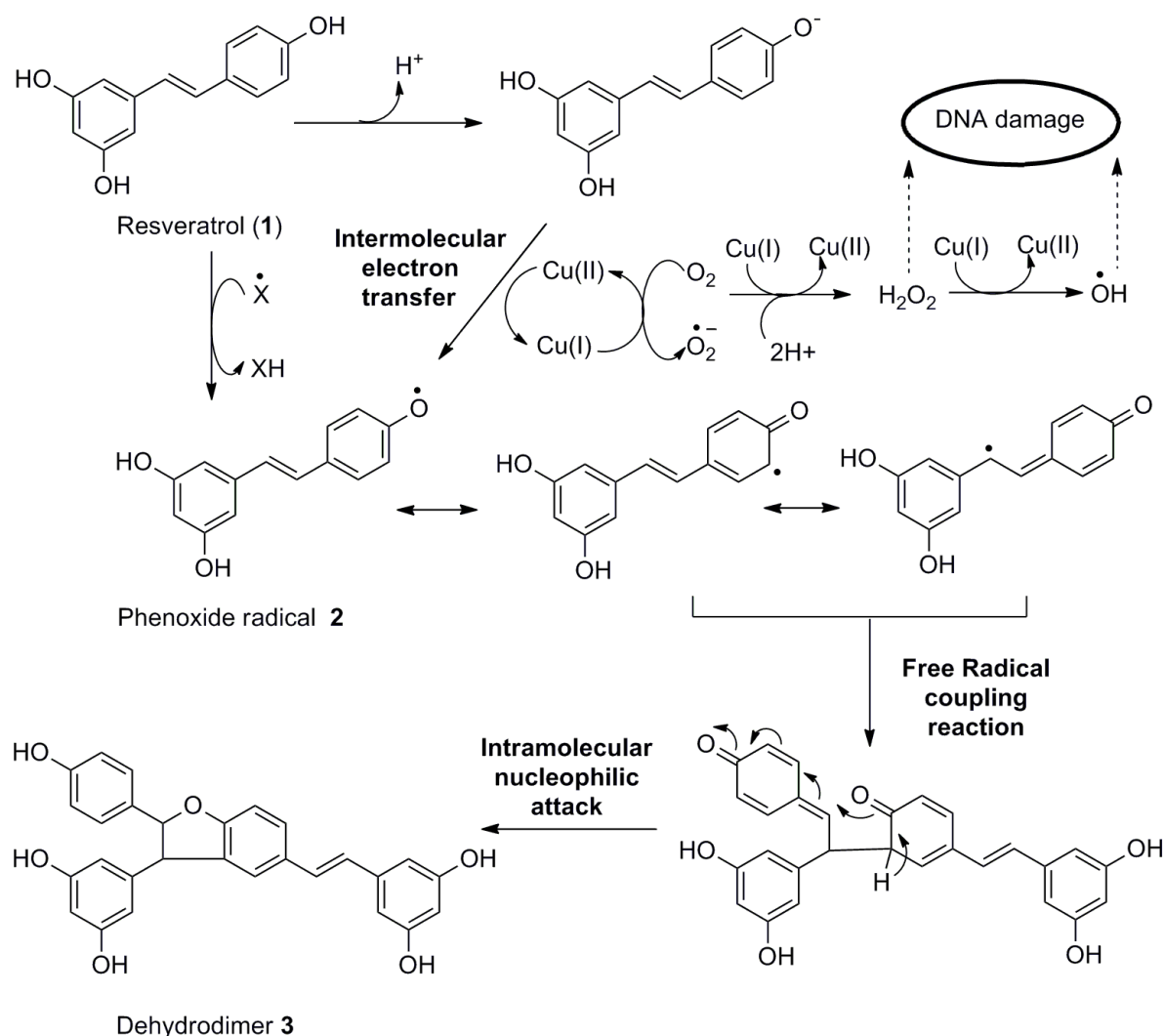


Figure 1.4 – Proposed antioxidant and prooxidant mechanisms of resveratrol, $X^\cdot =$ Free radicals.

Copper is an essential trace element present in living organisms, with the capability of switching between $Cu(II)$ and $Cu(I)$ and interacting with several ligands [22,23]. On these properties is based its role in biochemical processes, with its involvement in electron transfer processes in proteins and enzymes, as well as in redox reactions producing free radicals. Beside copper, also other metal ions, such as iron (III), have similar redox reaction with resveratrol [14,24,25].

Each antioxidant, including resveratrol, some vitamins, tannins and flavonoids, is a redox species, protecting against free radicals in some circumstances and promoting free radical generation in others [26–28]. Copper is one of the most redox-active metal ions present in living cells. In the presence of $Cu(II)$, resveratrol is able to become a

prooxidant producing reactive oxygen species (ROS), which in turn are able to damage DNA. The prooxidant mechanism of resveratrol is based on the acidity of the phenol group, involving a proton loss from the OH in *para* position, to give a phenoxide anion which participates in a redox reaction gives a phenoxide radical **2** while Cu(II) is reduced to Cu(I). Molecular oxygen is able to oxidize Cu(I) by conversion into a superoxide anion, the latter being able to generate hydrogen peroxide, which induces DNA damage directly or after conversion into a hydroxyl radical (Figure 1.4) [29,30]. Thus the resveratrol-copper system seems to play a relevant role and it has been shown to be biologically active by bacteriophage inactivation tests [31] and by mutagenicity in plasmid DNA [30]. The product of the last reaction is the phenoxide radical **2**, which gives the same final dehydrodimer **3** as in the antioxidant process (Figure 1.4) [21]. Later species has been isolated from plants where it is produced through a metabolic sequence induced in response to biotic or abiotic stress [32–34]. It has attracted intense interest for their intricate structures and diverse biological activities.

1.3 Mass spectrometric analysis of resveratrol

The biological interest of this natural product has stimulated the development of various analytical methods for the identification and quantification of resveratrol and related metabolites in red wine and plant extracts [34,35]. Organic solvent extraction, solid-phase extraction (SPE) and direct injection techniques without sample preparation has been used for the analysis of resveratrol by gas chromatography (GC), high-performance liquid chromatography (HPLC), capillary electrophoresis (CE) [7,36]. Most of the analyses were performed by high performance liquid chromatography (HPLC) coupled with UV detection, which is limited by its low selectivity and sensitivity.

Metal complexes of natural phenolic compounds, as flavonoids, have been studied by ESI-MS [37], whereas for resveratrol MS techniques have been so far limited to the analysis of chemicals in red wine and grapes by liquid chromatography atmospheric pressure photoionisation [38], fragmentation experiments, deuterium labeling and accurate mass measurements in negative ion mode [39]. Recently, a Matrix Assisted Laser Desorption Ionization (MALDI-MS) investigation has been reported [40]. The formation of Cu(II) ion complex of resveratrol has been studied by UV-visible spectroscopy in DNA breakage studies [29,31].

Chapter 2

Mass spectrometry

The search of analytical tools that can identify masses of particles, the unknown compounds, and elucidate the small inorganic molecules to biological macromolecules, had lead to the invention of the first mass spectrometry by J. J. Thomson in 1912 [41]. In the past 20 years, mass spectrometry has rapidly extended its applications invading every discipline of the sciences [42, 43]. High detection sensitivity (order of one part in 10^{12}) of mass spectrometry in chemically complex mixture provides valuable information to a wide range of applications starting from physics to life sciences. The present chapter of the thesis describes different mass spectroscopy techniques that have been used to investigate the oxidative coupling of resveratrol induced by metal ions.

2.1 Principles

Mass spectrometry (MS) concerns systems that separate ionized particles, which are then characterized by their mass to charge ration (m/z) and relative abundances.

MS consists of three basic modules. Ionization of chemical compounds, separation of the generated charged molecules and recording of the ions according to their m/z ratios [44]. In a typical MS process, the molecules of interest are introduced into the ionization source as a gas or in condensed phase. In the later case, liquid or solid first undergo vaporization and later get ionized to acquire positive or negative charges. The analyzer uses electrical or magnetic fields, or combination of both, to separate and transfer the ions from the region where they are produced to a detector, where they produce a signal which is then amplified. The analyzer is operated under high vacuum, so that the ions can travel to the detector. The final spectrum provides information on the mass to charge ratio of the desired molecular species [44–46].

Structural information can be generated using different types of mass spectrometers, usually those with multiple analyzers which are known as tandem mass spectrometers. This is achieved by fragmenting the sample inside the instrument and analyzing the generated products. Schematic diagram of a mass spectrometer is shown in figure 2.1.

The method of sample introduction to the ionization source often depends on the ionization method being used, as well as the type and complexity of the sample. It can be inserted directly into the ionization source, or can go through some type of chromatography route before reaching the ionization source. The later method usually involves the mass spectrometer being coupled directly to high pressure liquid chromatography (HPLC), liquid chromatography (LC), gas chromatography (GC) or capillary electrophoresis (CE) separation column, and hence the sample is separated into a series of components which then enter the ionization source of mass spectrometer sequentially for individual analysis.

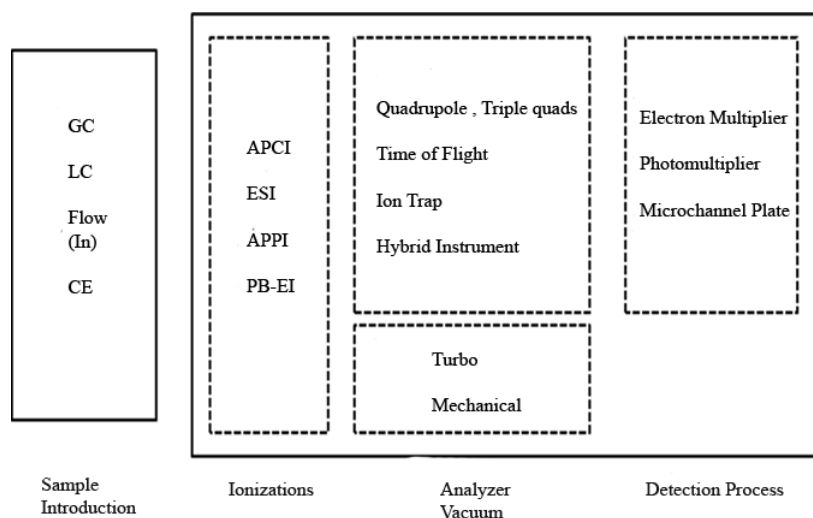


Figure 2.1 – Schematic diagram of a mass spectrometer.

Advantages

Apart from the mass spectroscopy, several other analytical techniques are available such as X-ray crystallography, ^1H or ^{13}C -Nuclear magnetic resonance spectroscopy, infrared absorption etc which can be useful for structural characterization of metal

complexes. Each technique has its own advantage and disadvantages. The advantages of MS over the other existing techniques are:

- It does not require any particular sample pre-treatment other than the dissolution of the sample in a suitable solvent.
- The sample can be introduced either directly or after chromatographic or electrophoretic separation.
- High sensitivity and speed of MS over other techniques, which enables to analyze very low concentrated complex mixtures.
- Specificity is a critical advantage of MS.
- Stoichiometry of relevant metal complexes can be easily analyzed by MS, because of the molecular weight of the complex is directly measured.
- MS can be coupled with online separation methods such as HPLC and capillary electrophoresis for the analysis of mixtures.
- MS is especially applicable to the identification of unknown molecule, because of the possibility to carry out MS/MS experiments leading to structural information.
- Unlike X-ray crystallography, MS do not demand the crystallization of high mass complexes, which itself is a risky process.
- MS has undisputed advantages over NMR for studying proteins with poor solubility and high molecular weight. NMR is limited to study proteins with molecular weight less than 30 kDa, while MS has been used to study over 1000 kDa protein-protein complexes [47].
- Sample purity is not important in MS.

MS has the following major disadvantages:

- Non-covalent complexes are often disrupted, except in a soft ionization system, as ESI.
- It cannot distinguish stereo isomers.
- Expensive instrumentation.

Application

Mass spectroscopy gives both qualitative (structure) and quantitative (molecular mass or concentration) information on the analyte molecules. Nowadays, MS extensively used for:

- Biomolecules or Biochemistry: analysis of protein, peptides, oligonucleotides, lipids, steroids, polysaccharides.
- Physical chemistry: studying fundamentals of gas phase ion chemistry, atomic physics, reaction kinetics, inorganic chemical analysis, determination of thermodynamic parameters.
- Pharmaceutical: unknown drug discovery, combinational chemistry, pharmacokinetics and many others.
- Clinical: neonatal screening, diagnosis of diseases, hemoglobin analysis, drug testing.
- Environmental: Polycyclic aromatic hydrocarbons (PAHs), Polychlorobiphenyls (PCBs), water and air quality, food contamination, heavy metals (as well as organic chemistry in general).
- Geological: isotopic composition, oil composition.
- Forensic: identification of unknown samples.
- Industry: monitoring of process streams.

2.2 Ionization Source

The role of the ion source is to convert neutral atoms or molecules into ions. This is required because all mass spectrometers use electromagnetic fields to manipulate atoms in the form of positive or negative ions. In addition to ionizing neutral atoms, the ion source provides some degree of focusing, collimation, and acceleration to ions. The choice of the ionization method depends upon the internal energy transferred during the ionization process and on the physico-chemical properties of the analytes that is to be ionized.

The ion sources usually employed can be divided into two main classes. The first class concerns sources that operate at low pressure and includes the electron ionization

(EI) and the chemical ionization (CI) sources. In the EI technique, ions are produced by the interaction of gas phase atoms or molecules with energetic electrons [48] and in CI technique, they are produced through the collision of atoms or molecules with the reagent gas that are present in the ion source chamber [49]. These two techniques are suitable for gas-phase ionization, and thus their use is limited to compounds sufficiently volatile and thermally stable [50]. Due to these limitations EI and CI techniques are not suitable for phenolic compounds.

The second category exists under two types: liquid-phase ion source and solid-phase ion sources. In liquid phase ion source, analyte is in the solution form. The solution is introduced as droplets into the source, where ions are produced at atmospheric pressure and focused into the mass spectrometer through some vacuum pumping stages. Atmospheric pressure chemical ionization (APCI) and electrospray ionization (ESI) correspond to liquid phase ion source [51, 52]. APCI but especially ESI techniques are suitable for charged, non polar - polar, non-covalent metal complexes. In the present study we have used both APCI and ESI techniques due to the polar nature of resveratrol compound.

In solid-phase ion sources, the analyte is in the form of non-volatile deposit. It is obtained by various preparation methods which frequently involve the introduction of a matrix that can be either a solid or a viscous fluid. This deposit is then irradiated by energetic particles or photons that desorb ions. These ions can be extracted by an electric field and focused towards the analyzer. Matrix-assisted laser desorption [53], secondary ion mass spectrometry [54], plasma desorption and field desorption [55] sources all use this strategy to produce ions.

2.2.1 Atmospheric Pressure Chemical Ionization (APCI)

It is an ionization technique, which takes place at atmospheric pressure and is analogous to chemical ionization [49, 51]. APCI generally produces protonated or deprotonated molecular ions from the sample via a proton transfer (positive ions) or proton abstraction (negative ions) mechanism. It is most commonly used in connection with high pressure liquid chromatography (HPLC) or other flow separation techniques. APCI has its primary applications in the areas of ionization of low mass organic compounds (unsuitable for the analysis of thermally labile compounds).

The first APCI source was developed in the 1970s by Horning et al. [56] at the Baylor College of Medicine (Houston, TX). Initially, ^{63}Ni foil was used as a source of electrons to perform ionization, but later a corona discharge electrode was introduced.

This class of electrode became the model for modern, commercially available APCI interfaces. Figure 2.2 shows the schematic diagram of a APCI instrument.

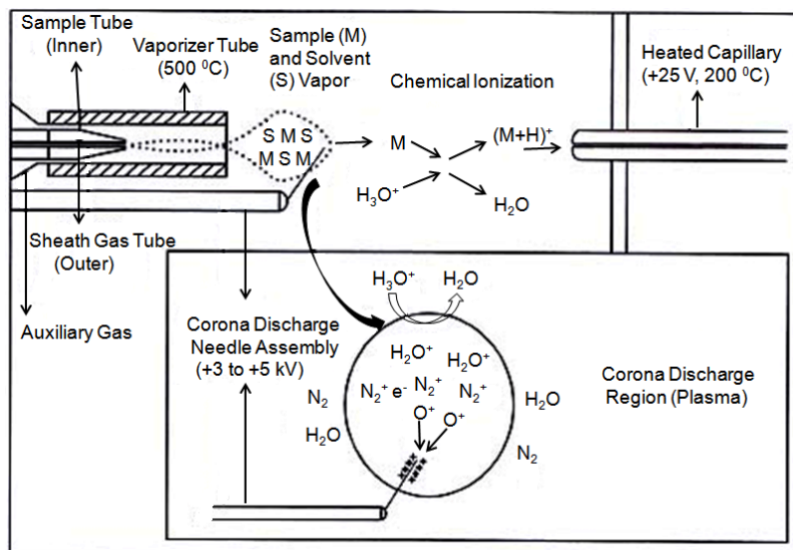


Figure 2.2 – A schematic figure of an APCI interface.

In APCI process, the solution of an analyte is passed through a heated capillary (typical temperature in the range 300-400 °C) and sprayed with high-flow rates of nitrogen coaxial to the capillary, which behaves as a vaporizer. The mixture of vaporized solvent and analyte molecules flows towards the ion formation region where a corona discharge initiates chemical ionization at atmospheric pressure using nitrogen and/or the vaporized solvent as the reagent gas (Figure 2.2). The needle generates a discharge current ($\sim 2\text{-}3 \mu\text{A}$) which produces primary ions. These primary ions react very rapidly, transferring their charge to solvent molecule to form secondary reactant gas ions. These secondary reactant gas ions then undergo repeated collisions with the analyte leading to the formation of analyte quasi molecular ions, by charge or proton transfer reactions. Under these conditions, the formation of protonated $[\text{M}+\text{H}]^+$ or deprotonated $[\text{M}-\text{H}]^-$ molecules occurs. Once ions are formed, they enter the pumping and focusing stage as the other atmospheric pressure ionization sources.

A potential advantage of APCI is that it is possible to use a non-polar solvent as a mobile phase solution, instead of a polar solvent, because the non polar solvent and molecules of interest are converted to the gaseous state before reaching the corona

discharge pin. Typically, APCI is a less "soft" ionization technique than ESI, i.e. it generates more fragment ions relative to the parent ion [57].

2.2.2 Electrospray Ionization (ESI)

ESI is a suitable technique for the analysis of thermally fragile and high-molecular-weight material including proteins and polymers; recently there has been an increase in applications involving coordination complexes. It is a very gentle ionization process (involving transfer of solution ions to the gas phase), and therefore typically yields molecular ions with little or no fragmentation. The spectra obtained by this technique are more beneficial for easy interpretation. ESI was developed primarily by Fenn and co-workers in the mid 1980s, an achievement for which Fenn won the Nobel Prize for Chemistry in 2002 [58, 59].

ESI process involves a complex series of events, all occurring during a few microseconds, including solvent electrolysis at the emitter tip, the establishment of charge gradient, the charge separation, solvent evaporation, acid-base reactions, and droplet fission [60, 61]. Furthermore, the physical and chemical properties (droplet size, charge, ion pairing, surface activity) of the analytes, buffer, solvent and instrument parameters are also important for the electrospray process. Electrospray ionization mechanism can be divided into the following steps: a) the production of charged droplets at the electrospray capillary tip; b) the evolution of charged droplets by repeated droplets disintegration and formation of very small highly charged droplets capable of producing gas phase ions; c) the actual mechanism, by which gas-phase ions are produced.

Production of charged droplets

In the electrospray process, a dilute solution is sprayed from a metal capillary held at a high voltage (2-5 kV) into a chamber which is at atmospheric pressure. Due to the high voltage, very high electric field is created between the end of the capillary tip and counter electrode. This leads to a partial separation of positive and negative electrolyte ions in the solution. The repulsion of the ions at the surface due to pull of the electric field overcomes the surface tension of the liquid and expands the liquid into a cone identified as Taylor cone [62]. The tip of the Taylor cone, being the least stable point, elongates into a liquid filament. This filament breaks up into individual small charged droplets as shown in figure 2.3.

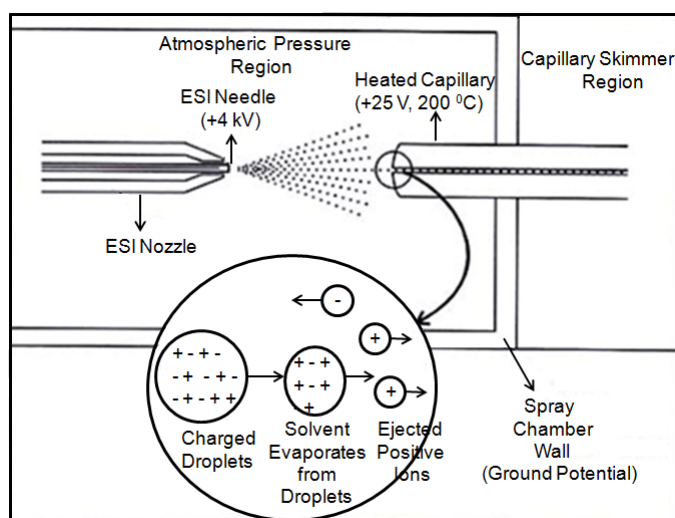


Figure 2.3 – Schematic of electro spray ionization. Ionization and nebulisation occurs at the tip of the capillary, which is at a potential of several kilo volts.

Charged droplet Shrinkage

Solvent evaporation promoted by heat supply from the ambient air leads to the decrease of the droplet size at constant charge. The droplet shrinks until it reaches the threshold point called Rayleigh limit where the Coulombic repulsion between the charges overcomes the cohesive force of the surface tension [63]. This leads to the Coulomb fission of the droplets. The radius of the generated droplets is about one-tenth of the parent droplet radius ($\sim 1 \mu\text{m}$) and carries 2% of the mass and 15% of the charge of the parent droplets (Figure 2.4). The process of diffusion continues until the radius of the droplets reaches to nanometer range. These droplets acquire few elementary charges and ultimately lead to the precursors of the gas-phase ions. The decomposition scheme is schematically shown in figure 2.4.

Formation of gas-phase ions from small and highly charged droplets

Two basic mechanisms have been proposed for the formation of gas phase ions from very small and highly charged droplets, the charge residue model (CRM) and the ion evaporation model (IEM). The CRM mechanism was proposed by Dole et al. [64] for the high molecular mass species such as proteins. According to this mechanism, when small droplets are formed by droplet evolution, some of these droplets possibly contain

one analyte molecule as well as the ionic charge on the surface of the droplet. Solvent evaporation from such a droplet will lead to a gas-phase analyte ion, whose charge originates from the charges at the surface of the vanished droplet. This assumption is known as the charged residue model (CRM).

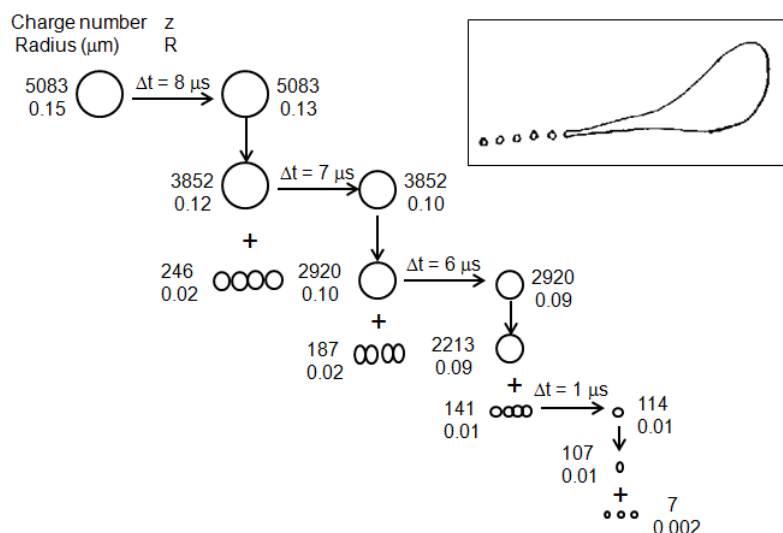


Figure 2.4 – Droplet evolution scheme due to solvent evaporation at constant charge and Coulomb fissions at the Rayleigh limit. Figure in inset at the top right, illustrates the fission of one such droplet.

The IEM model was proposed by Iribarne and Thomson [65,66] for small organic molecules. It is based on a continuous ion-evaporation process. When the droplet has reached a radius in the range of ~ 10 - 20 nm after solvent evaporation, the direct emission of analyte ions into the gas-phase will occur. The relevant explanation is that at this droplet radius a few charged molecules of the droplet experience a net Coulombic repulsive force from the remaining molecules of the droplet. As a result those charge molecules knock out of the droplet. This phenomenon is termed as ion evaporation model.

Ions can then be subjected to fragmentation processes in order to yield structural information. Collision induced dissociation (CID) can be easily achieved in most commercial ESI-MS by acceleration of the ions by means of an applied cone voltage (a potential difference applied across two cones which accelerates the ions, causing collisions with gas and residual solvent molecules). The advantage of this approach is that the degree of fragmentation can be carefully tuned. A singly charged parent

ion will often undergo loss of neutral ligand molecules in the initial stages, whereas a multiply charged ion will typically fragment by loss of a charged species or gain of a counter ion, to reduce the charge on the parent ion [67].

Energy-dependent electrospray ionization mass spectrometry (EDESI-MS) uses a graph of cone voltage versus m/z ratio upon which ion intensity is plotted, which provides a complete picture of the fragmentation pattern particularly suitable for the structural analysis of mixtures.

Due to all these extensive features, ESI is a relevant and constructive technique for a variety of biological applications. In addition, the ESI technique allows non-covalent biomolecular complexes to be ionized intact, which expand the utility of MS to the study of protein-protein, protein-drug complexes and generally any multi molecular complexes [68]. In the present thesis, we have used ESI technique for,

- Identification of non-covalent interaction of resveratrol and its analogues with metal ions.
- Study of oxidative products of resveratrol and its analogues.

2.3 Mass Analyzers

Once gas phase ions are produced, they need to be isolated for further detection. A mass analyzer is the part of the instrument in which ions are separated based on their m/z values. There are several different types of mass analyzers, all based on the interaction of charged particles with electric or magnetic fields. The five main features of an analyzer are:

- Mass range: it determines the m/z range in which measurements can be carried out.
- Transmission: the ratio between the number of ions reaching the detector, and the ions produced in the source.
- Analysis speed: the rate at which the analyzer measures over a particular mass range.
- Mass accuracy: it indicates the accuracy of the m/z provided by the mass analyzer.
- Resolving power: the ability to yield precise signals for two ions with a small mass difference.

Currently, four main analyzers are widely used in MS, namely quadrupole (Q), quadrupole ion trap (QIT), time of flight (TOF), and Fourier Transform Ion Cyclotron resonance (FT-ICR). These analyzers vary in terms of size, price, resolution, mass range, and the ability to perform tandem mass spectrometry experiments (MS/MS). The following sections will focus over details of the working principle of the Q and QIT mass analyzers, which were used in our experiments.

2.3.1 Quadrupole Analyzer

The principle of the quadrupole mass analyzer was first described by the Noble prize winning physicist, Paul Wolfgang [69] at the University of Bonn in 1953. This analyzer consists of two pairs of metal rods with a circular cross section, as shown in figure 2.5. Opposing pairs are electrically connected. One pair is biased positive, while the other pair is biased negative with respect to ground. RF voltages are applied between the positive and negative pairs of rods. When a positive ion enters the quadrupole midway between the four electrodes, it is repelled equally by both positive electrodes. If the negative electrodes were not present, these ions would tend to oscillate slightly between the two electrodes and remain in a stable condition independent of their m/z ratios. However, in the presence of two negative electrodes, the positive ions are instead swept towards whichever negative electrode happens to exert the greatest attractive force. The applications of an RF voltage between the two pairs of rods cause the ions to spiral between the four electrodes. The net result is a simultaneous oscillation of ions between the two positive and two negative electrodes.

Positive ions having a smaller m/z ratio tend to respond more to the RF fields than ions having larger m/z ratios. With each oscillation, the amplitude increases and eventually the positive ions of smaller m/z ratio strike the positive electrodes while the larger m/z ratio ions pass by them. Thus the positive electrodes work as a high-pass mass filter. Due to the little effect of RF potentials on positive ions having a larger m/z ratio, they tend to drift toward the negative electrodes, while positive ions with smaller m/z ratio tend to oscillate between these two electrodes. The resulting oscillations tend to stabilize the smaller m/z ratio, positive ions long enough to pass by the negative rods. The negative electrodes thus function as a low-pass mass filter for positive ions.

The positive and negative pair of quadrupole electrodes function together as a band-pass filter. In theory, the quadrupole mass filter has an infinitely sharp band-pass and only ions of a single m/z ratio are allowed to pass through it. The limit of the band-pass is determined by the ratio of the amplitude of the RF voltage (V)

to that of the DC voltage (U). Similarly, the negative ions are also filtered in the same manner as the positive ions, expect that those having a smaller m/z ratio tend to drift toward the negative electrodes, while larger m/z ratio tend to drift toward positive electrodes. Ions having the selected m/z ratio are able to pass through the quadrupole. Finally, they are analyzed by the detector. This simplified illustration of a quadrupole is based on a complicated second-order differential equation, known as the Mathieu equation [70, 71].

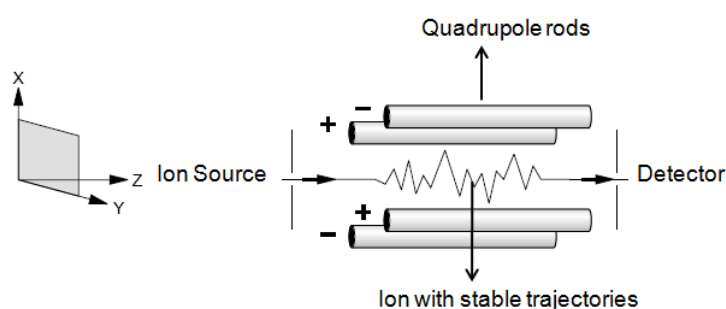


Figure 2.5 – Schematic diagram of a quadrupole mass filter.

The major advantages of quadrupole analyzers are low cost, relatively small size, robustness, and ease of maintenance. A quadrupole possesses, however, limited capability in terms of mass range (usually <4000 Da), resolving power, and the ability to perform MS/MS analysis. This drawback can be overcome by attaching a quadrupole to other analyzers such as additional quadrupole (triple quadrupole instrument) or a quadrupole linked to a TOF (Q-TOF).

Tandem Quadrupole System

In a typical tandem quadrupole system there are three quadrupoles arranged in a linear fashion, often called "triplequad" (Figure 2.6). The analyte ion of interest is mass-selected by the first quadrupole (Q1) and allowed to collide with a collision gas (usually N_2) in a second RF-only quadrupole collision cell (Q2), where the precursor ions are activated by collision and undergo further fragmentation. This process is known as collision-induced dissociation (CID). Daughter ions resulting from CID are related to the molecular structure of the ions and can be monitored by the third quadrupole mass analyzer (Q3) thus providing structural information of the molecular ions [72].

The following modes of data acquisition are commonly used in a tandem quadrupole system:

- Product scan (daughter scan): Q1 is static allowing only one ion of specific m/z ratio to pass through and Q3 scans the different CID product ions. This mode can be used for studying molecular structure.
- Precursor scan (parent scan): Q1 scans over a range of possible precursor ions and Q3 is static focusing on one unique product ion resulting from CID of a class of precursor ions.
- Neutral loss: Both Q1 and Q3 scan together at a constant difference of m/z ratio. This is used to monitor the loss of a neutral fragment for a class of molecules from CID.
- Multiple reaction monitoring: Both Q1 and Q3 are static for a pre-determined pair of precursor and product ions. This confers the highest specificity and sensitivity and is commonly used in ESI-MS/MS quantification procedures.

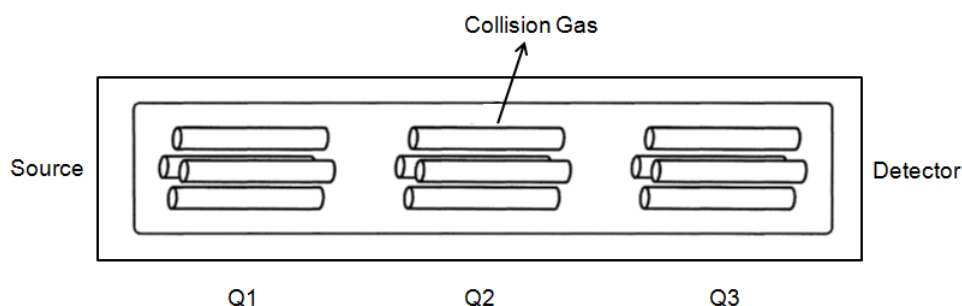


Figure 2.6 – Schematic diagram of a triple quadrupole system. The first (Q1) and third (Q3) are mass spectrometers and the center (Q2) is a collision cell.

2.3.2 Quadrupole Ion Trap Analyzer

The ion trap mass analyzer is essentially a 3-dimensional version of the quadrupole mass filter [70]. Its basic principle, theory and operation is similar to Quadrupole mass filter. The ion trap mass analyzer is a device that allows ions in the gas-phase to be selectively trapped by strong electric fields. Ions with different masses are present together inside the trap and are expelled according to their masses to

obtain the spectrum within milliseconds. The successive fragmentation of the ions is achieved by Collision Induced Dissociation (CID), the ability to isolate and fragment the selected ions known as MS^n . Due to this unique feature of QIT, deep insights on the structure of the ions can be obtained. This is one of the reasons for which the QIT mass spectrometer has been adopted for most of the work presented in this thesis.

An ion trap is made up of a rotationally symmetrical ring electrode of hyperbolic shape and two end cap electrodes of the same cross-section. Basic set-up of the ion trap mass analyzer is shown in figure 2.7.

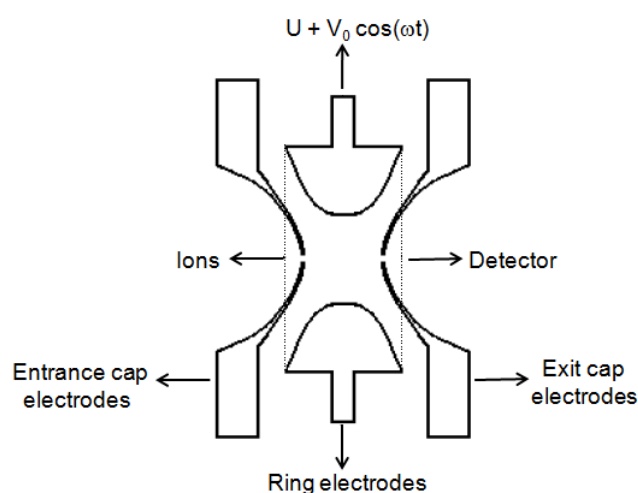


Figure 2.7 – Schematic diagram of a typical ion trap mass spectrometer.

Ions produced in the source travel through a capillary and are focused using a series of skimmers and octopoles into an ion beam that enters into the trap through an inlet at the end cap electrode; these ions are trapped within the system of three electrodes (Figure 2.7). When a suitable potential is applied to the ring electrode and the two end-cap electrodes are grounded, a quadrupolar field is generated in the inner side of the trap, in which the ions oscillate. The force on the ions increases linearly with the distance from the center of the trap. Therefore, all the ions are pushed towards the center of the trap. The stability of the oscillating trajectory of an ion within the trap is determined by the Mathieu equation. For detection of the ions, the potentials are altered to destabilize the ion motion in the axial direction resulting in ejection of the ions through the exit cap electrode. The ions are usually

ejected in order of increasing m/z by a gradual change in the potentials. Finally, the ions are received by a detector to produce the mass spectrum [73].

The "stability diagram" shows a theoretical region where radial and axial stability overlaps. Depending upon the amplitude of the voltage placed on the ring electrode, an ion of a given m/z will have a_z , q_z values that will fall within the boundaries of the stability diagram, and the ion will be trapped. If the a_z , q_z values at that voltage fall outside of the boundaries of the stability diagram, the ion will hit the electrodes and be lost (Figure 2.8).

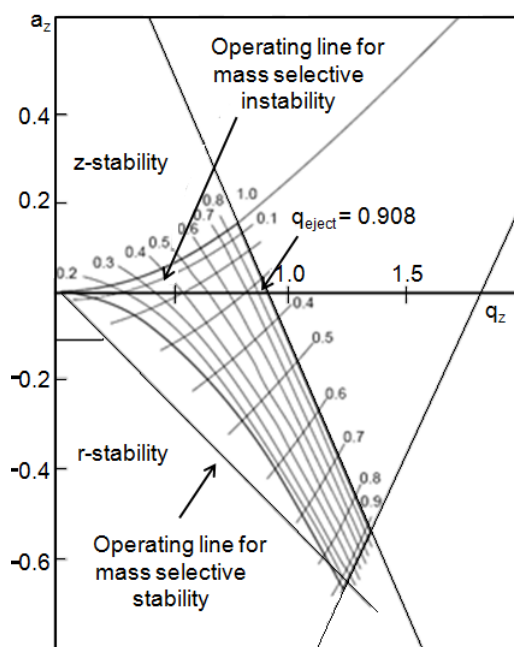


Figure 2.8 – Stability diagram in (a_z, q_z) space for the region of stability in both r- and z-directions near the origin for the three-dimensional quadrupole ion trap.

Further, the fragmentation can be induced by increasing the kinetic energy of ions of a selected m/z ratio for a specific amount of time. This is achieved by applying a small AC voltage to any of the electrodes at a frequency equal to the secular frequency of the ions. The same AC voltage can be used to assist in destabilizing selected ions and ejecting them from the trap.

Helium buffer gas is added to the trap to reduce the kinetic energy of the ions by collisional ion cooling. The addition of helium greatly increases the trapping efficiency of the ions.

2.3.3 Fourier transform ion cyclotron resonance analyzer

In infrared multiphoton dissociation spectroscopy (IRMPD) selected ions are irradiated by a tunable infrared laser at a particular frequency. If the laser frequency is in resonance with a vibrational mode of the molecule, the ion absorbs the laser photon. After absorption of an infrared photon by a particular normal mode of the ion, rapid intramolecular vibrational relaxation distributes the initial photon's energy to other vibrational modes, and the initial absorbing mode returns to its ground state level. This process is repeated with absorption of a second photon, subsequent distribution of energy into other vibrational modes of the ion, and return to its ground level. The process can be repeated with absorption of a third photon, etc. This continued absorption by the $\nu = 0$ level of a particular mode allows spectroscopic information to be obtained from the IRMPD process. Ion fragmentation results when the ions internal energy increases to a level above the dissociation threshold, after a sufficient number of photons are absorbed, without excessive collisional or radiative relaxation. The resulting dissociation of the ion leads to a change in the mass-to-charge ratio (m/z) which is detected by a mass spectrometer [74]. The proportion of the ion population that undergoes uni-molecular dissociation is related to the efficiency of light absorption at that laser frequency. In other words, the photo dissociation yield as a function of laser wavelength is related to the vibrational spectrum of the ion. Vibrational spectra can be predicted by modern computational chemistry approaches such as density functional theory (DFT). The comparison between the calculated and experimental spectra allows in many cases the assignment of structures.

IRMPD is most often used in Fourier transform ion cyclotron resonance (FT-ICR) mass spectrometry [75]. FT-ICR the charged particles move in a magnetic field, with a component of their velocity perpendicular to the magnetic field axis. As a result, the charged particles experience a net force. The resulting motion is known as "cyclotron motion". The cyclotron frequency is related to the mass-to-charge ratio of the ion. Detection of the ions occurs as the ion packets pass through two detector plates. As the ion packets move close to these plates, charge moves within the detection circuit to counteract the proximity of the ions. The voltage change between the detection plates can be measured as a function of time and raw data are obtained. The magnitude of the signal is proportional to the total charge and the proximity of the ions to the detection plates (orbital radius), and is independent on the magnetic field strength. The raw data represent the detection at the same time of all the ions, with their different cyclotron frequencies. It is therefore necessary to extract data about the

different ion packets. This is done by using the mathematical procedure known as a “Fourier transform” (FT).

When ions enter the FT-ICR analyzer cell, however, the radii of the cyclotron orbits are too small to be detected. The ions must be excited to detectable radii and this occurs by using a radio frequency (RF) potential applied to two excitation plates at the resonant frequency (i.e. resonant with the cyclotron frequency) of the ions, and the excitation additionally results in coherence of the ion packets. Figure 2.9 shows a schematic representation of a cross section of an FTICR analyzer cell, where ions are being excited by the RF potential applied to the excitation electrodes. Ions of different m/z values are excited to orbits of the same radius, though their cyclotron frequencies differ [76].

The FT-ICR analyzer cell (Figure 2.9) consists of the two excitation and two detection plates. In order to restrain the ions motion along the axis of the magnetic field, it is necessary to also include two trapping plates. A low potential (typically of an order of 1 V) is applied to the trapping plates to restrain the ions within the FT-ICR analyzer cell, so that they may be excited and detected. The schematic diagram of FT-ICR analyzer is shown in the figure 2.9.

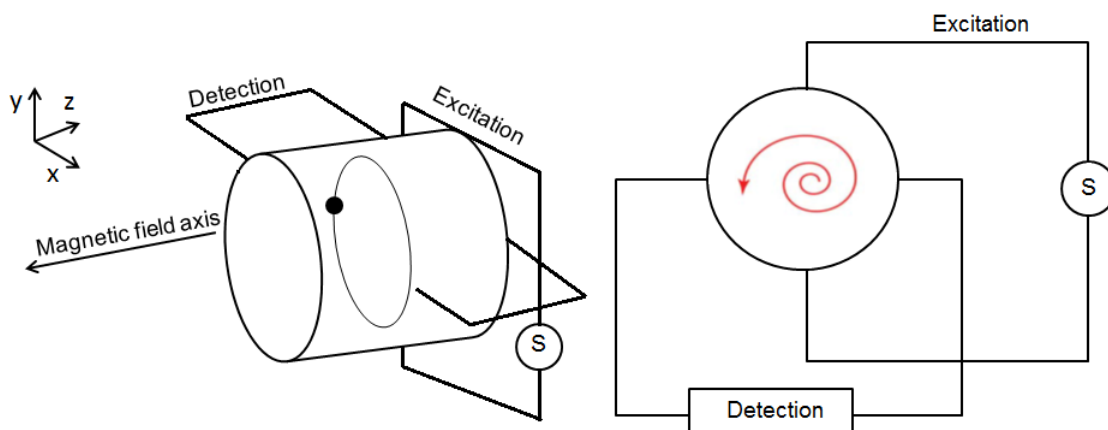


Figure 2.9 – Schematic representation of a cylindrical FT-ICR analyzer cell.

2.4 Detector

The ions passing through the mass analyzer are then detected and transformed into a usable signal by a detector. Today a variety of detectors are available. Choice

of detector depends on the design of the instrument and the analytical application. Detection of ions is always based on their charge, mass and velocities. Some detectors (Faraday cup) are based on the measurement of the direct charge current that is produced when an ion hits a surface and is neutralized. Others (electron multipliers or electro-optical ion detectors) are based on the kinetic energy transfer of the incident ion by collision with a surface that in turn generates secondary electrons, which give an electronic current. The number of ions leaving the mass analyzer at a particular instant is generally quite small; hence the amplification is necessary to obtain a usable signal.

Ion detectors can be divided into two classes. One class of detectors are made to count ions of a single mass at a time and therefore they detect the arrival of all ions sequentially at one point. Other detectors, such as photographic plates, image current detectors or array detectors, have the ability to count multiple masses and detect the arrival of all ions simultaneously along a plane (array collectors). The efficiency of these detectors decreases with the mass of the ions. This limitation of high mass ion detection leads to development of new detectors like charge or inductive detectors and cryogenic detectors.

Chapter 3

Experimental

3.1 Chemicals and Materials

Resveratrol, CuCl, laccase (from *Trametes versicolor*, activity measures >20 Units/mg), 3,4-dihydroxy benzaldehyde, 3,5-dihydroxy benzaldehyde, tert-butyldimethylsilyl chloride, benzyl triphenyl phosphonium bromide, tert-butyl ammonium fluoride (1M solution in THF), 1,8-diazabicycloundec-7-ene and galvinoxyl radical were supplied by Sigma Aldrich (St.Louis, USA), CuSO₄ · 5H₂O, anhydrous CuSO₄, CuBr, CuO, FeSO₄ · 7H₂O, FeCl₃, potassium carbonate, phenol, glacial acetic acid, sulphuric acid and zinc were obtained from Carlo Erba (Milano, Italy). Chloral hydrate was obtained from Acros Organics, 4-hydroxy benzaldehyde from Lancaster (Eastgate, Morecambe, England), Pd/C from Engelhard (Roma). High purity LC-MS grade acetonitrile, methanol, ethanol, isopropanol, ethyl acetate, tetrahydrofuran solvents were purchased from Merck (Darmstadt, Germany). Sodium acetate buffer solution (20 mM, pH 4.5) was prepared freshly and stored at room temperature. Deionized, double distilled water was used for all solutions and eluent for chromatography. Silica gel for chromatography (Si60 F₂₅₄, 0.5 mm) was purchased from Merck (Germany). All the chemicals and reagents were used without any purification.

3.2 Instrumentation

3.2.1 Mass Spectrometry

MS data and tandem fragmentation spectra (MSⁿ) were recorded by using a API-3000 (Applied Biosystems/MDS Sciex) triple quadrupole mass spectrometer and a Bruker Esquire LCTM (Bruker Daltonics, Germany) ion trap mass spectrometer,

equipped with atmospheric pressure chemical ionization (APCI) or electrospray ionization (ESI) ion source operated in the positive or negative ion mode, the latter instrument equipped with ESI source used for the most of the experiments. The following values of the experimental parameters were used: cone voltage 26 V; capillary exit 96 V; spray capillary voltage 4 kV; source temperature 300°C; flow rate of nitrogen as drying gas 6 L/min; nebulizer pressure 20 psi. The samples to be analyzed were diluted in either 1:1 methanol/water or acetonitrile/water, the latter solvents used for all the experiments. All the solutions were mixed at room temperature and directly infused in the source using a syringe pump (Harvard Apparatus, Holliston, MA), with a flow rate of 5µl/min. Mass spectra were acquired by scanning in the range m/z 50-600.

Possible ions of interest were identified by comparing spectra of the analyte to spectra of the blank or the reactants. Fragmentation experiments were carried out by using helium to collisionally activate the selected primary ions. When isotopic clusters were selected at the center, a width of m/z 4 was used. The collision energy was optimized for each MS/MS experiment. Spectra were collected and displayed using data analysis version 3.0 software (Bruker Daltonics 4.1, Bremen, Germany). MS and MS/MS instrument parameters for a particular ion were then optimized and selected using Esquire 4.0 software.

3.2.2 Nuclear Magnetic Resonance

Principles

The phenomenon of magnetic resonance results from the interaction of the magnetic moment of an atomic nucleus with an external magnetic field. It involves the change of the spin state of a nuclear magnetic moment, when the nucleus absorbs electromagnetic radiation in a strong magnetic field and re-emit electromagnetic radiation [77]. This energy is at a specific resonance frequency which depends on the strength of the magnetic field and the magnetic properties of the isotope of the atoms.

The NMR spectrum can provide indications for different kinds of hydrogen nuclei, depending from their environments in a molecular structure. Chemical shift depends from the position of a specific nucleus in the chemical environment. The chemical shift of a nucleus is the resonance frequency related to a standard, and its given as:

$$\delta(\text{ppm}) = (\nu - \nu_{REF}) \times 10^6 / \nu_{REF}$$

Where the reference is tetramethylsilane(TMS) having $\nu=0$ for convenience.

Moreover, an NMR spectrum contains additional information than just the chemical shift. Signals corresponding to the resonance frequencies of nuclei are often seen as multiple lines (doublet, triplet, quartet), with splitting characteristic of their interactions with other close nuclei with a spin-spin coupling (J in Hz) providing further valuable indications about molecular structure.

NMR spectroscopy can be applied not only to ^1H nucleus, but also to ^{13}C nucleus of carbon, which is much less abundant than ^{12}C isotope (which has a spin quantum number of zero and is not magnetically active), and requires a more sensitive instrumentation or a longer acquisition time, possible by Fourier Transform (FT) method.

Experimental details

^1H NMR spectra were acquired by an Avance 400 Bruker spectrometer at 400 MHz, in CDCl_3 or acetone- d_6 relative to the solvent residual signals at 7.26 or 2.05 ppm respectively, and J values in Hz. Bidimensional Heteronuclear Multiple Bond Correlation (HMBC) experiments were performed to obtain indications on C signals and for long range ^1H , ^{13}C correlations .

3.2.3 Ultraviolet–Visible Spectroscopy

Principles

UV-visible spectroscopy investigates the absorption of electromagnetic radiation in the range of wavelength 190-780 nm by matter. In this wavelength range the absorption of the electromagnetic radiation is caused by the excitation (i.e. transition to a higher energy level) of the bonding and non-bonding electrons of ions or molecules. The measured spectrum is continuous, due to the fact that the different vibration and rotation states of the molecules make the absorption band wider [78]. A graph of absorbance against wavelength gives the sample's absorption spectrum.

This spectroscopic technique is used for both qualitative and quantitative investigations of samples, the latter ones based on Lambert-Beer's Law described as follows:

$$A = \epsilon cl$$

where A = absorbance (defined as $A = \log_{10}(I_0/I)$, where I_0 is the incident light intensity and I is the light intensity after it passes through the sample), ϵ = molar absorption coefficient (in $\text{dm}^3 \text{mol}^{-1} \text{cm}^{-1}$ units), c = concentration (in molarity) of

the compound in the solution (in mol dm⁻³ units), and l = path length of light in the sample (in cm units).

Experimental details

UV spectra were performed at a room temperature with a Lambda 25 UV/Vis spectrophotometer (Perkin Elmer). In particular, for 4,4'-dihydroxy-(*E*)-stilbene an acetonitrile solution (50 μ M) was kept at room temperature, and the spectral tracing was started by addition of CuSO₄ (50 μ M in water). The spectra were recorded every 5 min after addition of CuSO₄.

3.3 MS analysis of resveratrol-metal complexes

Regarding solvent conditions used to achieve the higher sensitivity, and for maintaining the resveratrol metal complex intact, acetonitrile/water (1:1) was found to be better than methanol/water (1:1), especially in providing signal for metal complexes. The positive ion mode has been the best condition for the analysis of metal complex system with following experimental parameters: cone voltage 26 V; capillary exit 96 V; spray capillary voltage 4 kV; source temperature 300 °C.

3.4 Synthesis and structural characterization of resveratrol analogues

3.4.1 Dihydro-resveratrol

This compound was prepared as reported in figure 3.1.

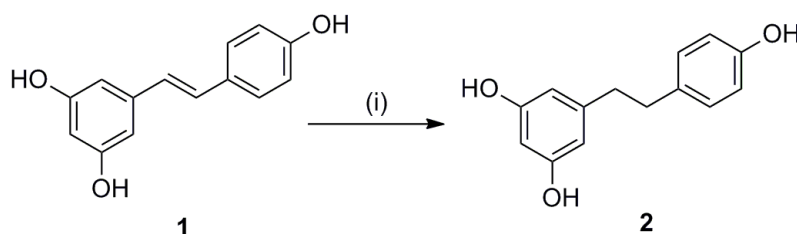


Figure 3.1 – Conversion of resveratrol (1) into dihydro-resveratrol (2). Reagent and conditions: (i) H₂, Pd/C, ethanol, 1 h.

Resveratrol (5 mg, **1**) and Pd/C (1 mg) were mixed in ethanol (8 ml) and the mixture was stirred under hydrogen atmosphere at room temperature. The reaction was monitored by thin layer chromatography (TLC) and stopped after 1 h. The mixture was filtered and evaporated *in vacuo* to obtain a residue, which was purified by preparative TLC on silica gel eluting with dichloromethane/methanol (9:1), to give pure dihydro-resveratrol **2**. (80%).

^1H NMR analysis gave a spectrum super imposable to the reported in data [79].

^1H NMR ($(\text{CD}_3)_2\text{CO}$, 400 MHz): δ 2.73 (m, 4H), 6.19 (d, $J = 2$ Hz, 1H), 6.22 (d, $J = 2$ Hz, 1H), 6.74 (d, $J = 8$ Hz, 2H), 7.03 (d, $J = 8$ Hz, 2H).

ESI (-) MS: m/z 229 (M-H) $^-$; MS/MS (229): m/z 123

3.4.2 (*Z*)-Isomer of resveratrol

This compound was prepared by photoisomerization of natural resveratrol (Figure 3.2).

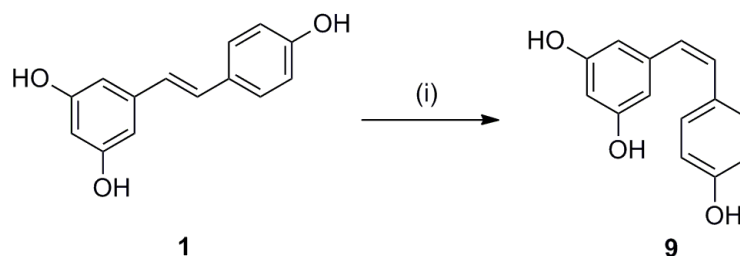


Figure 3.2 – Isomerization of natural (*E*)-resveratrol to (*Z*)-isomer **9**. conditions: (i) $h\nu$, 350 nm, ethanol.

A solution of resveratrol (**1**, 2 mg) in ethanol (0.8 mL), was degassed by using a nitrogen in NMR tube [80–82]. The tube was then inserted in a photochemical reactor (Applied Photophysics, Photochemical Reactors Ltd, UK) and irradiated at 350 nm over 2 h. At time intervals (every 10, 20, 40, 80 and 100 min), the NMR tube was scanned directly by ^1H NMR analysis. The obtained residue was purified by reversed phase HPLC technique using a Merck HITACHI AC-220V system with UV-vis detector (UVIDEDEC-100V) at a flow rate of 1 mL/min. The stationary phase consisted of a 7 μm Lichrosorb® C18 column and the mobile phase was water/methanol (40:60)

with single UV detection at 254 nm. The purified compound **9** collected at $t_R = 40$ min was characterized by ^1H NMR and directly used for MS experiments [83].

^1H NMR (CDCl_3 , 400 MHz): δ 6.22 (t, $J = 2.2$ Hz, 1H), 6.29 (d, $J = 2.2$ Hz, 2H), 6.37 (d, $J = 13.2$ Hz, 1H), 6.41 (d, $J = 13.2$ Hz, 1H), 6.69 (d, $J = 8.4$ Hz, 2H), 7.13 (d, $J = 8.4$ Hz, 2H), 8.14 (s, 2H), 8.40 (s, 1H).

ESI (-) MS: m/z 227 (M-H) $^-$; MS/MS (227): m/z 212, 199, 185, 183, 159, 157.

3.4.3 4,4'-Dihydroxy-(*E*)-stilbene

Synthesis of 4,4'-DHS (**11**) is reported in figure 3.3.

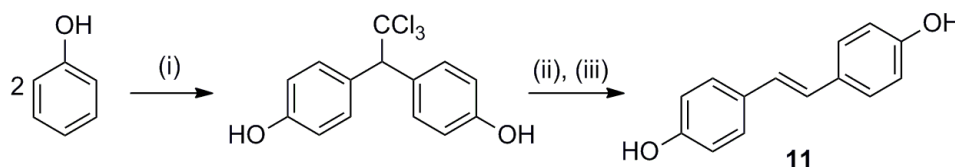


Figure 3.3 – Synthesis of 4,4'-DHS (**11**). Reagents and conditions: (i) chloral hydrate, acetic acid, H_2SO_4 ; (ii) Zn, ethanol, reflux, 4 h; (iii) MW irradiation, 2 h.

The reaction is carried out as reported [84]. A solution of phenol (100 mg , 1.06 mmole) and chloral hydrate (351 mg , 2.12 mmol) in glacial acetic acid (10 mL) was treated with 98% sulphuric acid (84 μL) under vigorous stirring at room temperature. The reaction was monitored by TLC and stopped after 12 h. The mixture was poured on to the crushed ice, the obtained precipitate was filtered, and taken to dryness. The residue was crystallized to give a pure as a 4, 4'-(2,2,2-trichloroethane-1,1-diyl) diphenol as a white crystalline solid. Its structure was confirmed by ^1H NMR analysis: ($(\text{CD}_3)_2\text{CO}$, 400 MHz): δ 2.9 (s, 1H), 6.72 (d, $J = 8$ Hz, 4H), 7.04(d, $J = 8$ Hz, 4H). Later it was used in the following step.

The latter product (16 mg , 0.05 mmol) in ethanol (0.6 mL), was added of zinc powder (15 mg , 0.15 mmol), and the mixture refluxed for 3 h. The reaction was monitored by TLC. After 4 h, the mixture was cooled and filtered. The residue was washed 2-3 times with acetone and ethanol, and concentrated *in vacuo* to obtain a residue, which was purified by preparative TLC on silica gel eluting with *n*-hexane/ethyl acetate (6:4) to give an isomeric mixture of 4,4'-DHS (*E/Z*, 1:1), characterized by ^1H NMR analysis.

This *E/Z* isomer was subjected to microwave irradiated for 2 h. The reaction was monitored by ^1H NMR analysis. After irradiation for 2 h, the residue was fractionated by preparative TLC on silica gel eluting with *n*-hexane/ethyl acetate (6:4) to give pure (*E*)-4,4'-DHS. It was characterized by MS and ^1H NMR analysis and comparison with reported data [85].

^1H NMR ($(\text{CD}_3)_2\text{CO}$, 400 MHz): δ 6.83 (d, $J = 8$ Hz, 4H), 6.95 (s, 2H), 7.40 (d, $J = 8$ Hz, 4H).

ESI (-) MS: m/z 211 (M-H) $^-$; MS/MS (211): m/z 193, 183, 169, 155.

3.4.4 4-Hydroxy-(*E*)-stilbene, 3,4-dihydroxy-(*E*)-stilbene, and 3,5-dihydroxy-(*E*)-stilbene

These resveratrol analogues were synthesized by Wittig reaction as reported in figure 3.4.

Preparation of 4-hydroxy-(*E*)-stilbene (4-HS,10)

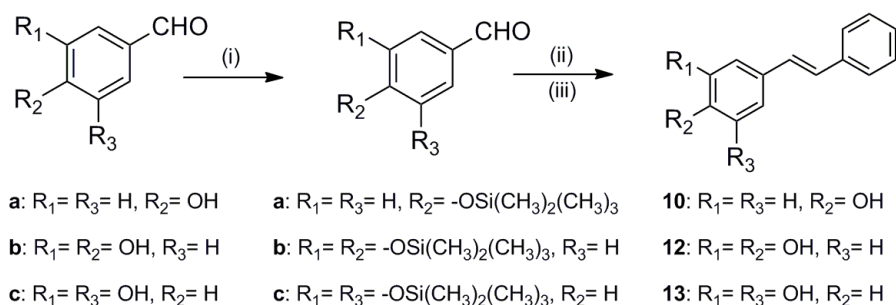


Figure 3.4 – Synthesis of stilbene analogues **10**, **12**, and **13**. Reagents and conditions: (i) tert-butyl dimethylsilyl chloride, 1,8-diazabicycloundec-7-ene, dichloromethane, (ii) benzyl triphenyl phosphonium bromide, K_2CO_3 , iso-propanol, reflux, 4 h; (iii) tert-butyl ammonium fluoride (1M in THF), THF, 1 h.

To a solution of 4-hydroxy benzaldehyde (100 mg, 0.81 mmole) in dichloromethane (10 mL), 1,8-diazabicycloundec-7-ene (0.16 mL, 1.06 mmole) was added followed by t-butyl-dimethyl silyl chloride (185 mg, 1.23 mmole), and the mixture was taken under vigorous stirring at room temperature. After stirring for 3 h, the reaction

was monitored by showing complete conversion of aldehyde by TLC. The mixture was concentrated, added to H₂O (15 mL) and extracted with ethyl acetate (3×10 mL). The combined organic layers were washed with H₂O, dried over anhydrous Na₂SO₄ and concentrated to give the protected aldehyde, as characterized by ¹H NMR analysis.

¹H NMR ((CDCl₃, 400 MHz): δ 0.26 (s, 6H), 1.0 (s, 9H), 6.95 (d, *J* = 8.9 Hz, 2H), 7.79 (d, *J* = 8.9 Hz, 2H), 9.89 (s, 1H).

(*E*)-tert-butyldimethyl (4-styrylphenoxy) silane was prepared as reported [86]. To a solution of (*E*)-tert-butyldimethyl (4-styrylphenoxy) silane (50 mg, 0.21 mmole) in iso-propanol (5 mL), potassium carbonate (44 mg, 0.318 mmole) and benzyl triphenyl phosphonium bromide (137 mg, 0.32 mmole) was added, and the mixture refluxed for 4 h monitoring by TLC. The reaction mixture was cooled, concentrated, added to H₂O (10 mL) and extracted with ethyl acetate (3×5 mL). The combined organic layers were washed with H₂O, dried over anhydrous Na₂SO₄ and evaporated to dryness to obtain a residue, which was fractionated on a silica gel column using a gradient of *n*-hexane/ethyl acetate as the eluent. Fraction eluted with *n*-hexane/ethyl acetate (97:3) gave pure product as oily solid.

¹H NMR ((CDCl₃, 400 MHz): δ 0.26 (s, 6H), 1.0 (s, 9H), 6.84 (d, *J* = 8 Hz, 2H), 6.97, 7.07 (each 1H, d, *J* = 16.3 Hz), 7.35 (t, *J* = 6.7 Hz, 1H), 7.40 (d, *J* = 8.8 Hz, 4H), 7.49 (d, *J* = 7.16 Hz, 2H).

A t-butyl ammonium fluoride solution (0.72 mL, 0.072 mmole, 1M in THF) was added to a solution of (*E*)-tert-butyldimethyl (4-styrylphenoxy) silane (15 mg, 0.048 mmole) in tetrahydrofuran (1.5 mL) at 0°C, and the mixture was stirred at room temperature. After 1 h, the reaction mixture was taken to dryness, added of H₂O (5 mL), neutralized with 0.1 N HCl and extracted with ethyl acetate (3× 5 mL). The combined organic layers were washed with H₂O, dried over anhydrous Na₂SO₄ and concentrated to obtain a residue, which was fractionated by preparative TLC with *n*-hexane/ethyl acetate (97:3), to give pure 4-HS (**10**). It was characterized by MS and ¹H NMR analysis and comparison with reported data [32].

¹H NMR ((CD₃)₂CO, 400 MHz): δ 6.76 (d, *J* = 8 Hz, 2H), 6.94, 7.06 (d, *J* = 18 Hz, 1H), 7.17 (td, *J* = 8, 2 Hz, 1H), 7.29 (t, *J* = 8 Hz, 2H), 7.35 (br d, *J* = 8 Hz, 2H), 7.47 (d, *J* = 8 Hz, 2H).

ESI (-) MS: m/z 195 (M-H)⁻; MS/MS (195): m/z 180, 165.

In order to synthesize 3,4-dihydroxy-(*E*)-stilbene (3,4-DHS, **12**) and 3,5-dihydroxy-(*E*)-stilbene (3,5-DHS, **13**), reactions under the same conditions as for were carried out but NMR spectra for the purified products were compared with reported data [87, 88].

Data for 3,4-DHS (**12**):

¹H NMR ((CD₃)₂CO, 400 MHz): δ 6.79 (d, $J = 8$ Hz, 1H), 6.89 (dd, $J = 8, 2$ Hz, 1H), 6.98, 7.01 (d, $J = 16.4$ Hz, each 1H), 7.09 (d, $J = 2$ Hz, 1H), 7.19 (t, $J = 7.4$ Hz, 1H), 7.31 (t, $J = 7.4$ Hz, 2H), 7.51 (d, $J = 7.4$ Hz, 2H).

ESI (-) MS: m/z 211 (M-H)⁻; MS/MS (211): m/z 193, 183, 165, 155, 141, 115.

Data for 3,5-DHS (**13**):

¹H NMR ((CD₃)₂CO, 400 MHz): δ 6.27 (t, $J = 2.1$ Hz, 1H), 6.56 (d, $J = 2.1$ Hz, 2H), 7.05, 7.07 (d, $J = 16.6$ Hz, each 1H), 7.22 (t, $J = 7.3$ Hz, 1H), 7.33 (t, $J = 7.3$ Hz, 2H), 7.53 (d, $J = 7.3$ Hz, 2H).

ESI (-) MS: m/z 211 (M-H)⁻

3.5 Synthesis and structural characterization of dehydrodimers

3.5.1 From resveratrol under different conditions

In the presence of copper(II)sulfate

Synthesis of dehydrodimer **3** is reported in figure 3.5.

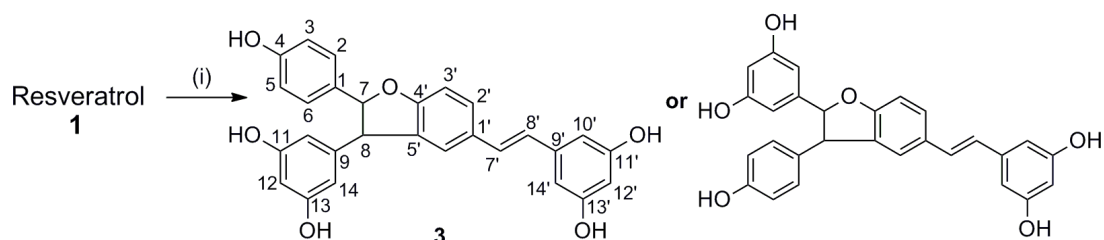


Figure 3.5 – Synthesis of dehydrodimer **3**. Reagent and condition (i) anhydrous CuSO₄, anhydrous acetonitrile, rt, 24h, Numbering is for convenience.

A solution of resveratrol (5 mg, 0.021 mmole) and anhydrous copper sulfate (6 mg, 0.032 mmole) were mixed in anhydrous acetonitrile (2 mL) and stirred for 24 h at room temperature, monitoring by TLC (*n*-hexane/ethyl acetate/methanol, 6:4:0.5). The reaction mixture was concentrated, added H₂O (2 mL) and extracted with ethyl acetate (3×5 mL). The combined organic layers were dried over anhydrous Na₂SO₄ and concentrated to obtain a residue, which was subjected to preparative TLC with *n*-hexane/ethyl acetate/methanol (6:4:0.5) to give the pure **3**. Assignment of structure **3** and not the isomer one reported in figure 3.5 was established by NMR and HMBC analysis.

¹H NMR ((CD₃)₂CO, 400 MHz): δ 4.47 (d, *J* = 8 Hz, 1H, H-8), 5.45 (d, *J* = 8 Hz, 1H, H-7), 6.20 (d, *J* = 2.2 Hz, 2H, H-10,14), 6.26 (t, *J* = 2.1 Hz, 1H, H-12'), 6.29 (t, *J* = 2.2 Hz, 1H, H-12), 6.54 (d, *J* = 2.1 Hz, 2H, H-10',14'), 6.85 (d, 2H, H-3,5), 6.87 (d, *J* = 8.3 Hz, 1H, H-3'), 6.90 (d, *J* = 16.3 Hz, 1H, H-8'), 7.06 (d, *J* = 16.3 Hz, 1H, H-7'), 7.24 (d, 2H, H-2,6), 7.26 (broad s, 1H, H-6'), 7.43 (dd, *J* = 8.3, 1.6 Hz, 1H, H-2').

¹³C NMR deduced by HMBC experiment ((CD₃)₂CO, 400 MHz, numbering from figure 3.5): δ58.5 (C-8), 94.72 (C-7), 106.86 (C-10,14), 101.79 (C-12), 102.12 (C-12'), 105.15 (C-10',14'), 109.86 (C-3'), 115.62 (C-3,5), 123.44 (C-6'), 126.7 (C-8'), 128.09 (C-2,6), 128.60 (C-7'), 128.14 (C-2'), 131.26,131.67, and 132.05 (C-1,1',5'), 140.28 (C-9'), 144.73 (C-9), 157.88 (C-4), 159.00 (C-11',13'), 159.22 (C-11,13), 161.3 (C-4').

ESI (-) MS: *m/z* 453 (M-H)⁻; MS/MS (453): *m/z* 435, 411, 369, 359, 347, 333.

ESI (+) MS: *m/z* 455 (M-H)⁺; MS/MS (455): *m/z* 437, 361.

Catalyzed by Laccase enzyme

Dehydrodimer **3** was obtained according to the procedure reported by Nicotra *et al.* [89]. Resveratrol (5 mg, 0.021 mmole) was dissolved in ethyl acetate (0.4 mL), while laccase (9 mg, 20 U) was dissolved in 20 mM acetate buffer, (pH 4.5, 0.4 mL). The biphasic system was stirred at room temperature for 24 h. The organic solvent was evaporated and the residue purified by preparative TLC (eluent: *n*-hexane/ethyl acetate/methanol, 6:4:0.5) to give resveratrol dehydrodimer **3**. ¹H NMR spectrum was super imposable to the previously recorded for resveratrol/copper(II)sulfate product. By using enzyme, an optically active product was obtained: $[\alpha]_D = -28^{\circ}$ (MeOH, *c* = 1.1 mg/mL).

ESI (-) MS: m/z 453 (M-H)⁻; MS/MS (453): m/z 435, 411, 369, 359, 347, 333, 317.

ESI (+) MS: m/z 455 (M-H)⁺; MS/MS (455): m/z 437, 361.

In the presence of galvinoxyl radical

Resveratrol dehydrodimer was prepared according to the Shang *et al.* [21]. A galvinoxyl radical (37 mg, 0.09 mmole) was added to a solution of resveratrol (10 mg, 0.05 mmole) in ethanol (5 mL), and the mixture was vigorously stirred at room temperature. The reaction mixture was monitored by TLC, stopped after 8 h. And then concentrated, added of H₂O (5 mL), and extracted with ethyl acetate (3×5 mL). The combined organic layers were washed with H₂O, dried over anhydrous Na₂SO₄ and concentrated *on vacuum* to obtain a residue, which was purified by preparative TLC in reverse phase (methanol/water, 8:2) to give dehydrodimer **3**, as established by NMR analysis.

In the presence of iron(III)chloride

Synthesis and structure of dehydrodimer **4** are reported in figure 3.6.

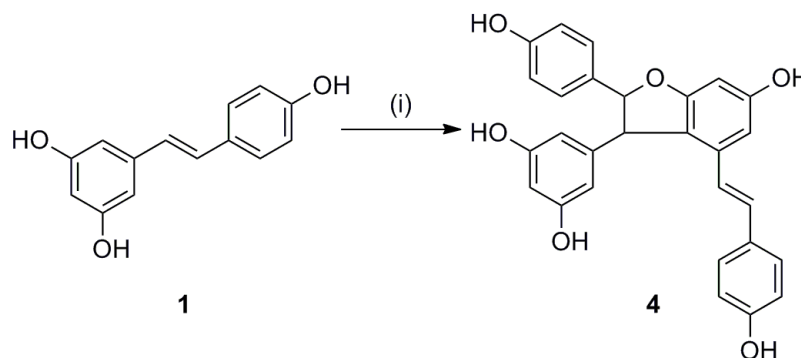


Figure 3.6 – Synthesis of dehydrodimer **4**. Reagent and condition: (i) FeCl₃, MeOH/H₂O (1:1), rt, 49h.

The procedure reported by Chun-Suo *et al.* [90, 91] was followed. A solution of FeCl₃ (1.4 mg, 0.032 mmole) in water (0.5 mL) was added drop wise to resveratrol (5 mg, 0.021 mmole) in methanol (0.5 mL) under stirring. The mixture was stirred at room temperature for 49 h. After removal of the methanol *in vacuo*, the residue was

diluted with water and extracted with ethyl acetate (3×5 mL). Then the combined organic layers were washed with H₂O and evaporated to give a residue, which was subjected to preparative TLC (*n*-hexane/ethyl acetate/methanol, 6:4:0.5) to give pure **4**. The structure was characterized by MS and ¹H NMR analysis and comparison with reported data [92], establishing that it was regioisomer of **3**.

¹H NMR ((CD₃)₂CO, 400 MHz): δ 4.46 (d, *J* = 5.4 Hz, 1H), 5.44 (d, *J* = 8 Hz, 1H), 6.24 (br s, 3H), 6.33 (d, *J* = 2 Hz, 1H), 6.71 (d, *J* = 16.3 Hz, 1H), 6.74 (d, *J* = 7 Hz, 2H), 6.77 (d, *J* = 2 Hz, 2H), 6.83 (d, *J* = 7 Hz, 2H), 6.91 (d, *J* = 16.3 Hz, 2H), 7.19 (d, *J* = 7 Hz, 2H), 7.21 (d, *J* = 7 Hz, 2H).

ESI (-) MS: *m/z* 453 (M-H)⁻; MS/MS (453): *m/z* 435, 411, 369, 359, 347, 333.

3.5.2 From 4-HS in the presence of copper(II)sulfate

Synthesis of dehydrodimer **14** is reported in figure 3.7.

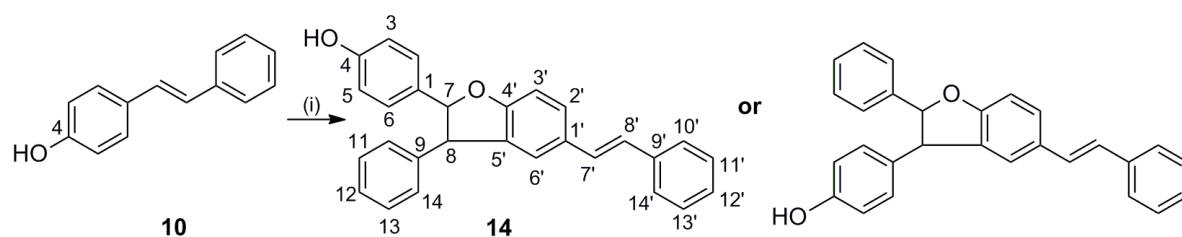


Figure 3.7 – Synthesis of dehydrodimer **14**. Reagent and conditions: (i) anhydrous CuSO₄, dry acetonitrile, rt, 24h, Numbering is for convenience.

A copper sulfate (6 mg, 0.04 mmole) was added to a solution of **10** (5 mg, 0.03 mmole) in acetonitrile (2 mL), and the mixture was stirred at room temperature. The reaction mixture was monitored by TLC. After 24 h the reaction mixture was added of with H₂O (5 mL), and extracted with ethyl acetate (3×5 mL). The combined organic layers were dried over anhydrous sodium sulphate and taken to dryness. The residue was purified by preparative TLC on silica gel eluting with *n*-hexane/ethyl acetate/methanol (6:4:0.5), to give pure dehydrodimer. Structure **14** and not the regioisomer structure reported in figure 3.7 was established by NMR and HMBC analysis and comparison with reported data [91].

^1H NMR ($(\text{CD}_3)_2\text{CO}$, 400 MHz): δ 4.63 (d, $J = 8.5$ Hz, 1H), 5.49 (d, $J = 8.5$ Hz, 1H), 6.83 (d, $J = 8$ Hz, 2H), 6.88 (d, $J = 8.4$ Hz, 1H), 6.98, 7.13 (d, $J = 16.4$ Hz, 2H), 7.14 (t, d, $J = 8$ and 2 Hz, 1H), 7.16 (d, $J = 2$ Hz, 1H), 7.19 (d, $J = 8$ Hz, 1H), 7.19 (d, $J = 8.3$ Hz, 2H), 7.21 (t, $J = 8$ Hz, 1H), 7.21 (t, d, $J = 8$ and 1.5 Hz, 1H), 7.29 (t, d, $J = 8$ and 2 Hz, 2H), 7.34 (t, d, $J = 8$ and 1.5 Hz, 1H), 7.46 (d, $J = 8.4$ Hz, 1H), 7.49 (t, d, $J = 8$ and 2 Hz, 2H).

^{13}C NMR deduced by HMBC experiment ($(\text{CD}_3)_2\text{CO}$, 400 MHz, numbering from figure 3.7): δ 57.1 (C-8), 94.2 (C-7), 107.3 (C-10,14), 102.2 (C-12), 110.1 (C-3'), 116.00 (C-3,5), 128.5 (C-6'), 128.5 (C-2,6), 123.6 (C-2'), 132.3, 131.9, and 131.6 (C-1,1',5'), 138.5 (C-9'), 142.5 (C-9), 158.3 (C-4), 142.5 (C-11,13), 160.5 (C-4').

ESI (-) MS: m/z 389 (M-H) $^-$; MS/MS (389): m/z 371, 295.

3.5.3 From 3,4-DHS in the presence of copper(II)sulfate

Synthesis of Diels Alder product **19a** is reported in figure 3.8.

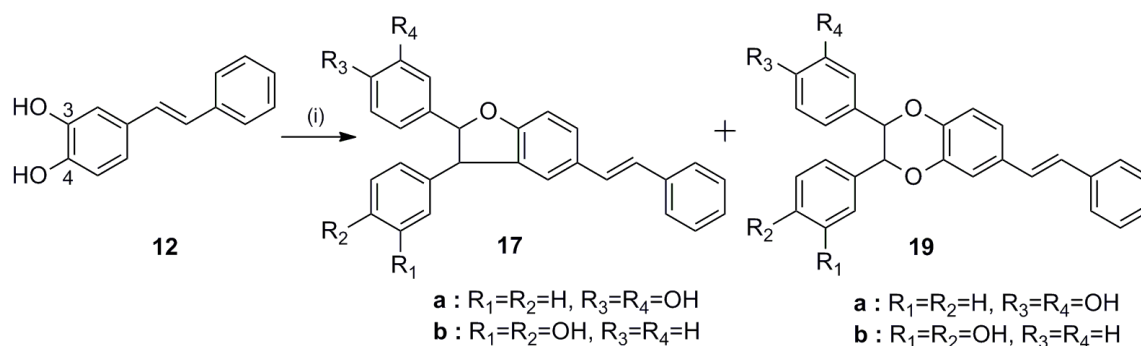


Figure 3.8 – Synthesis of **17a/17b** and **19a/19b**. Reagent and condition: (i) anhydrous CuSO_4 , dry acetonitrile, rt, 24h.

A copper sulphate (7 mg, 0.036 mmole) was added to a solution of **12** (5 mg, 0.023 mmole) in acetonitrile (2 mL), and the mixture was stirred at room temperature. The reaction mixture was monitored by TLC and stopped after 24 h. The reaction mixture was evaporated *in vacuo* obtaining a residue, which was purified by preparative TLC on silica gel eluting with *n*-hexane/ethyl acetate/methanol (6:4:0.5), to give a pure product. Its structure was established to be dioxane-like dimer **19a** (and not 17a, 17b, or 19b) by MS analysis and NMR spectra compared to known data [21].

^1H NMR ($(\text{CD}_3)_2\text{CO}$, 400 MHz): δ 4.92 (d, $J = 8$ Hz, 1H), 5.05 (d, $J = 8$ Hz, 1H), 6.51 (d, $J = 8$ Hz, 1H), 6.68 (d, $J = 8$ Hz, 1H), 6.77 (d, $J = 2$ Hz, 1H), 6.97 (d, $J = 8$ Hz, 1H), 7.13, 7.19 (d, $J = 16.4$ Hz, 2H), 7.17 (d, $J = 8$ Hz, 1H), 7.23 (m, 2H), 7.24 (d, $J = 7.8$ Hz, 1H), 7.25 (m, 1H), 7.26 (m, 2H), 7.27 (d, $J = 2.4$ Hz, 1H), 7.35 (d, $J = 7.8$, 2H), 7.57 (d, $J = 7.8$, 2H).

ESI (-) MS: m/z 421 (M-H) $^-$; MS/MS (421): m/z 211.

3.6 Density functional theory calculations

Quantum chemical calculations on resveratrol-copper complexes (Section 4.1.2) were performed by using the Gaussian 03W revision E.01 package [93]. Geometry optimization and subsequent vibrational analysis were carried out at B3LYP/6-311G(d) level of theory [94, 95]. Additional calculations by using the TZVP basis set were performed by using the NWCHEM (Pacific North West National Laboratory, USA) software [96].

For the dehydrodimers, all calculations were performed with the Jaguar 7.5 quantum chemistry package [97] using density functional theory (DFT) with the B3LYP hybrid functional [94, 98](Section 4.4), which is known to give a good description of reaction profiles for organic compounds.

The 1s-3p core electrons of the copper and iron atoms were described with the Hay and Wadt core-valence relativistic effective core-potential (ECP) leaving the outer electrons to be treated explicitly by a basis set of double- ξ quality [99], whereas all electrons were considered for the remaining atoms with the 6-31G** basis set (denoted as LACVP** in Jaguar) [100]. For all the considered molecules, preliminary conformational search using a Monte Carlo Multiple Minimum approach at MM level (using the MMFFs force field) was carried out. The most stable conformers for each molecule were optimized in gas phase with this basis set and the B3LYP functional. Frequency calculations were performed to verify the correct nature of the stationary points and to estimate zero-point energy (ZPE) and thermal corrections to thermodynamic properties.

The Poisson-Boltzmann (PB) continuum solvation model, as implemented in Jaguar [101], was used to estimate the energetical and structural changes in aqueous solution, addressed by performing single point calculations on the gas phase optimized geometries with a larger 6-311++G** basis set for the main group elements and LACV3P+*, consisting of Hay and Wadt core-valence ECP basis set of triple- ξ quality plus one diffuse d function, for the metal atom [99, 100].

Chapter 4

Results and discussion

4.1 Resveratrol-copper complexes

This section describes metal complexes of resveratrol produced as gas phase ions by electrospray ionization mass spectrometry (ESI-MS). Mass spectrometry has been extensively applied for investigating non-covalent metal complexes, mainly in the gas phase [102] and sometimes in liquids [103]. It is worth noting that transition metal chemistry is usually investigated in solution or solid state, whereas mass spectrometry allows to study the gas phase, a situation in which interactions with the solvent molecules are eliminated or strongly reduced, and ions may be present as bare species. ESI-MS technique is used extensively in the analysis of metal ion complexes, also of biological relevance, due to its capability to produce ions in the gas phase which are strongly correlated to their solution structures [104].

4.1.1 Mass spectrometric analysis

After addition of an equimolar amount of copper(II)sulphate to a solution of resveratrol in acetonitrile/water(1:1), a clear change in the spectra was observed, in comparison to the MS spectrum recorded for resveratrol.

The positive ion mode full scan ESI spectrum of a water/acetonitrile (1:1) solution of resveratrol and copper(II)sulfate is shown in figure 4.1. In addition to the $[M+H]^+$ ion of resveratrol at m/z 229 and to the peak at m/z 455 imputable to its dehydrodimer, intense cluster signals indicating the presence of copper ions are observed. Copper occurs as two stable natural isotopes, ^{63}Cu (69.15 %) of accurate mass 62.9296 Da and ^{65}Cu (30.85 %) of accurate mass 64.9278 Da, that show a characteristic ~2:1 ratio. The peak at m/z 519 is assigned to a mono charged complex formed by two

resveratrol molecules and one copper ion, since its isotopic distribution is in agreement with the simulated pattern for the molecular composition $C_{28}H_{24}CuO_6$ (Figure 4.2).

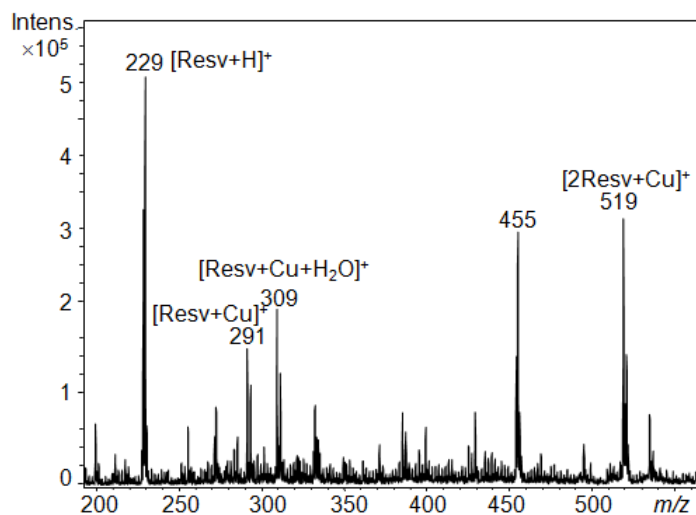


Figure 4.1 – ESI (+) MS spectrum obtained by injection of a 1:1 resveratrol/ $CuSO_4$ solution in CH_3CN/H_2O (1:1).

As copper was present in the initial solution as $Cu(II)$, a reduction has occurred to $Cu(I)$ ion as often reported in the case of ESI-MS of Cu -complexes [22, 104, 105]. Other peaks are observed at m/z 291 and m/z 309, attributable to $[Resv+Cu]^+$ and $[Resv+Cu+H_2O]^+$ respectively.

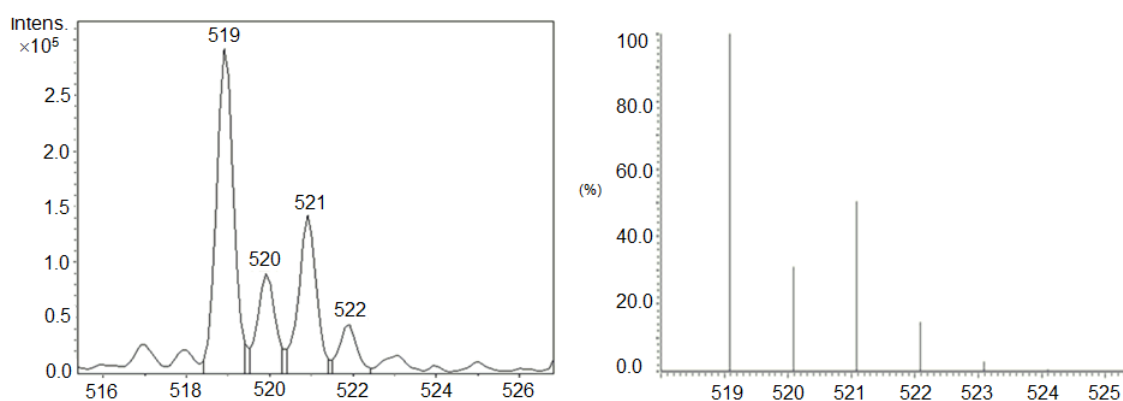


Figure 4.2 – Expanded region of the ESI(+)-MS spectrum obtained by injection of a 1:1 resveratrol/ $CuSO_4$ solution in CH_3CN/H_2O (1:1) corresponding to cluster at $m/z = 519$ for $[2Resv+Cu]^+$ in the experimental (left) and simulated (right) cases.

Fragmentation experiments were carried out to gain insight into the structures of the clusters. MS/MS experiments on the whole cluster centered at m/z 520 yield

intense cluster peaks at m/z 291 and m/z 309 showing the contributions of both the copper isotopes (Figure 4.3 (a)). The assignment is supported by MS/MS experiment performed on precursors with different isotopic composition, with the selection of the signal at m/z 519 producing the more abundant single peaks at m/z 309 and 291 corresponding to the presence of ^{63}Cu isotope (Figure 4.3 (b)). The former peak corresponds to the loss of one neutral resveratrol molecule, the latter results from the addition of H_2O present in trace in the ion trap, to the ion at m/z 291.

MS^3 experiments performed on ions at m/z 309 give an intense signal at m/z 291, attributable to the loss of one water molecule. We obtained the spectrum shown in figure 4.4.

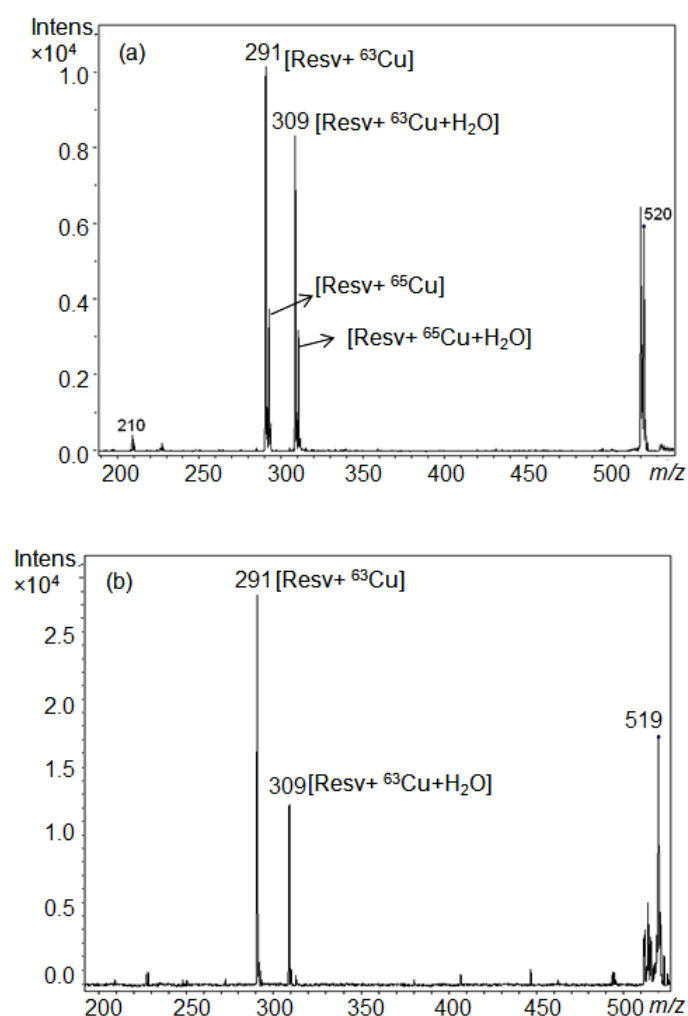


Figure 4.3 – Positive-ion MS/MS fragmentation on: (a) m/z 520 \pm 2 corresponding to the selection of the whole cluster ascribed to $[2\text{Resv}+\text{Cu}]^+$ ion and (b) m/z 519 corresponding to the most intense peak of the cluster due to the contribution of ^{63}Cu isotope.

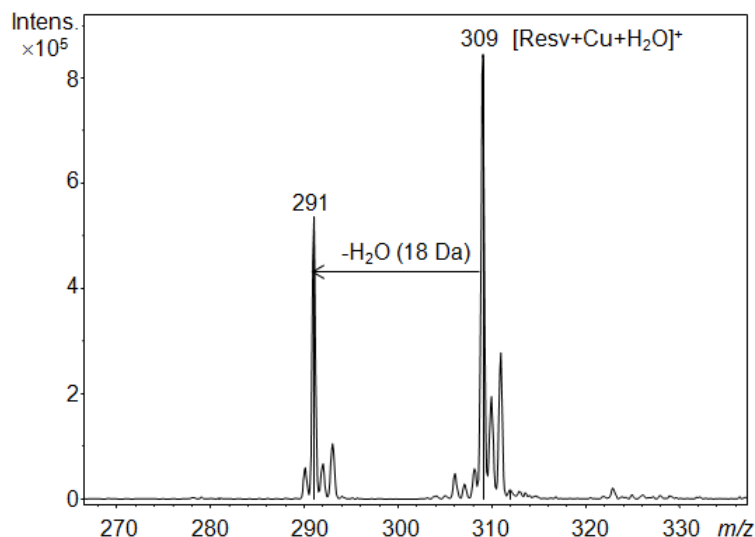


Figure 4.4 – MS³ experiment on the signal selected at m/z 309, corresponding to $[\text{Resv} + \text{Cu} + \text{H}_2\text{O}]^+$ ion.

In figure 4.5 the ESI spectrum, for the complex formed at m/z 291 $[\text{Resv} + \text{Cu}]^+$ is reported. By increasing the skimmer voltage from the standard 26 V value up to 50 V, the ratio of the ions at m/z 309 and 291 changes from 2.2/1 to 1/2.5. MS/MS experiments on the m/z 291 ion produce intense fragments at m/z 228, 210 and 187, all of them with a cluster showing the loss of copper.

The formation and stability of resveratrol/copper complexes have been investigated also in solution phase, in order to verify if complexes are produced in solution or in the gas phase. Experiments were performed by using ¹H NMR analysis of resveratrol in presence of an equimolar amount of copper salt. We observed no evident changes on the spectrum registered immediately after the addition of the salt and one hour later (Figure 4.6). Moreover, no detectable alterations appeared in the ¹H NMR spectrum of the preformed resveratrol-copper salt solution after one day. These evidences indicate that metal complexes mainly formed in the ion source.

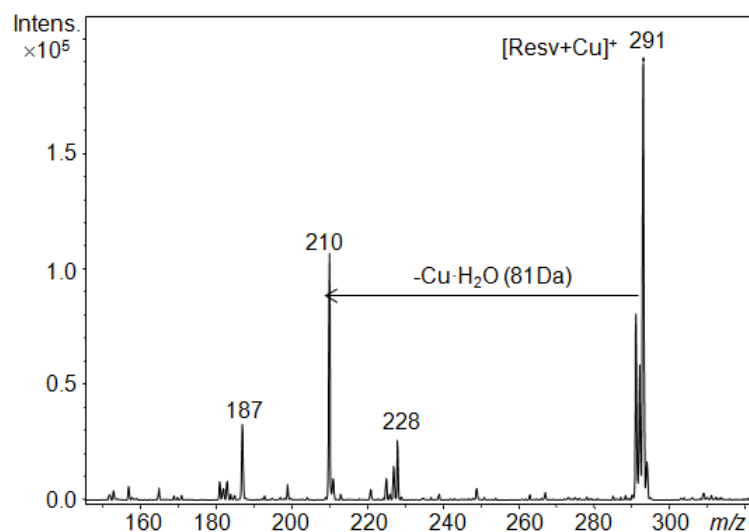


Figure 4.5 – MS^3 experiment on the signal selected at m/z 291, corresponding to $[\text{Resv}+\text{Cu}]^+$ ion.

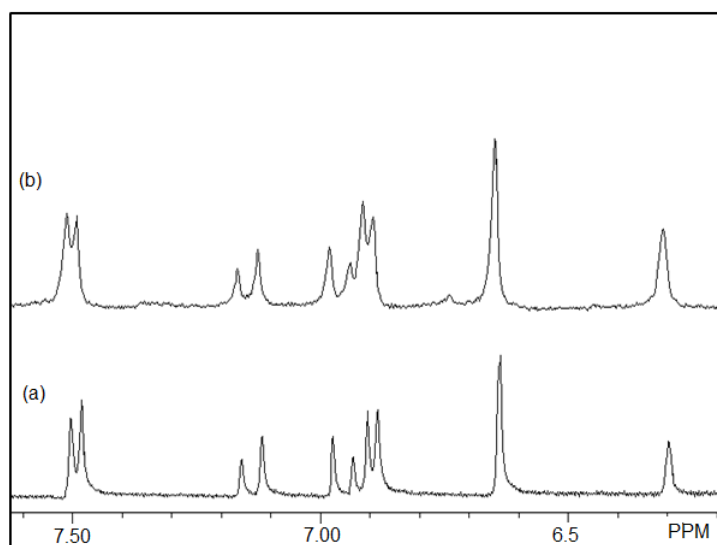


Figure 4.6 – ^1H NMR spectrum recorded in D_2O in presence of CD_3CN , for resveratrol (a) and in the presence of anhydrous CuSO_4 after 1h (b) in spectral range 7.7:6.2 ppm.

It has previously outlined that the observed complexes are monocharged cations. As copper(I) was not present in the initial sample solution, a reduction process from Cu(II) to Cu(I) has occurred in the gas phase. To further support this conclusion, we carried out measurements by replacing CuSO_4 with both Cu(I)Cl and Cu(I)Br salt. We obtained similar spectra, although with a higher noise probably because of

the extremely low solubility of copper(I)salt. In addition, fragmentation experiments involving ions at m/z 519, 309 and 291 gave the same fragmentation patterns.

In order to evaluate how the molecular structure affects the interaction with the copper ion, we have compared resveratrol with a derivative compound lacking of the double bond between the two aromatic rings. To this purpose we prepared the synthetic dihydro-resveratrol (DHResv) by hydrogenation of resveratrol (Section 3.4.1). Its solution in acetonitrile/water added of an equimolar amount of copper(II)sulfate was analyzed by ESI-MS technique. Only weak signals related to copper complexes were observed. However, if acetonitrile is replaced by methanol (2:1 DHResv/CuSO₄ in MeOH/H₂O,1:1), an intense peak appears at m/z 293, attributable to the [DHResv+Cu]⁺ ion (Figure 4.7).

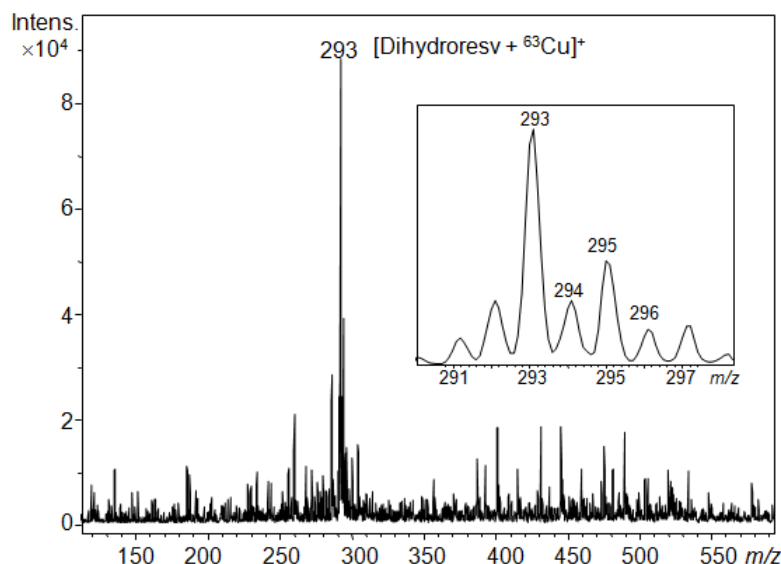


Figure 4.7 – ESI(+)-MS spectrum obtained by injection of 1:1 dihydro-resveratrol /CuSO₄ solution in MeOH/H₂O (1:1) with a zoom on the isotopic cluster at m/z 293/295.

In this experiment also a reduction of copper ion has occurred. The same signal is detected by using CuCl instead of CuSO₄. MS/MS experiments by selection of the whole cluster at m/z 294±2 produce fragments at m/z 211 and m/z 187 (Figure 4.8(a)). The cluster pattern for the most intense peak at m/z 187 corresponds to the loss of 4-methylenecyclohexa-2,5-dienone and points to the presence of Cu(I), supported by fragmentation experiments on the selected ion at m/z 295 which produced

single signals both at m/z 211 and 189, the latter one corresponding to the presence of ^{65}Cu isotope (Figure 4.8(b)). The other daughter ion at m/z 211 as a single peak indicates the absence of Cu(I) ion and corresponds to $[\text{DHResv-H}_2\text{-H}_2\text{O+H}]^+$ ion.

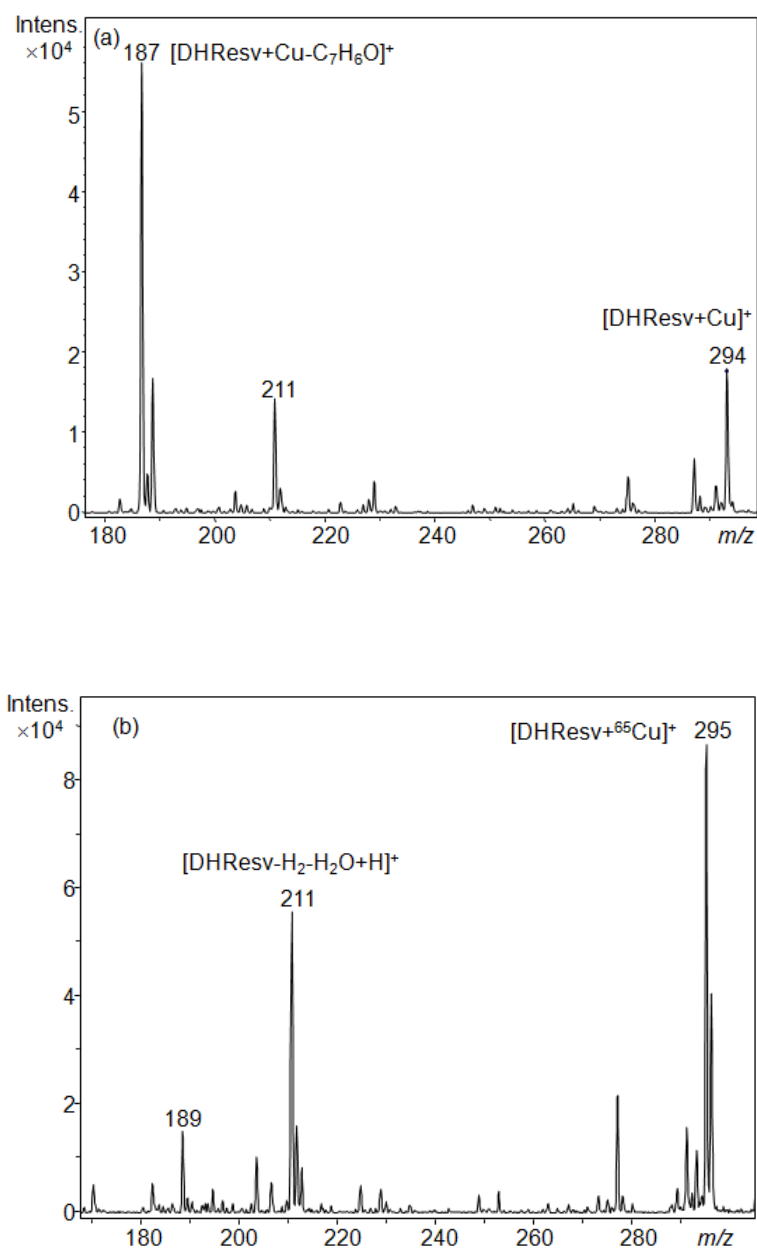


Figure 4.8 – MS/MS experiment on : (a) m/z 294 ± 2 , corresponding to the selection of the whole cluster ascribed to $[\text{DHResv+Cu}]^+$ ion, and (b) on the signal selected at m/z 295, due to the contribution of ^{65}Cu isotope.

4.1.2 Density functional theory calculations

Resveratrol was investigated by DFT calculations [17–19], however, structures of resveratrol/copper complexes have not been reported so far. For this reason we have carried out calculations at B3LYP/6-311G(d) level of theory with the aim to establish geometries for the complexes experimentally detected.

The calculated structure of the $[\text{Resv}+\text{Cu}]^+$ complex detected at m/z 291 is shown in figure 4.9. Its binding energy, calculated with respect to the energies sum the of the separated moieties (Resv and Cu^+) is 3.3 eV. Interestingly, the Cu ion binds to C(6), and not to the electronegative oxygen atoms of the resveratrol molecule. The bond C(6)-Cu (length 1.93 Å) could have been predicted by the nucleophilic trait of the C-atoms if the resonance forms are taken into account.

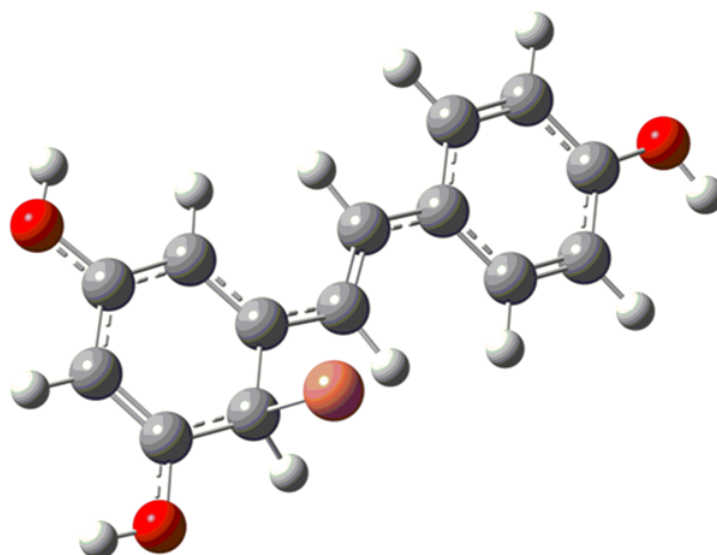


Figure 4.9 – Energy minimized structure of the $[\text{Resv}+\text{Cu}]^+$ complex at B3LYP/6-311G(d) level of theory.

It is worth noting that the preferential coordination of copper at carbon at first seems unexpected, but coordination to the aromatic ring of copper ion is consistent with metal ion coordination [106–108], and crystallographic evidences for coordination of copper ion to arenes exists [109–111]. Our results for the structures and energetic ordering of coordination of the Cu ion to the aromatic ring of resveratrol are in full agreement with previous investigations. In fact, a similar behavior was described for

[Phenol+Cu]⁺, in which case the most stable structure is that with the Cu ion bonded to the carbon atom in *para* position [112, 113].

The optimized structure of the [Resv+Cu+H₂O]⁺ ion detected at *m/z* 309 is shown in figure 4.10. Cu is bonded to C(6), with C(6)-Cu = 1.95 °A and Cu-OH₂ = 1.91 °A. The binding energy is 5.4 eV, with respect to the sum of the energies of resveratrol, Cu⁺ and H₂O.

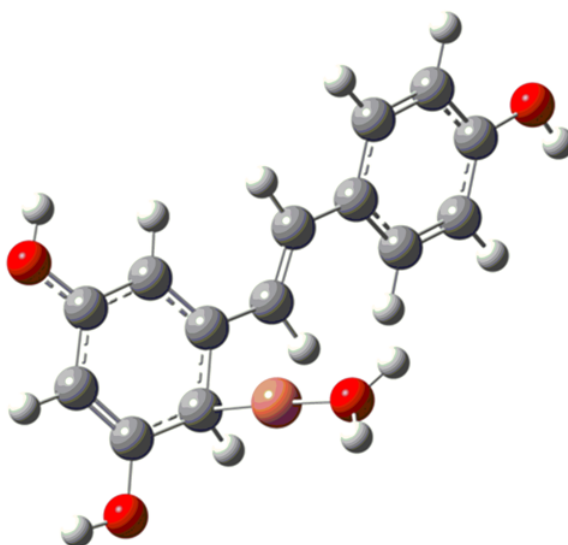


Figure 4.10 – Energy minimized structure of the [Resv+Cu+H₂O]⁺ complex at B3LYP/6-311G(d) level of theory.

The [2Resv+Cu]⁺ complex at *m/z* 519 has the structure reported in figure 4.11 and its binding energy is 5.9 eV with respect to the sum of the energy of two free resveratrol molecules and copper ion. Our results show that the Cu ion interacts with the carbon atoms of the alkenyl bond in resveratrol, which have nucleophilic features as clearly deduced by the Highest Occupied Molecular Orbitals (HOMO) map (Figure 4.12). In more details, the geometry of the complex in figure 4.11 shows a C(7)-Cu bond distance of 2.05 °A in the first resveratrol, and distances C(7)-Cu = 2.09 °A and C(8)-Cu = 2.09 °A for the second resveratrol molecule.

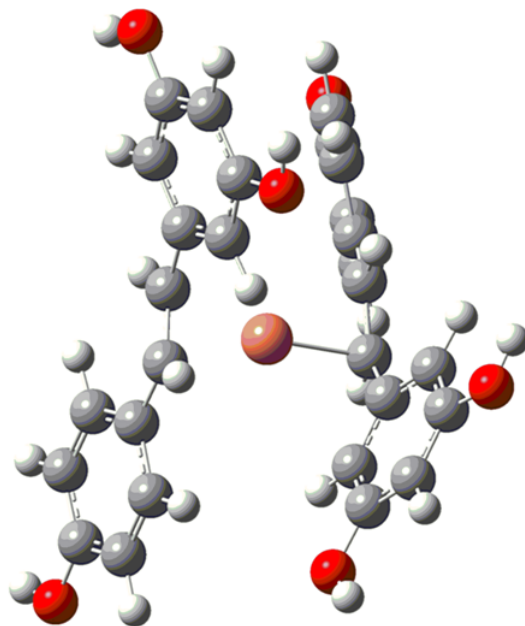


Figure 4.11 – Energy minimized structure of the [2Resv+Cu]⁺ complex at B3LYP/6-311G(d) level of theory.

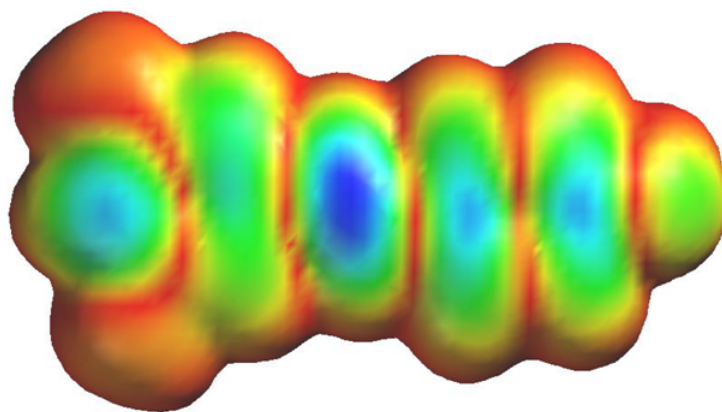


Figure 4.12 – HOMO map of resveratrol at B3LYP/6-311G(d) level of theory. Colors near blue represent large positive values of the highest-occupied molecular orbital.

In the case of dihydro-resveratrol the Cu(I) complex corresponding to m/z 293 has an intramolecular sandwich structure with distances C(2)-Cu = 2.08 Å and C(11)-Cu = 2.07 Å (Figure 4.13). This peculiar geometry arises from the lack of the double bond connecting the two rings, which allows their rotation around the single C-C bond, so that they eventually encapsulate the copper atom. The related steric

constraints might explain the non formation of 3-particle clusters, as instead observed in the case of resveratrol. The binding energy results to be 4.8 eV with respect to the sum of energies of DHResv molecule and copper ion.

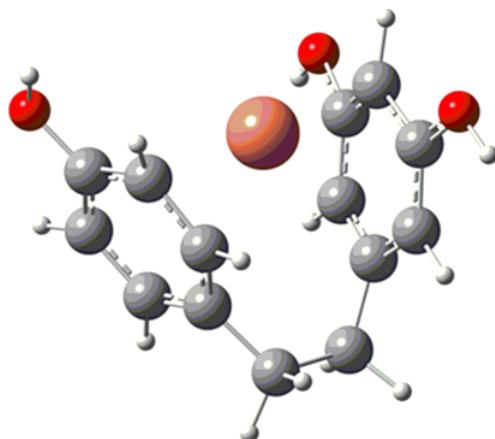


Figure 4.13 – Energy minimized structure of the $[\text{DHResv}+\text{Cu}]^+$ complex at B3LYP/6-311G(d) level of theory.

In conclusion B3LYP/6-311G(d) calculations have been carried out for the detected complexes, with the aim to establish their geometries and energies. In resveratrol/copper complex system, the most stable structures are characterized by bonds /interactions between the copper atom and the carbon atoms in the aromatic ring and/or in the alkenyl group. For dihydro-resveratrol, the geometry indicates an intramolecular sandwich structure, containing the metal ion between the two aromatic rings.

4.1.3 Infrared multiple photon dissociation spectroscopy

The technique of IRMPD spectroscopy has shown its ability to determine the structure of gaseous ions. By using this technique, structures of small biologically relevant molecules in the gas-phase were studied [114, 115]. In particular, the IRMPD spectrum of gaseous ion is related to the calculated vibrational spectrum, which can be predicted by modern computational chemistry approaches. By comparing calculated and experimental frequencies, it is possible to determine the molecular geometry of the complexes.

By using this method, the $[\text{Resv}+\text{Cu}]^+$ complex at m/z 291 is studied. Its experimental and calculated frequencies in -OH stretch region with stable isomer is shown

in figure 4.14. Our preliminary results shows that the Cu ion interacts with the carbon atoms of the alkenyl bond in resveratrol, which show nucleophilic features in agreement with result indicated by the HOMO map (Figure 4.12). This study is in progress.

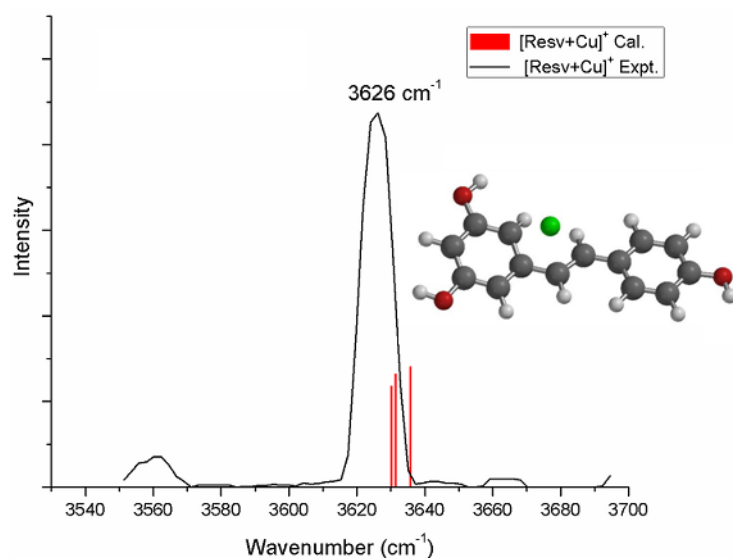


Figure 4.14 – IRMPD spectra recorded in -OH stretch range for [Resv+Cu]⁺ ion; experimental (black line) and calculated IR frequencies (red line) of most stable isomer.

4.2 Resveratrol dehydrodimer in the presence of Cu(II) ions

Later we focused our attention on the formation of dehydrodimer **3** induced by copper ions in the gas phase. MS spectra recorded in positive and negative ion modes, we observed new signals corresponding to the pseudomolecular ion of dehydrodimer **3** (Figure 3.5).

In particular, ESI (+) MS spectrum recorded for resveratrol and copper(II)sulfate in acetonitrile/water (1:1) solution (Figure 4.15(a)) shows [M+H]⁺ ion of resveratrol at m/z 229, signals related to the described three Cu(I) complexes, and an intense peak at m/z 455 [116]. The latter one can be assigned to [M+H]⁺ ion, where M is for dehydrodimer **3**. MS/MS experiments on this ion gave intense signals at m/z 437 and m/z 361, corresponding to the loss of water and phenol respectively (Figure 4.15 (b)).

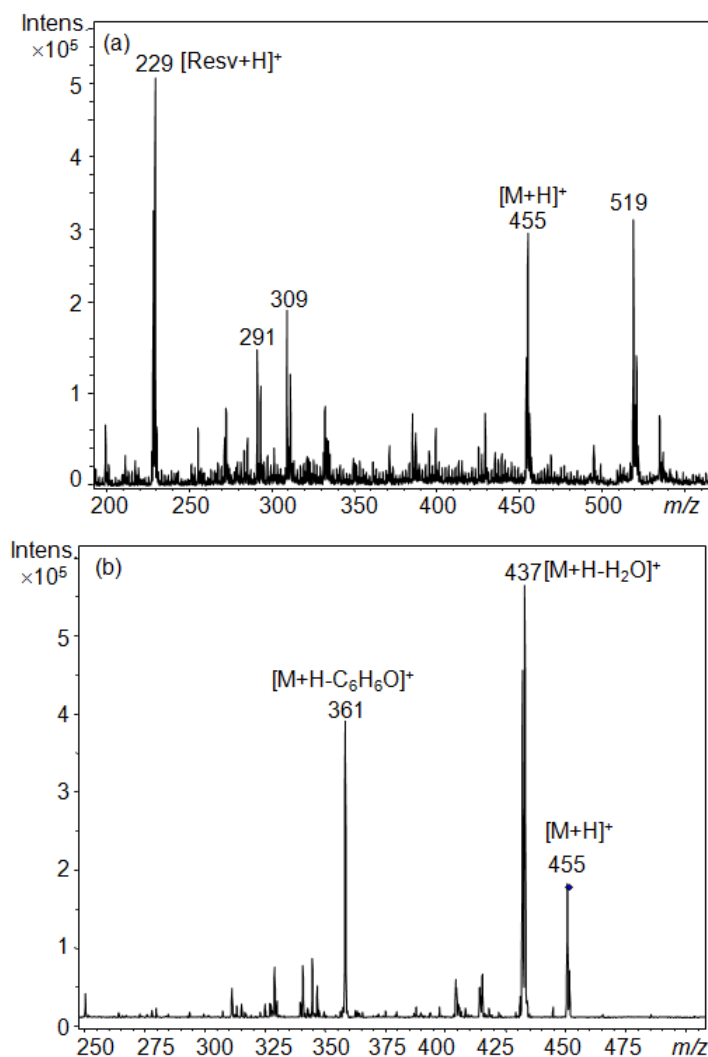


Figure 4.15 – (a) ESI(+)MS spectrum obtained by injection of a 1:1 resveratrol/ CuSO_4 solution in $\text{CH}_3\text{CN}/\text{H}_2\text{O}$ (1:1); (b) MS/MS spectrum on $[\text{M}+\text{H}]^+$ ion at m/z 455; M is for the dehydrodimer **3**.

MS^3 experiments performed on ion at m/z 361 produced diagnostic fragments: at m/z 343, due to the loss of a water molecule; at m/z 251 corresponding to the loss of resorcinol (hydroxy phenol) moiety ($\text{C}_6\text{H}_6\text{O}_2$); and an intense signal at m/z 237 corresponding to $[\text{M}-\text{C}_7\text{H}_8\text{O}_2]^+$. Similarly, MS^3 experiments on ion at m/z 437, produced fragments: at m/z 419 due to loss of a water molecule; m/z 343 due to the loss of a phenol; m/z 327 corresponding to the loss of resorcinol moiety, and at m/z 313 due to the loss of $\text{C}_7\text{H}_8\text{O}_2$ group. These results indicate the presence of two resorcinol units in the structure of compound corresponding to m/z 455, in agreement with dehydrodimer **3**. This is also in line with the involvement of the *para* OH group in the formation of **3**, as reported in the biological mechanism (Figure 1.4) [21].

In ESI-MS spectrum recorded in the negative ion mode there is no evidence for resveratrol-copper complexes, but it shows the presence of $[\text{Resv-H}]^-$ ion at m/z 227, and the pseudomolecular ion at m/z 453 for product **3** (Figure 4.16(a)). In particular, the negative ion mode resulted the best condition for analysis of this compound, due to the easy loss of proton from a OH group in phenol, known to have acidic property. MS/MS on m/z 453 produced peaks: at m/z 435 due to the loss of water; at m/z 359 due to the loss of a phenol; at m/z 347 due to the loss of 4-methylenecyclohexa-2,5-dienone ($\text{C}_7\text{H}_6\text{O}$); at m/z 333 corresponding to $[\text{M-H-C}_7\text{H}_6\text{O}_2]^-$; at m/z 411 and m/z 369 related to the loss of one or two $\text{C}_2\text{H}_2\text{O}$ groups respectively (Figure 4.16 (b)).

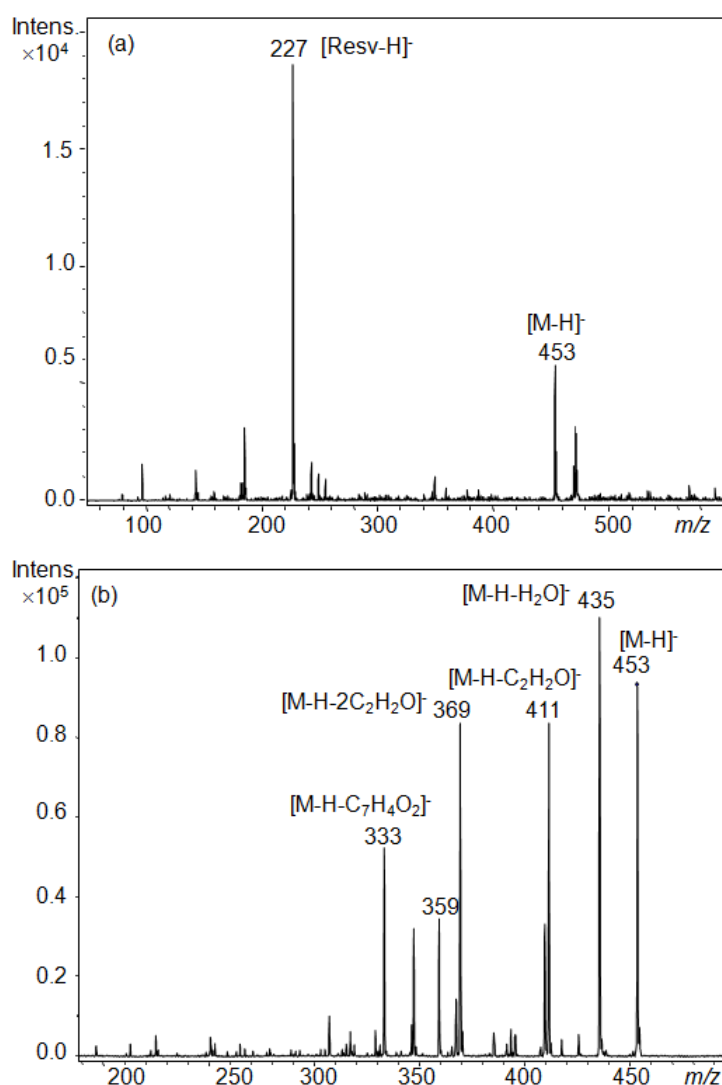


Figure 4.16 – (a) ESI(-)MS spectrum obtained by injection of a 1:1 resveratrol/ CuSO_4 solution in $\text{CH}_3\text{CN}/\text{H}_2\text{O}$ (1:1); (b) MS/MS spectrum on $[\text{M-H}]^-$ ion at m/z 453, M is for the dehydrodimer **3**.

MS³ experiments performed on ion at m/z 369 produced intense signals at m/z 285, 327 corresponding to the loss of one and two C₂H₂O, respectively (Figure 4.17). In addition, MS³ experiments on ion at m/z 411 give an intense fragments at m/z 393 and 367 due to the loss of water and CO₂ molecules, respectively.

Negative ion mode MS/MS experiments on m/z 227 corresponding to [Resv-H]⁻ gave ions at m/z 185 and 143, due to the loss of one and two C₂H₂O moieties, in line with the fragment data reported by Stella *et al.* [117]. Hence, one could conclude that fragment ion C₂H₂O is also obtained from the resorcinol ring in structure **3**, as already proposed for the identification of isomeric resveratrol dimers isolated from wine grapes by HPLC/MSⁿ analysis [118].

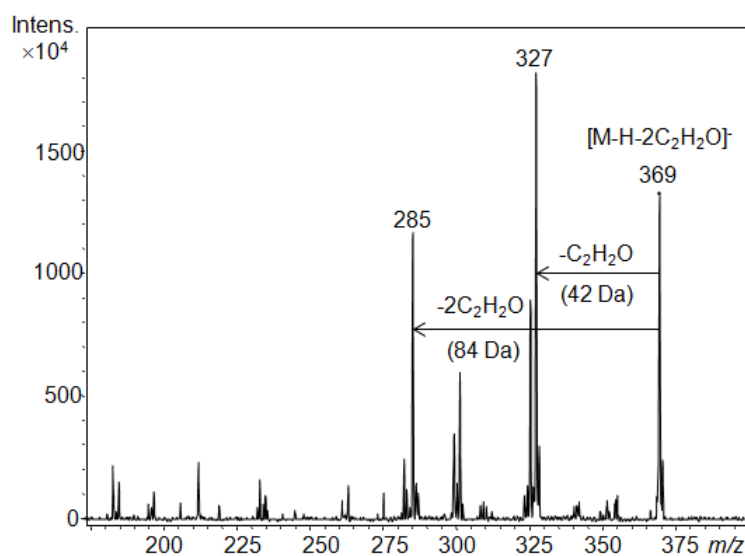


Figure 4.17 – MS³ experiment on the signal selected at m/z 369. M is for dehydrodimer **3**.

In order to summarize MS data obtained for dehydrodimer **3**, a scheme of fragmentation pathway is reported in figure 4.18, in agreement with reported data [118].

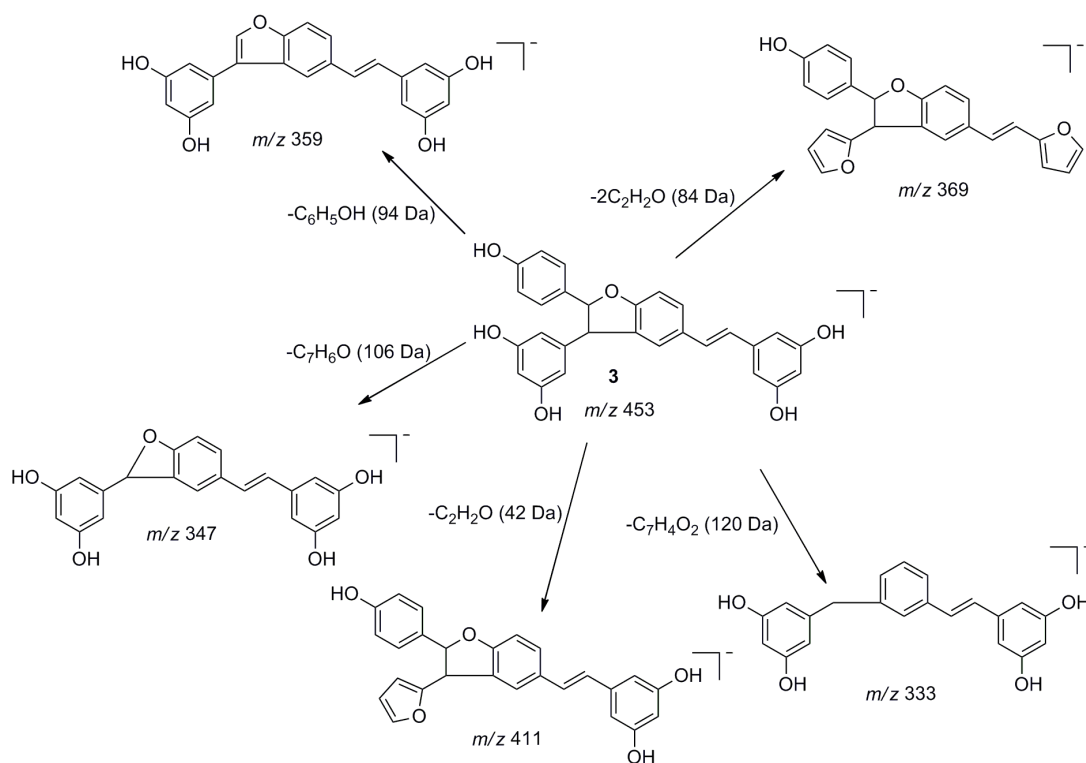


Figure 4.18 – Fragmentation pathway proposed for $[M-H]^-$ ion at m/z 453 of dehydrodimer **3**.

As a confirm of dehydrodimer **3** structure, this compound was synthesized by reaction of resveratrol with copper(II)sulfate (Section 3.5.1), characterized by NMR analysis, and these data compared with the ones previously reported [21].

In figure 4.19 $^1\text{H-NMR}$ spectrum recorded in acetone- d_6 for dehydrodimer **3** is given. In details: i) the two doublets at 6.94 and 7.05 ppm, with coupling constant $J = 16.4$ Hz are assigned to olefinic protons H-7' and H-8' respectively and the corresponding constant $J = 16.4$ Hz supports their *trans* position ii) two doublets at 4.45 and 5.44 ppm, $J = 8.0$ Hz for the aliphatic protons H-7 and H-8, respectively. These results are in agreement with those previously reported by Nicotra *et al.* [89]

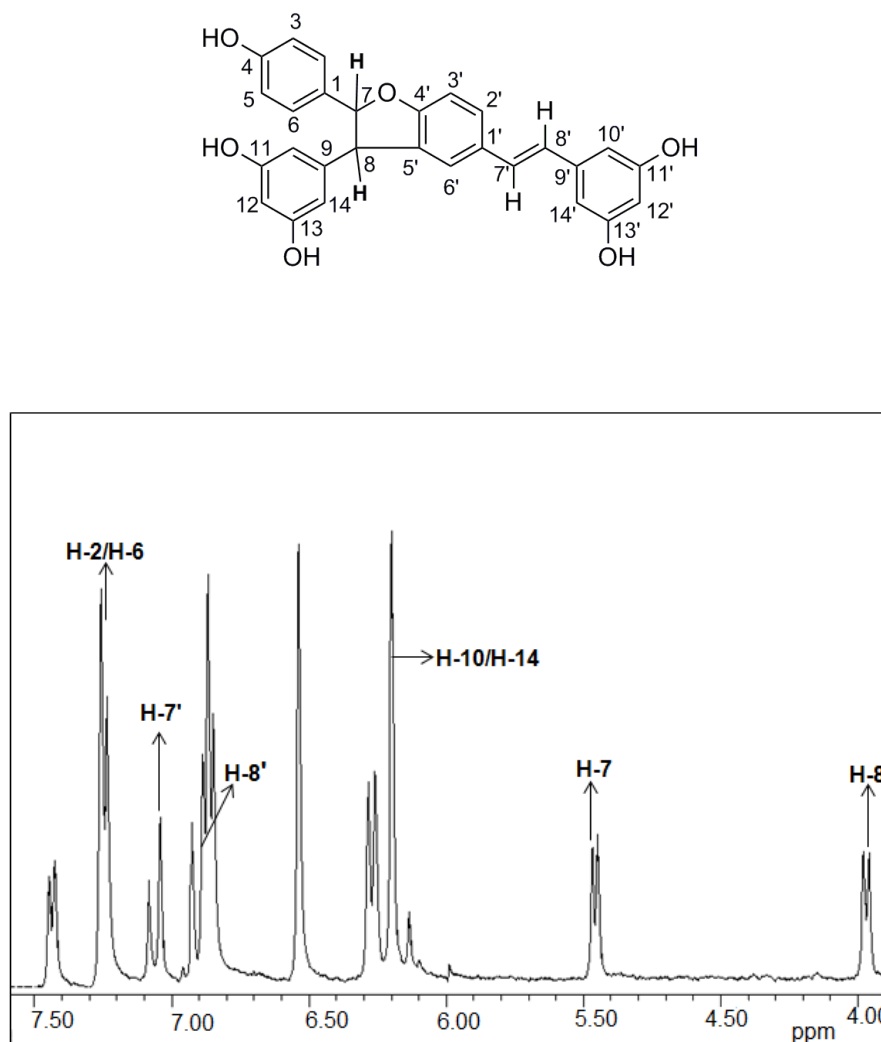


Figure 4.19 – Chemical structure of dehydrodimer **3** with indication of numbering adopted for ¹H NMR assignment (above) and ¹H NMR spectrum, recorded in acetone-d₆, for dehydrodimer **3** in spectral range 7.5:4.5 ppm (below).

Additional structure assignments came from long range ¹H, ¹³C correlations by Heteronuclear Multiple Bond Correlation (HMBC) experiments. In details, we observed i) the magnetically equivalent H-2/H-6 protons as multiplet with $J = 8$ Hz at 7.24 ppm showed correlation with C-7 at 94.72 ppm, ii) H-10/H-14 protons as singlet $J = 2.2$ Hz at 6.20 ppm correlate with C-8 at 58.52 ppm. iii) the weak correlation between proton H-7 at 5.45 ppm with C-4' at 161.3 ppm (Figure 4.20). These corre-

lations allowed us to establish that aromatic ring with *para*-OH (phenol) is linked to C-7 and with two *meta*-OH (resorcinol) is linked to C-8. Furthermore, the HMBC data was found to be in agreement with the reported data. [34]

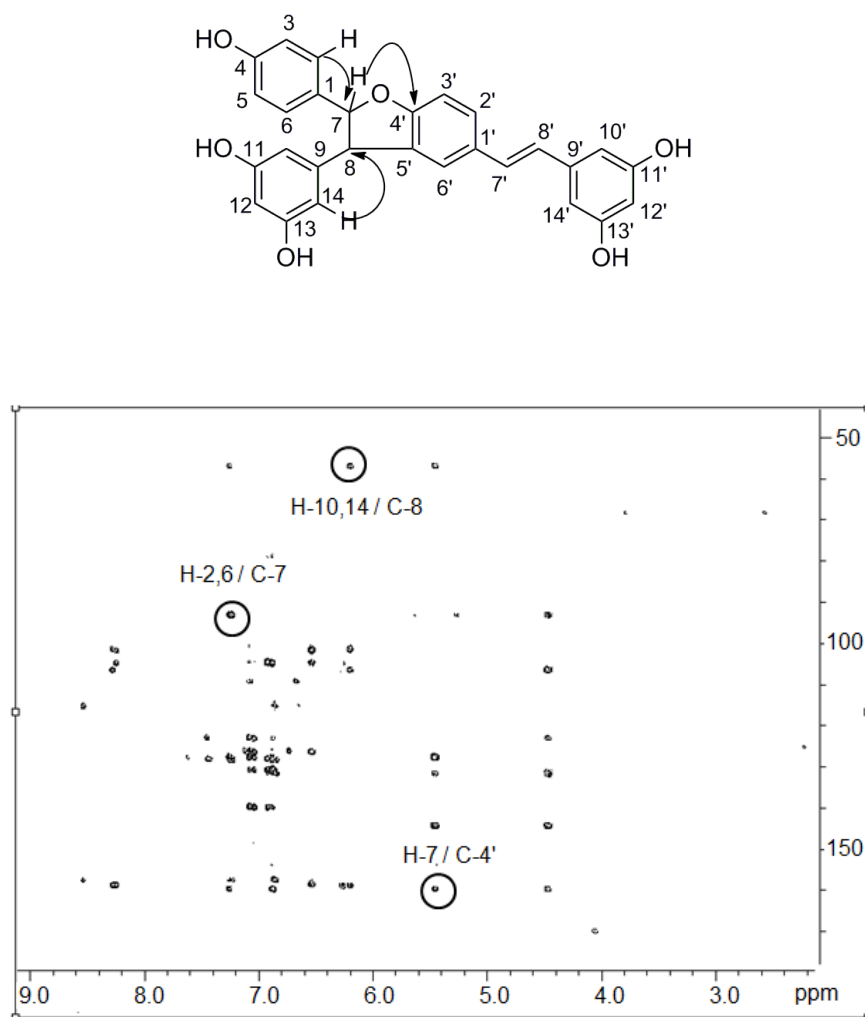


Figure 4.20 – Significant ^1H , ^{13}C long range correlations by HMBC experiments of synthetic dehydrodimer **3**, recorded in acetone- d_6 .

The synthetic dehydrodimer established to have structure **3** by NMR analysis, it was analyzed by MS analysis in order to compare its spectrum with that obtained for the dehydrodimer produced directly in MS experiments starting from the injection of a resveratrol/copper(II)sulfate solution.

Mass spectrum carried out in negative ion mode for the synthetic product indicated a pseudomolecular ion at m/z 453. MS/MS spectra showed the same fragmentation as in the case of the dehydrodimer detected (Figure 4.16(b)) after injection of resveratrol with copper(II)sulfate solution. From all above observations, we could conclude that the product formed in the ESI-MS of a resveratrol/copper(II)sulfate solution is likely to own the structure dehydrodimer **3** [119].

4.2.1 MS analysis under different instrumental conditions

ESI and APCI ionization techniques (Section 2.2.1 and 2.2.2) have different ranges of applicability in terms of polarity and molecular mass of the analytes. ESI is a soft method of ionization and it is the best ionization technique for complexes where metal ions are bound through coordinate bonding (weak interaction) to protein and biomolecules. For such a reason we choose to study the interaction of resveratrol (and its analogues) with metal ions by ESI-MS analysis.

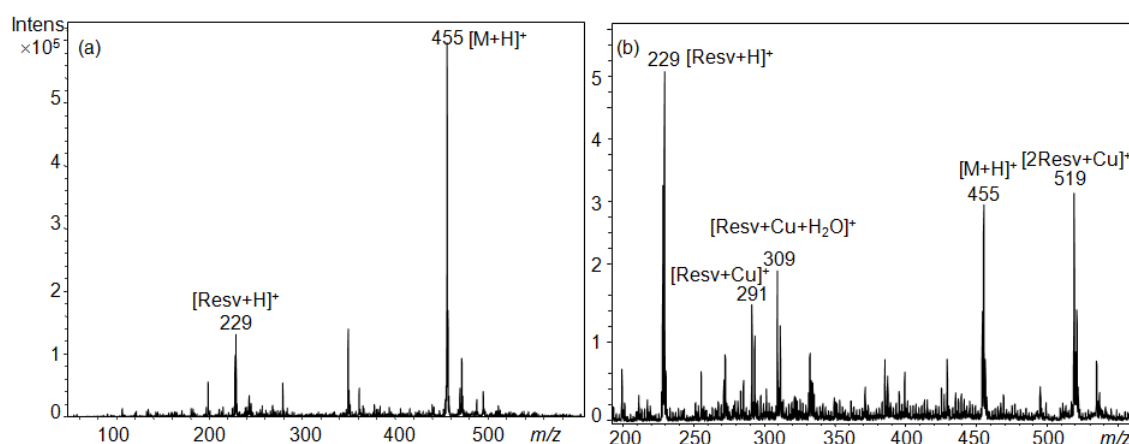


Figure 4.21 – APCI(+) (left) and ESI(+) (right) mass spectrum obtained by injection of a 1:1 resveratrol/CuSO₄ solution in CH₃CN/H₂O (1:1).

Positive ion APCI (Figure 4.21(a)) and ESI (Figure 4.21(b)) spectra show signals for the pseudomolecular ion of resveratrol and the corresponding oxidative product, the dehydrodimer (Figure 4.21(M)). The measured limit of detection indicates that

ESI is significantly more efficient than APCI in the positive ion mode for the compounds studied. On the other hand, MS/MS was found to be less sensitive, but more reliable and simple than MS due to the absence of chemical noise.

4.2.2 Time dependent formation

An interesting aspect to be investigated is to verify if dehydrodimer **3** formation occurs in solution before injection, or in gas phase after injection.

It is difficult and it was not possible to set up a technical system able to verify it. By carrying out the laboratory reaction of resveratrol/copper(II)sulfate and monitoring the conversion to product **3** by thin layer chromatography (TLC) and ^1H NMR analysis, it was evident that the kinetics of the reaction was not so fast, occurring in hours (a good yield of product **3** was obtained after 24 hours). This evidence mainly to the formation of **3** in gas phase, but it resulted difficult to be investigated more deeply with our ESI-MS device.

ESI(+)-MS analysis was performed by injection of resveratrol/copper(II)sulfate solution at different time monitoring spectra every 15 minutes. We observed and evaluated: i) the decreasing intensity of $[\text{M}+\text{H}]^+$ peak at m/z 229 for resveratrol. ii) the corresponding formation of metal complexes $[\text{Resv}+\text{Cu}]^+$ at m/z 291, $[\text{Resv}+\text{Cu}+\text{H}_2\text{O}]^+$ at m/z 309, and $[2\text{Resv}+\text{Cu}]^+$ at m/z 519, iii) the relative intensity at different time of dehydrodimer **3** and the copper-complexes (Figure 4.22).

In general these time dependent experiments indicate: i) decreasing of resveratrol concentration, ii) $[2\text{Resv}+\text{Cu}]^+$ as the most intense complex, iii) all the Cu-complexes decrease their intensity in corresponding to an increasing concentration of dehydrodimer **3**, at least until 33 minutes after the mixing of resveratrol and copper sulfate solution.

In negative ion mode detection, we have followed the slowly decreasing of intensity of m/z 227 for $[\text{M}-\text{H}]^-$ ion of resveratrol and the formation of the peak at m/z 453 for $[\text{M}-\text{H}]^-$ of dehydrodimer **3**, whereas metal complex were not detected (Figure 4.23).

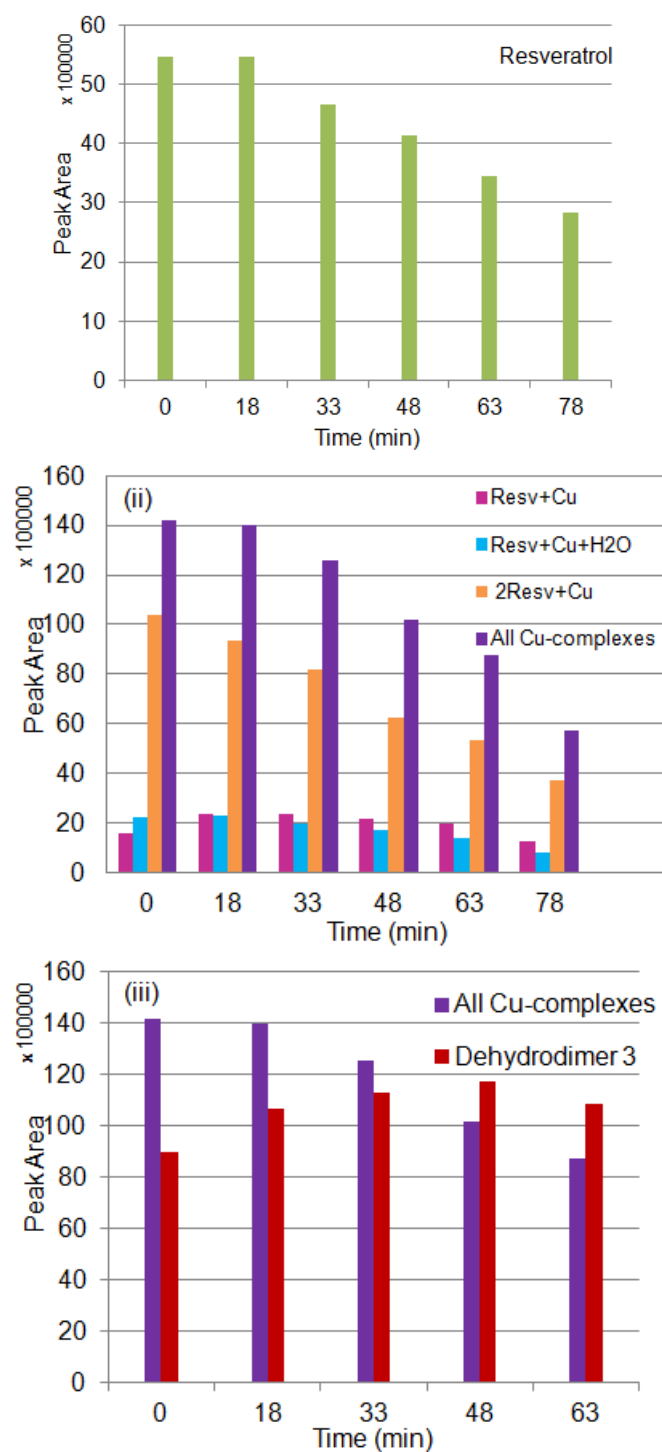


Figure 4.22 – Abundance of i) resveratrol, ii) resveratrol-copper complexes and iii) dehydrodimer **3** and all Cu-complexes by ESI(+)-MS spectra recorded in time range by injection of 1:1 resveratrol/CuSO₄ solution in CH₃CN/H₂O (1:1).

4.2: Resveratrol dehydrodimer in the presence of Cu(II) ions

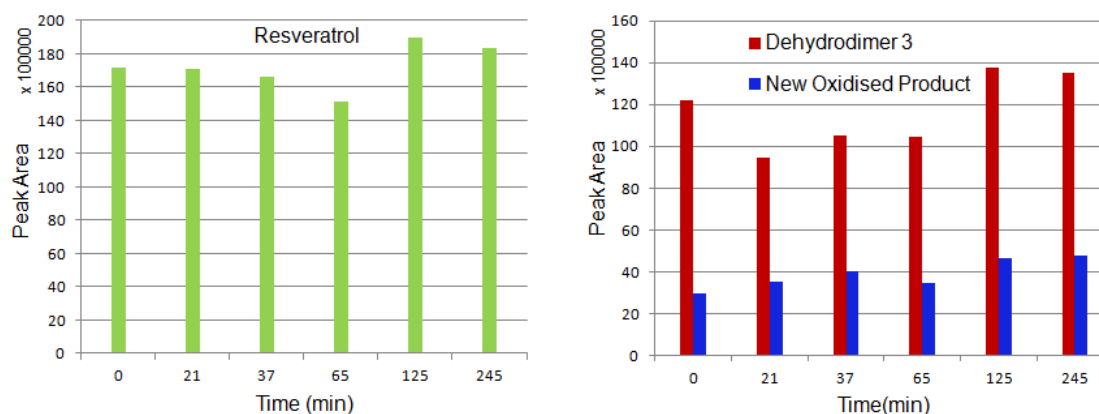


Figure 4.23 – Abundance of resveratrol and oxidation products by ESI(-)-MS spectra recorded in time range by injection of 1:1 resveratrol/CuSO₄ solution in CH₃CN/H₂O (1:1).

We obtained small difference, but practically the same behaviors by considering the dehydrodimer **3**/resveratrol ratio over by chromatography and mass analysis (Figure 4.24).

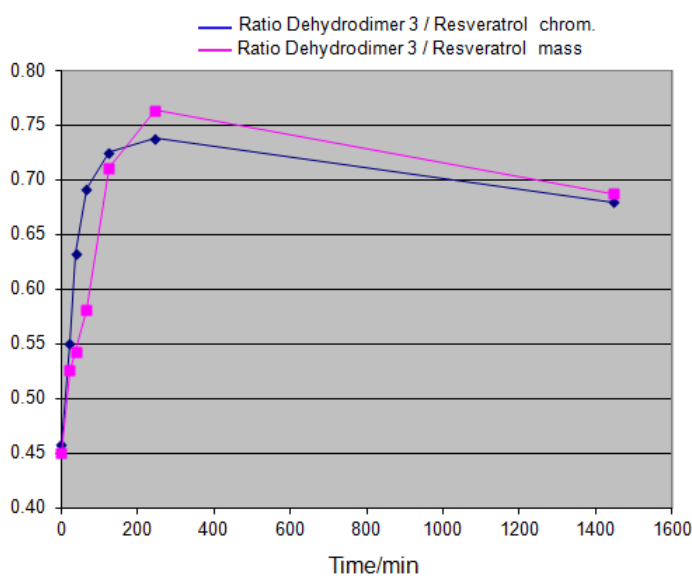


Figure 4.24 – ESI(-)-MS chromatography comparison spectra obtained by injection of 1:1 resveratrol /CuSO₄ solution in CH₃CN/H₂O (1:1).

In this MS study as a function of time the main evidence is the increasing formation of the signal at m/z 471, having an intensity which becomes constant after about 2h (Figure 4.25).

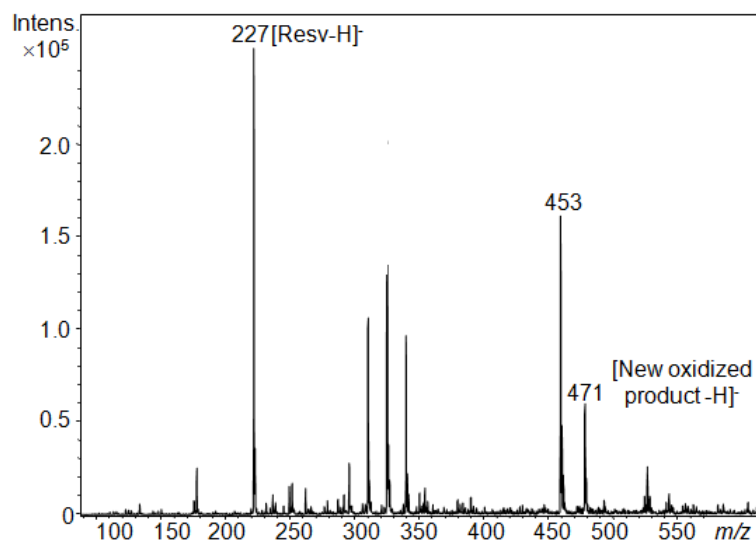


Figure 4.25 – ESI(-)-MS spectrum showing the signal at m/z 471 obtained by injection of 1:1 resveratrol/ CuSO_4 solution in $\text{CH}_3\text{CN}/\text{H}_2\text{O}$ (1:1) after 125 minutes from the mixing of the solution.

MS/MS experiments on m/z 471 show the fragment ion at m/z 377 attributable to the loss of a phenolic group $[\text{M}-\text{H}-\text{C}_6\text{H}_6\text{O}]^-$, the ion at m/z 349 corresponding to the $[\text{M}-\text{H}-\text{C}_6\text{H}_6\text{O}-\text{CO}]^-$ ion and the most abundant peak at m/z 255 corresponding to $[\text{M}-\text{H}-\text{C}_6\text{H}_6\text{O}-\text{CO}-\text{C}_6\text{H}_6\text{O}]^-$ ion (Figure 4.26).

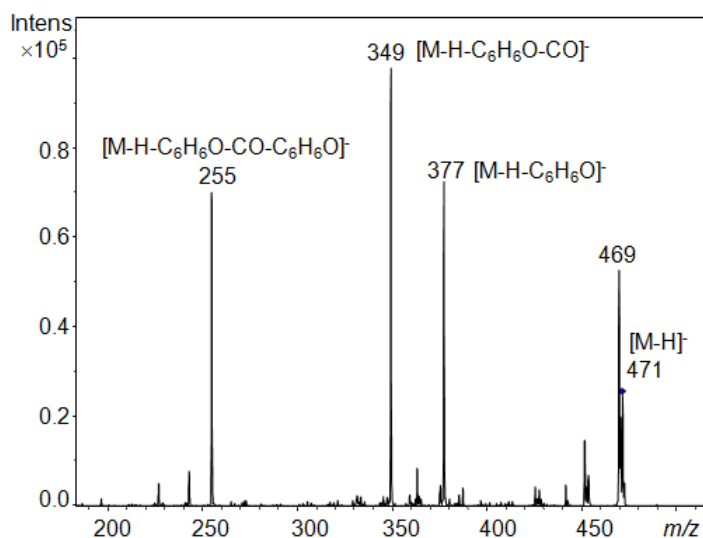


Figure 4.26 – ESI(-) MS/MS spectrum on $[\text{M}-\text{H}]^-$ ion at m/z 471, obtained by injection of 1:1 resveratrol/ CuSO_4 solution in $\text{CH}_3\text{CN}/\text{H}_2\text{O}$ (1:1) after 125 minutes from the mixing; M is for the new oxidized product.

Regarding the structure of this product, the fragmentation pattern is in agreement with data reported by J. Denis and co-workers for the natural products called viniferenol by isolation from cell cultures of *Vitis vinifera* [120,121]. We can conclude that product corresponding to m/z 471 is one of the two possible diastereoisomers of the natural retrisols A or B (Figure 4.27).

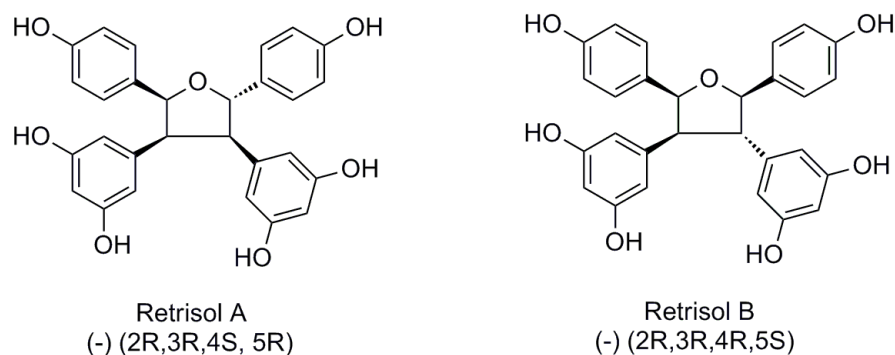


Figure 4.27 – Chemical structure of the natural products retrisols A and B.

In conclusion, in negative ion mode an addition oxidative product was detected, with the planar structure as retrisols or a regioisomer of them. Its formation increased when resveratrol/ CuSO_4 solution was injected after some minutes or 1h later, after the preparation of the solution.

4.2.3 In the presence of laccase enzyme

Laccase is an oxidoreductase enzyme containing four copper ions (Figure 4.28), all of them being involved in redox processes *via* a radical cyclic mechanism [122]. Laccase is widely distributed in fungi and in higher plants, which are able to catalyze the oxidation of various phenolic compounds at the expense of molecular oxygen. Further, it shows an exceptional substrate versatility and therefore is a potentially suitable biocatalyst for the mild oxidation of several organic compounds [123,124]. This enzyme was used to oxidize phenolic derivatives, such as estradiol and penicillin to give dimers and higher oligomers [125]. However, the main disadvantage of these transformations is the extensive polymerization in the oxidation process, with production of complex mixtures of poly-phenolic oligomers.

When used to catalyze the oxidation of resveratrol, laccase has been provided very selective giving quite pure optically active dehydrodimer **3** [89]. We decided to investigate by ESI-MS analysis a resveratrol solution in buffered ethyl acetate in the

presence of laccase. The same results were obtained by MS/MS experiments on $[M-H]^-$ ion at m/z 453 for the product formed by injection of the previously described solution and by the dehydrodimer **3** purified by the bench reaction. The latter one was analyzed also by NMR analysis confirming its structure. It is noteworthy that this dehydrodimer **3**, presents the stereogenic centers at C-7 and C-8 positions, so that when produced in the laccase catalyzed reaction is formed as optically active (Section 3.5.1), as expected in the case of the involvement of a chiral catalyst.

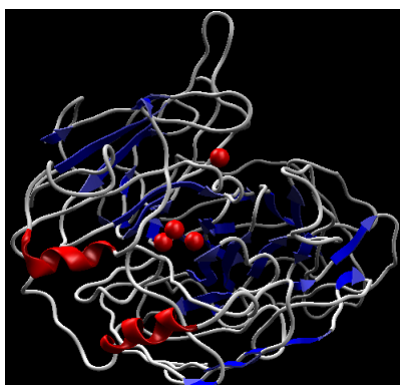


Figure 4.28 – Crystal structure of laccase from *Trametes versicolor*, as reported in Protein Data Bank (PDB ID 3KW7) Four Cu ions present in the active site are indicated in red.

Bi-dimensional Nuclear Overhauser Effect (NOESY) indicated no correlation between H-7 and H-8, supporting the *trans* position of H-7/H-8. By comparing the negative value of optical activity observed for the laccase catalyzed reaction (Section 3.5.1) with the negative optical activity of the natural (-)(7S,8S)- δ -viniferin, we can conclude that enzyme oxidation produces the same natural isomer [89].

In conclusion MS results show that the same dehydrodimer **3** is formed both with copper(II)sulfate and laccase catalyzed reactions.

4.3 Resveratrol dehydrodimer in the presence of Fe(III) ions

By replacing Cu(II) with Fe(III) ions in resveratrol solution, we detected the spectrum reported in figure 4.29. Differently from the copper case, ESI(+)-MS analysis produced a more intense ion at m/z 228 attributable to the radical cation, together with the protonated resveratrol at m/z 229 (Figure 4.29). The spectrum show also a peak

at m/z 455. The formation of the radical cation in ESI-MS is in line with previously reported data [126,127]. MS/MS experiments on this ion produced intense fragments at m/z 437 and m/z 361, as in the case of copper(II)sulfate and a new minor fragment at m/z 349, attributable to the loss of 4-methylenecyclohexa-2,5-dienone. Another peculiarity of the iron system is that no metal complexes could be detected. This is in line with previous report on the inability of resveratrol to chelate Fe (III) or Fe (II) ions [128,129].

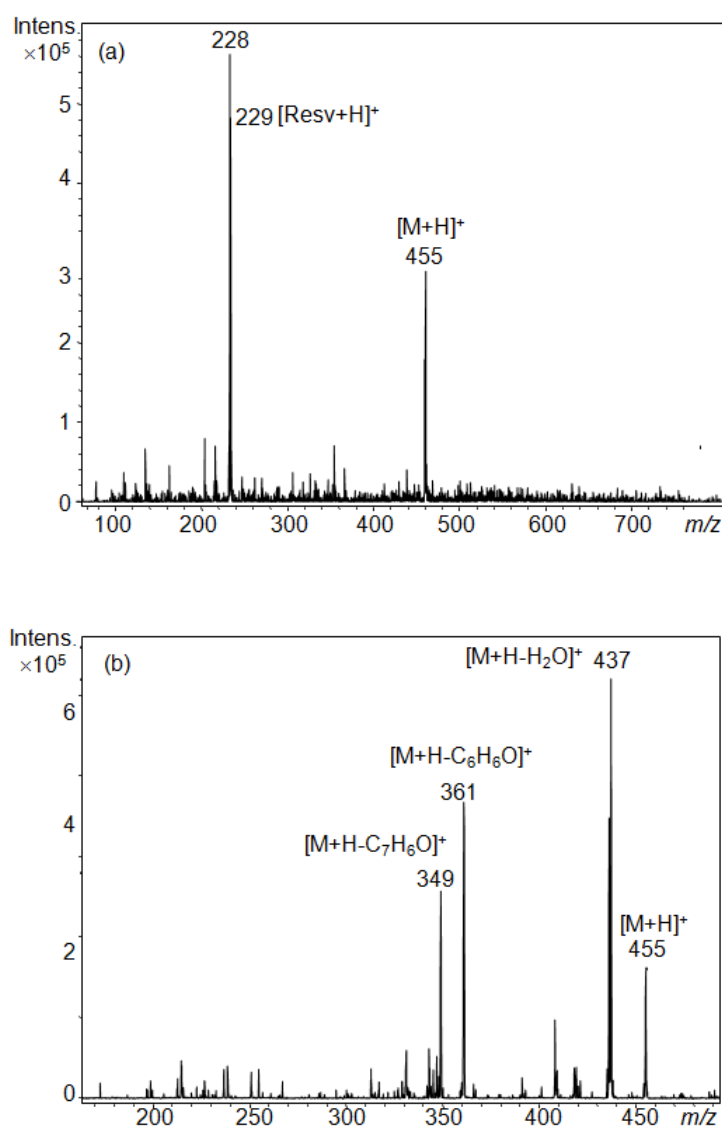


Figure 4.29 – (a) ESI(+)-MS spectrum obtained by injection of a 1:1 resveratrol/FeCl₃ solution in CH₃CN/H₂O (1:1) ; (b) MS/MS spectrum on [M+H]⁺ ion at m/z 455, M is for a dehydrodimer.

MS³ experiments performed on fragment ion at m/z 361 produced intense signals at m/z 343, 251 and 237, as in the case of copper(II)sulfate; and a new intense fragment appears at m/z 267, corresponding to the loss of a phenol molecule (C₆H₆O). In addition, MS³ experiments on fragment ion at m/z 349 (Figure 4.30), produced more intense signals at m/z 255, attributable to the loss of a phenol and m/z 239 due to the loss of a resorcinol moiety (C₆H₆O₂). Based on these findings, we conclude that the dehydrodimer structure formed in the presence of Fe(III) ions is different from the dehydrodimer **3**.

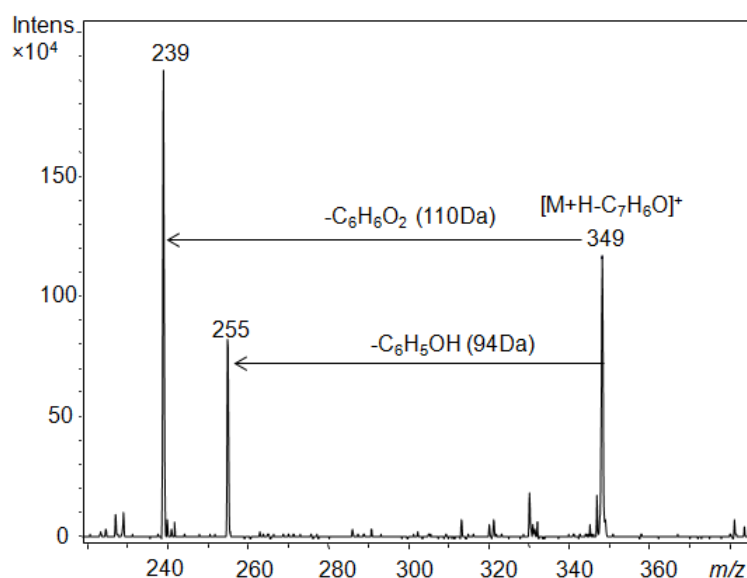


Figure 4.30 – MS³ experiment on the signal selected at m/z 349. M is for a dehydrodimer.

The negative ion mode ESI-MS spectrum showed the expected peaks at m/z 227 for resveratrol, and at m/z 453 for the dehydrodimer. MS/MS experiments on the latter ion produced the same fragments as for the copper(II)sulfate case, but the signal at m/z 359 is the most intense (Figure 4.31), whereas it was a minor fragment in the MS analysis of resveratrol/copper(II)sulfate (Figure 4.16)

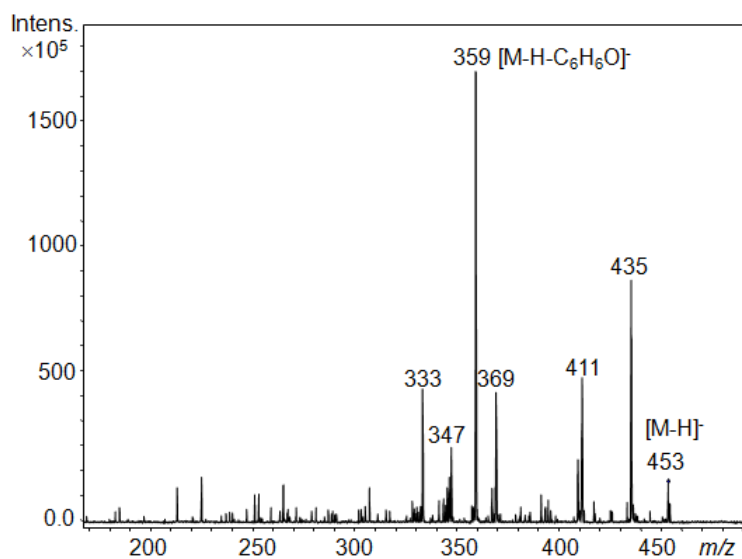


Figure 4.31 – ESI (-) MS/MS spectrum by fragmentation experiment on the ion at m/z 453, obtained by injection of 1:1 resveratrol/ FeCl_3 solution in $\text{CH}_3\text{CN}/\text{H}_2\text{O}$ (1:1); M is for the dehydrodimer.

MS^3 experiments performed on ion at m/z 359 (Figure 4.32) gave fragment signals at m/z 265, corresponding to the neutral loss of a phenol molecule. Interestingly, only a dehydrodimer different from **3** can lose two phenolic groups and produce the signal at m/z 265, as evident by comparison of the spectra reported in figures 4.32 and 4.17.

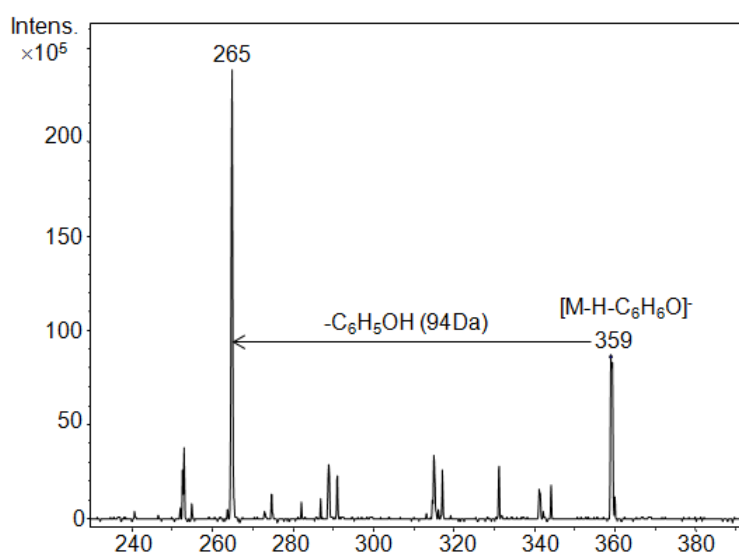


Figure 4.32 – MS^3 experiment on the signal selected at m/z 359. M is for dehydrodimer.

For assigning the structure of the dehydrodimer produced in presence of iron ions, this product was synthesized by bench reaction of resveratrol with FeCl_3 (Section 3.5.1), and characterized by NMR analysis, comparing the data with the one previously reported [91].

As expected, ^1H NMR spectrum was different from the dehydrodimer **3**. In details, it showed : i) the presence of two doublets at 6.73 and 6.94 ppm with common coupling constant $J = 16.2$ Hz, to be assigned to the two olefinic protons in *trans* position. ii) two coupled aliphatic protons at 4.46 and 5.44 ppm with the coupling constant $J = 5.1$ Hz.

Mass measurements carried out in negative ion mode for this synthetic dehydrodimer showed a signal at m/z 453, whose MS/MS spectra corresponded to the product formed in the gas phase in MS study of resveratrol/ FeCl_3 solution. All these data support the structure **4** for this dehydrodimer (Figure 4.33).

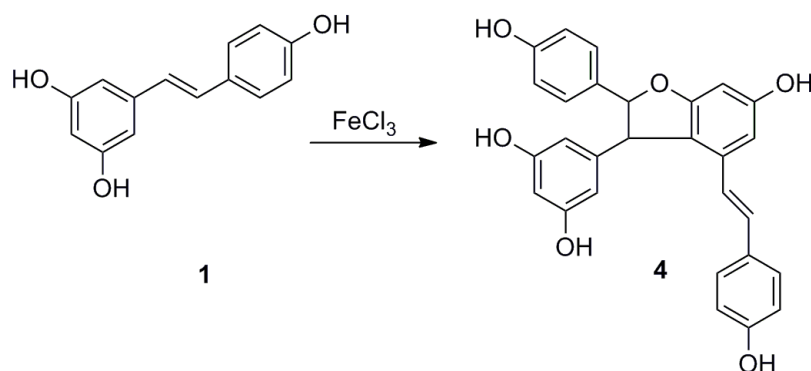


Figure 4.33 – Structure of the dehydrodimer **4** obtained from resveratrol in the presence of FeCl_3 .

It is noteworthy that dehydrodimers **3** and **4** obtained in our experiments in racemic form, have planar structure as for natural δ -viniferin [130] ((-), with 7S,8S, absolute configuration) and ϵ -viniferin [131] with ((-), with 7R,8R configuration and also as (+) enantiomer [92]), isolated from grapevine leaves (Figure 4.34).

In order to confirm the structure of dehydrodimers **3** and **4**, MS/MS data of these products were compared with those obtained from natural δ -viniferin and ϵ -viniferin [132]. In particular, negative ion mode fragmentation spectra for δ -viniferin and ϵ -viniferin are shown in figure 4.35. The results are in agreement with the fragments obtained in our MS study for dehydrodimer **3** (Figure 4.16 (b)) and dehydrodimer **4** (Figure 4.31).

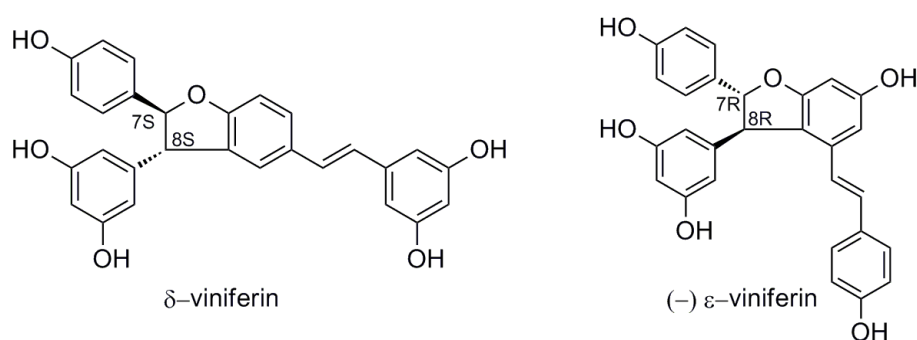


Figure 4.34 – Natural δ -viniferin (left) and $(-)\epsilon$ -viniferin (right) with indication of absolute configuration.

It is worth noting that both these molecules show two fragment ions at m/z 369 and 359, but their relative abundances are strongly different. It has been previously observed that the ion at m/z 359 can be related to the loss of a phenolic group typical for both viniferins, but as the most abundant in MS/MS spectrum of ϵ -viniferin. In particular, the origin of the fragment ions at m/z 369, more abundant in the MS/MS spectrum of δ -viniferin has been verified [132].

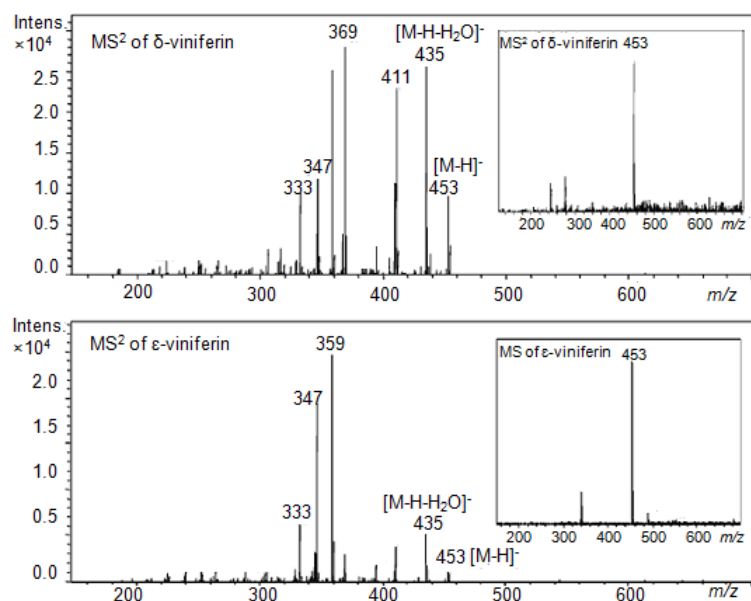


Figure 4.35 – Mass spectra from fragmentation experiments of natural δ -viniferin and ϵ -viniferin obtained by HPLC-MS of *P.viticola* [132].

4.3.1 Metal ion induced selectivity

Our studies established that dehydrodimer **3** is the oxidative product of resveratrol in the presence of copper(II)sulfate, whereas the isomeric dehydrodimer **4** is selectively obtained replacing Cu(II) with Fe(III) ions. An explanation for this selectivity can be found by applying Hard and Soft Acids and Bases (HSAB) theory.

This theory is a qualitative concept to describe the stability of metal complexes and the mechanisms of reactions where they are involved [25]. It has been also used to help in understanding the predominant factors which derive chemical properties and reactions. In general “Hard” is atomic centers of small ionic radius, net positive charge, low electron affinity, high energy LUMO and are strongly solvated, and “Soft” is large radius, has low positive charge, electron pairs in their valence shells, easy to polarize and oxidize and low energy LUMO [133]. According to theory, a soft acid reacts with a soft base and a hard acid with hard base. It is especially used in transition metal chemistry, where experiments have been done to determine the coordination of ligands and transition metal ions in terms of their hardness and softness.

According to Pearson HSAB theory, we can say that in the system under investigation Fe and Cu ions have different behaviors, in particular Fe(III) is classified as hard acid, Cu(I) as soft acid, and Cu(II) has a borderline effect [134].

The properties of metal ion would affect the electronic distribution over the resveratrol molecule and orientation of the reacting species. Copper (I) ion is a soft acid and prefers to coordinate with soft base, because orbitals involved are close in energy, a condition which allows the maximum overlap for a covalent bonding [135]. It has previously outlined that the observed complexes are coordinated with the olefinic bridge of resveratrol (Section 4.1.2), which acts as a soft base [136]. As a result, it tends to form stable quinone methide radical, which eventually gives the dehydrodimer **3** [24].

In contrast, Fe(III) ion is a hard acid and so prefers to coordinate with hard base largely by electrostatic interactions [137]. Hard acids and bases have the HOMO of the base and the LUMO of the acid far apart in energy. This leads to a more *ionic* bond with low overlap. Also, the smaller the ion or molecule, the harder it is, because the charges can get closer in the *ionic* bond. In our system, it was considered that Fe(III) ion coordinated with oxygen atoms of the phenolic groups, giving the formation of dehydrodimer **4**.

4.4 Theoretical investigation of dehydrodimer formation

In order to gain insights on the formation of the dehydrodimers, DFT calculations on the formation of the phenoxide radicals from resveratrol, and their dimerization have been carried out in collaboration with Prof. Nazzareno Re. We first considered the formation of the two possible phenoxide radicals originating from the oxidation of the corresponding deprotonated resveratrol anions on the oxygen atom in the 4' or 3 position, respectively (Figure 4.36).

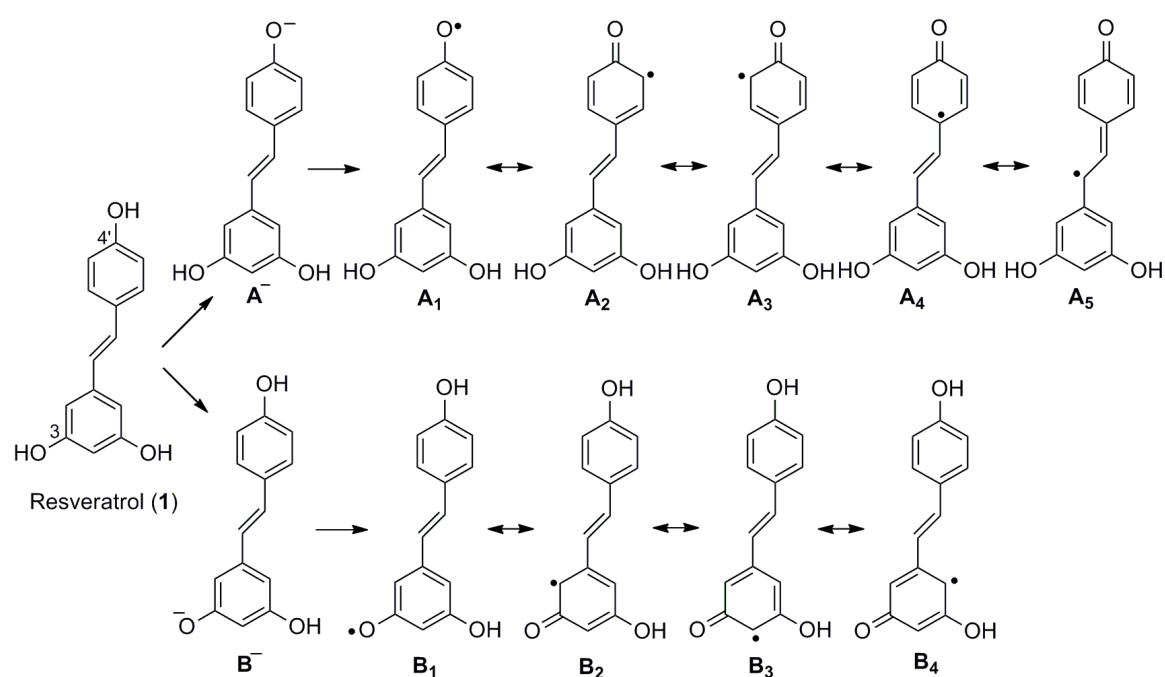


Figure 4.36 – Formation of two possible phenoxide radicals **A** and **B**.

Both 4'-O and 3-O resveratrol radicals **A** and **B** show several possible resonance structures, the most significant ones shown in figure 4.36. The importance of these structures for each of the two radicals can be estimated from the calculated spin densities, reported in figure 4.37. We see that the most important structures are those with the unpaired electron localized on the oxygen atom involved in the H-abstraction and on the *ortho* and *para* carbon atoms of the corresponding phenyl

ring, **A**₁-**A**₄ and **B**₁-**B**₄, and, only for the 4'-O radical, on the distal carbon atom of the ethylene unit, **A**₅.

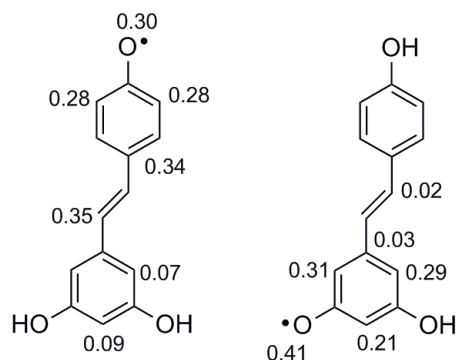


Figure 4.37 – Spin densities calculated for the two possible phenoxide radicals, **A**₁ (left) and **B**₁ (right).

Our calculations indicate that the 4'-O anion **A**⁻ is more stable than the 3-O anion **B**⁻, by 1.1 kcal mol⁻¹ in enthalpy at 298 K, and that the corresponding 4'-O radical **A** is also more stable than **B** by a larger extent, 7.2 kcal mol⁻¹, in agreement with previous theoretical studies [17–20].

We then considered the thermodynamics of the most plausible mechanisms proposed for the dimerization of the resveratrol to products **3** and **4** (Figure 4.38). The dehydrodimer **3** is obtained from the coupling reaction of the radical structures **A**₅ and **A**₂ (or **A**₃), to give an intermediate dimer **5** which then undergoes an intramolecular nucleophilic attack. On the other hand, the dehydrodimer **4** is obtained from the coupling reaction of the radical structures **A**₅ and **B**₂ (or **B**₄), to give an intermediate dimer **6** which then also undergoes a similar intramolecular nucleophilic attack (Figure 4.38).

The calculated enthalpies for both reaction paths are reported in Table 4.1. Both values in gas phase and in water solution are reported and show that the solution environment do not significantly change the qualitative picture, as expected for radical reactions, and suggest that the ESI-MS approach is an adequate technique to investigate the reaction in solution.

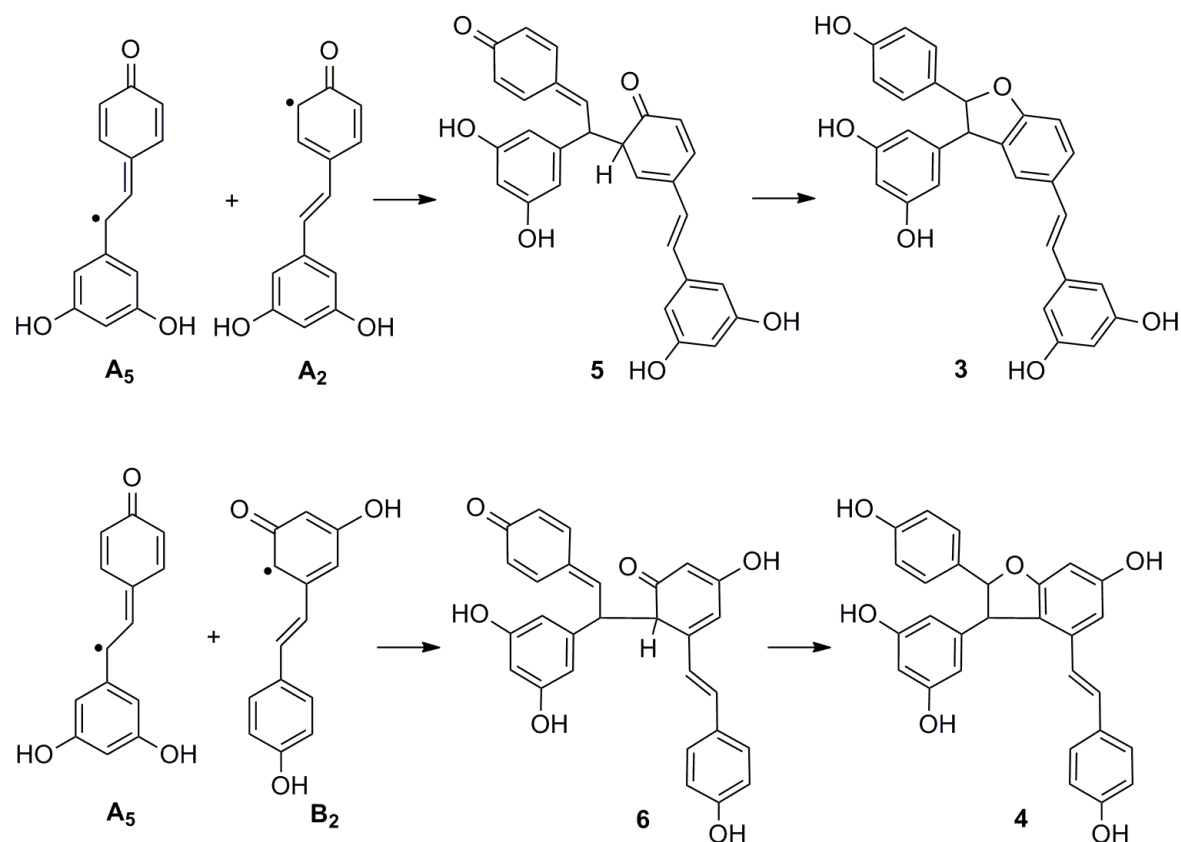


Figure 4.38 – Proposed reaction paths leading to the dehydromers **3** and **4**.

Reaction	Gas phase	Solution
$A_5 + A_2 \rightarrow 5$	-6.5	-3.6
$5 \rightarrow 3$	-37.5	-33.2
$A_5 + B_2 \rightarrow 6$	-19.2	-13.7
$6 \rightarrow 4$	-29.6	-27.6
$A_2 + \text{Resveratrol (1)} \rightarrow 7$	+25.0	+15.7
$A_2 + A_2 \rightarrow 8$	-5.4	-2.3
$A_5 + A_5 \rightarrow 8a$	-10.0	-11.6

Table 4.1 – Reaction enthalpies at 298 K for the paths leading to the dehydromers **3** and **4** as illustrated in Figure 4.38.

The results in Table 4.1 indicate that both steps, radical coupling and subsequent intramolecular nucleophilic attack, are exoergic for each of the two possible mechanisms. It is worth noting that although **A** is more stable than **B** (by 7.2 kcal mol⁻¹) and thus forms more easily, once **B** is formed, it reacts more favorably with **A** to give

the intermediate dimer **6**: indeed, while the coupling of **A**₅ and **A**₂ has a reaction energy of -3.6 kcal mol⁻¹, while that between **A**₅ and **B**₂ has a much higher reaction energy (-13.7 kcal mol⁻¹). These results explain the contradictory experimental data according to which either dimer **3** and **4**, or both, may form from the oxidation of resveratrol, depending on the experimental procedure. The subsequent intramolecular nucleophilic attack, **5** → **3** and **6** → **4**, are both highly exoergic with similar reaction energies, respectively -33.2 and -27.6 kcal mol⁻¹.

We also considered (i) the attack of the **A**₂ radical to the ethylene unit of a neutral resveratrol molecule, which is a statistically more plausible alternative to the formation of an initial dimer **7** with the same backbone of **5**; (ii) the coupling of two radicals **A**₂ through the formation of a different dimer **8** featuring a C-C bond between two phenyl rings; (iii) the coupling of two radicals **A**₅ through the formation of a different dimer **8a** featuring a C-C bond between two ethylene units (Figure 4.39). The thermodynamics of both reactions are also reported in Table 4.1 and indicate: (i) an endothermic reaction energy for the attack of the **A**₂ radical to a neutral to the ethylene resveratrol molecule, by 15.7 kcal mol⁻¹; and (ii) a reaction energy for the the coupling of two radicals **A**₂ through their phenyl ring lower than that between **A**₂, only -2.3 kcal mol⁻¹, suggesting that these processes are not or less plausible. The reaction energy for the coupling of two radicals **A**₅ through their ethylene units has a rather high value, -11.6 kcal mol⁻¹: this results indicate that this is a plausible reaction in agreement with experimental studies indicating the formation of different dehydrodimers, such as pallidol, when resveratrol is treated with peroxidase [14].

We finally considered the oxidation of the 4'-O and 3-O phenoxide anion, **A**⁻ and **B**⁻, by Cu(II) and Fe(III) ions. The most plausible mechanism for these oxidation reactions consists of (i) the approach and coordination of the phenoxide oxygen to the metal ion; (ii) an electron transfer from the organic anion to the metal center leading to a complex whereby the oxidized phenoxo radical is still coordinated to the reduced metal ion; and (iii) the detachment of the radical from the reduced metal ion. An accurate calculation of the intermediates geometry and energies and of possible energy barriers involved in these processes is a very difficult task and should be treated by rigorous wave function methods, such as CASSCF and CASPT2, which are too computationally demanding for the size of the considered systems. For this reason, we employed an approximate approach in which we limit ourselves to estimate the relative stabilities of the final products of the oxidation process, i.e. the complex between the oxidized phenoxo radical and the reduced metal ions, at DFT level. We assumed the coordination of only one phenoxide anion, and the metal

coordination was saturated to four, for the Cu(II) ion, and six, for the Fe(III) ion (based on the most common coordination numbers for these metal ions), with water molecules (Figure 4.40). Both 4'-O and 3-O phenoxide anions were considered, and we performed geometry optimization starting from the geometrical parameters expected for phenoxo radicals and the reduced Cu(I) and Fe(II) ions.

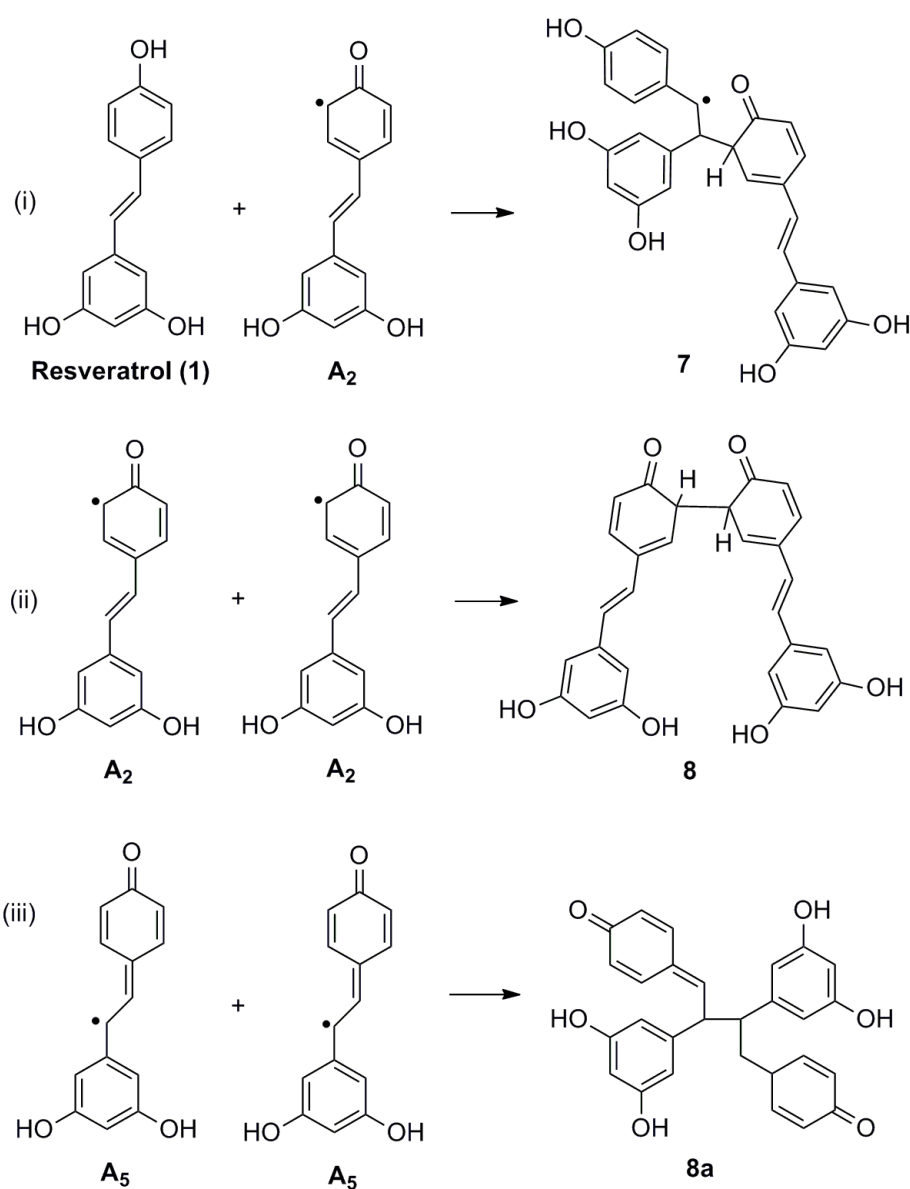


Figure 4.39 – Possible alternative initial reaction paths: (i) the attack of the A_2 radical to the ethylene unit of a neutral resveratrol molecule, (ii) the coupling of two radicals A_2 and (iii) the coupling of two radicals A_5 .

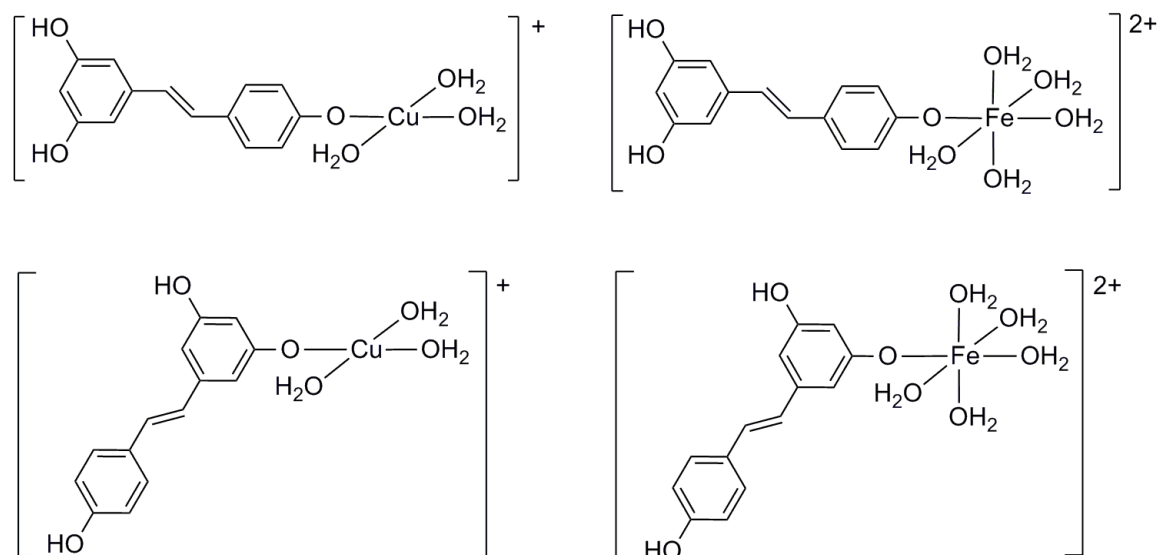


Figure 4.40 – Considered complexes between the oxidized phenoxo radical and the reduced copper and iron metal ions.

The analysis of the final optimized geometries and spin densities confirms that in all considered complexes the electron transfer has occurred. It is worth noting that the optimization of both the Cu(II) complexes spontaneously leads to the detaching of two water molecules, giving a dicoordinated species, as expected for a Cu(I) ion, and confirming once more that the electron transfer has indeed occurred. No such effects could be observed for the Fe(III) complexes, as the Fe(III) and Fe(II) ions both prefer hexa coordination.

The results show that while for the Cu(II) ion, the final 4'-O phenoxo radical complex was lower in energy than the 3-O phenoxo radical complex, by 7.7 kcal mol⁻¹, for the Fe(III) ion the final 3-O phenoxo radical complex was lower than the 4'-O phenoxo radical complex, by 1.2 kcal mol⁻¹. These results explain why the use of Cu(II) ion leads to the dehydrodimer **3**, involving only the 4'-O radical **A**, while the use of Fe(III) ion preferentially leads to the regioisomeric product **4**, requiring the formation of the 3-O radical **B**.

In conclusion, computational results suggest that dehydrodimers **3** and **4** are formed by coupling reactions, and subsequent intramolecular nucleophilic attack, of phenoxide radicals. The latter are produced in the oxidation reaction of phenoxide

anions by Cu(II) and Fe(III) ions. We find that Cu(II) preferentially produces the 4'-O resveratrol radical **A**, while Fe(III) produces easier the 3-O resveratrol radical **B**. Given that the formation of dehydrodimer **3** requires **A** radicals as reactants, whereas that of dehydrodimer **4** needs also **B** radicals, these computational findings explain why reactions of resveratrol with Cu and Fe ions eventually result in the production of species **3** and **4**, respectively [119].

4.5 MS analysis for synthetic analogues of resveratrol

Due to the well-known antioxidant and cancer chemo-preventive properties, along with its structural simplicity and lack of toxicity, resveratrol is taking an ideal lead for development of new bio-active agents. Present work describes an ESI-MS study on resveratrol analogues that enable us to deduce a structural-activity relationship. Synthetic hydroxystilbenes **9-13** have been investigated in order to evaluate the role of number and position of OH groups on the reactivity (Figure 4.41).

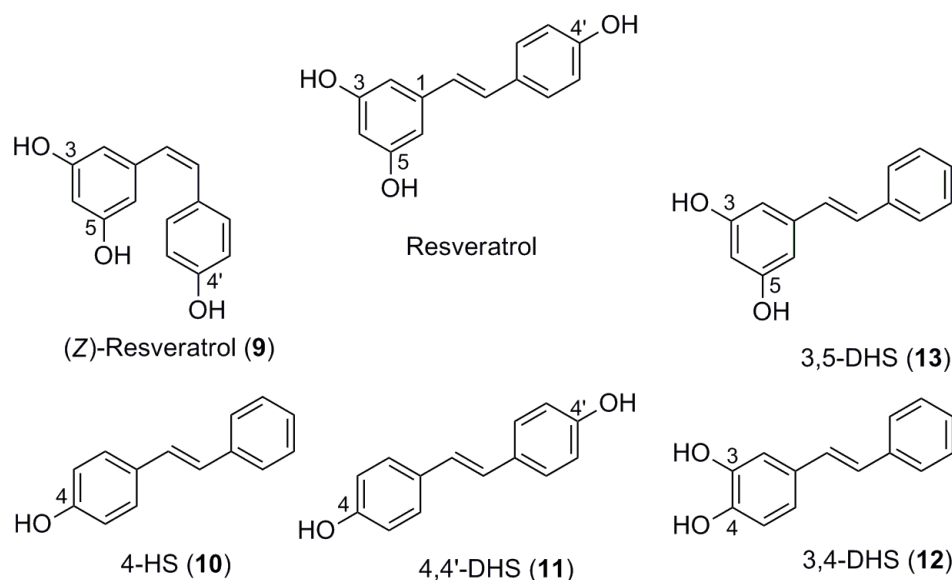


Figure 4.41 – Synthetic hydroxystilbene analogues **9-13**. Numbering is for convenience.

4.5.1 (*Z*)-Isomer of resveratrol

(*Z*)-Resveratrol (**9**) obtained by photoisomerisation of the natural compound (Section 3.4.2) has been analyzed in presence of copper(II)sulfate under the same conditions adopted for resveratrol investigation. ESI-MS measurements gave signals for copper complexes at m/z 291, m/z 309, and m/z 519 attributable to $[\text{Resv}+\text{Cu}]^+$, $[\text{Resv}+\text{Cu}+\text{H}_2\text{O}]^+$, and $[2\text{Resv}+\text{Cu}]^+$ respectively with the presence of signal at m/z 455 attributable to the corresponding dehydrodimer. Most probably, this dehydrodimer is isomeric to **3** on the double bond, but MS technique cannot give this information. Finally, we can conclude that (*Z*)-isomer show with copper(II)sulfate the same behavior like resveratrol.

4.5.2 4-Hydroxy-(*E*)-stilbene

The oxidative product from resveratrol has shown that hydroxyl group at 4'-position is much easier to undergo oxidation than other hydroxyl groups in *meta*-positions on the other aromatic rings. However, in order to understand the role of 4-OH group in the formation of dehydrodimer, analogue **10** was synthesized (Section 3.4.4), characterized by NMR and used for ESI-MS/MS study.

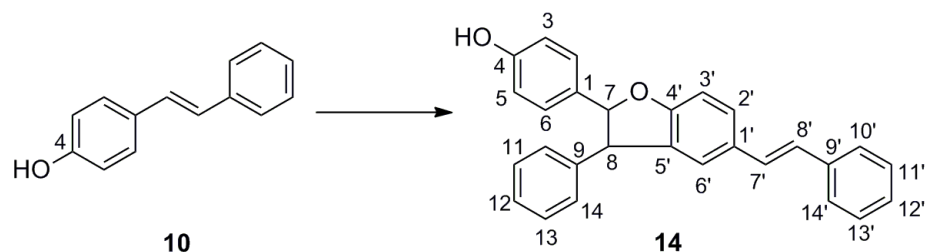


Figure 4.42 – Dehydrodimer **14** detected by ESI-MS spectrum obtained by injection of 1:1 4-HS (**10**)/CuSO₄ solution in CH₃CN/H₂O (1:1). Numbering is for convenience.

The positive ion mode ESI spectrum of **10** with copper(II)sulfate in acetonitrile/water (1:1) is reported in figure 4.43. It shows the signal at m/z 391 and m/z 390 corresponding to $[\text{M}+\text{H}]^+$ ion and radical cation of dehydrodimer **14**, respectively. In addition a signal at m/z 196 is detected, corresponding to the radical cation of **10**. The formation of radical cation in ESI-MS process is in line with reported data [126, 127].

MS/MS experiments on m/z 390 ion produces intense fragments at m/z 296, attributable to the loss of a phenol (C_6H_6O) molecule and at m/z 299, corresponding to $[M-C_7H_7]^+$ ion (Figure 4.44).

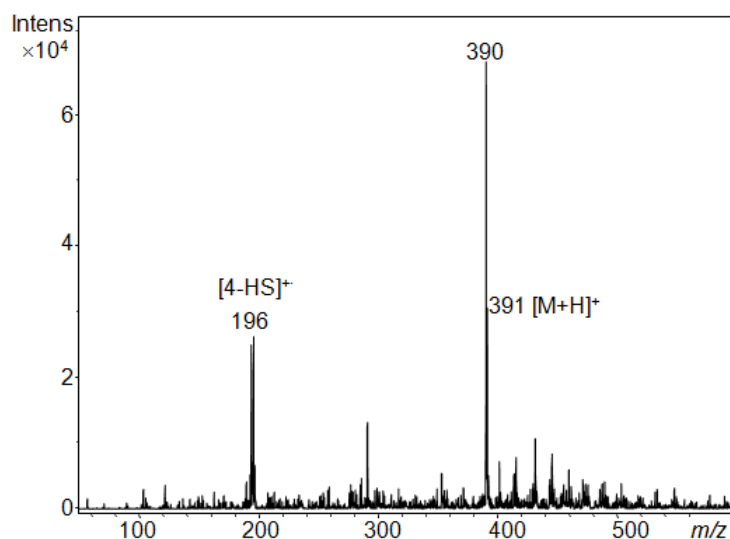


Figure 4.43 – ESI(+)-MS spectrum obtained by injection of a 1:1 4-HS (**10**)/CuSO₄ solution in CH₃CN/H₂O (1:1). M is for dehydrodimer **14**.

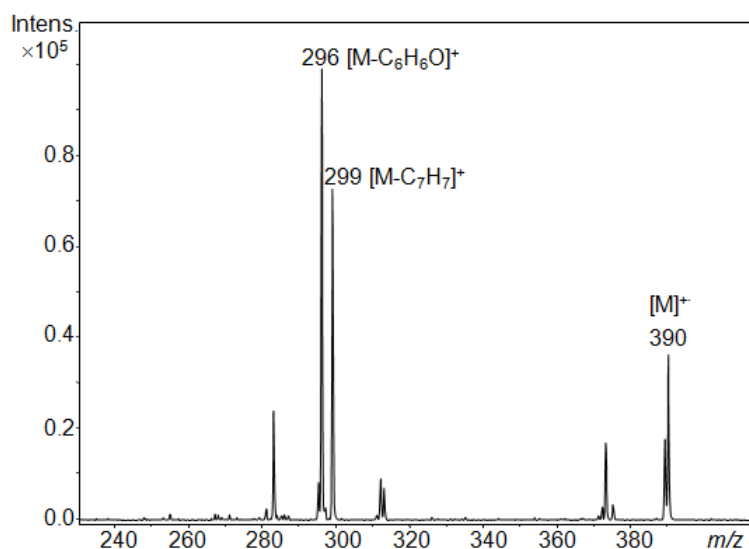


Figure 4.44 – ESI (+) MS/MS spectrum by fragmentation of m/z 390 ion, obtained for a 1:1 4-HS(**10**)/CuSO₄ solution in CH₃CN/H₂O (1:1); M is for the dehydrodimer **14**.

ESI(-)MS spectrum of the same solution showed the $[M-H]^-$ ion at m/z 389, for the dehydrodimer **14**, together with m/z 195 attributable to the $[4\text{-HS-H}]^-$ ion. MS/MS experiment on m/z 389 gave m/z 371 and m/z 295 ions due to the loss of water and phenol molecules, respectively (Figure 4.45).

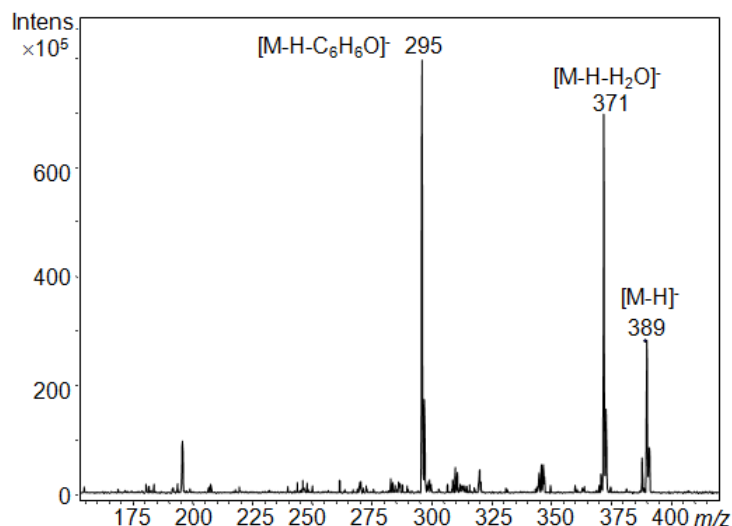


Figure 4.45 – ESI(-)MS spectrum by fragmentation experiment on $[M-H]^-$ ion at m/z 389, obtained by injection of 1:1 4-HS(**10**)/CuSO₄ solution in CH₃CN/H₂O (1:1); M is for the dehydrodimer **14**.

Similarly to the procedure adopted for the structural assignment of dehydrodimer produced from resveratrol (Section 4.2), product **14** was synthesized by reaction of **10** with copper(II)sulfate and its structure characterized by NMR analysis (Section 3.5.2) [32, 138].

In figure 4.46 ¹H NMR spectrum recorded in acetone-d₆ for dehydrodimer **14** is reported. In particular, we obtained characteristics signals of two *trans*-olefinic protons (two doublets at 6.98 and 7.13 ppm, with a large coupling constant of 16.4 Hz, H-7' and H-8', respectively) and two aliphatic protons (doublets at 4.65 and 5.51 ppm, $J = 8.5$ Hz, H-8 and H-7, respectively).

Structure assignment has been made on the basis of long range ¹H and ¹³C correlations by HMBC experiments. In details, i) the magnetically equivalent H-2/H-6 protons at 7.19 ppm showed correlation with C-7 at 94.2 ppm, ii) H-10/H-14 protons at 6.20 ppm correlate with C-8 at 57.1 ppm. iii) a weak correlation between proton H-7 and C-4' (Figure 4.47). These correlations allowed us to establish that 4-hydroxybenzyl moiety is linked to C-7 and phenyl ring is linked to C-8 position.

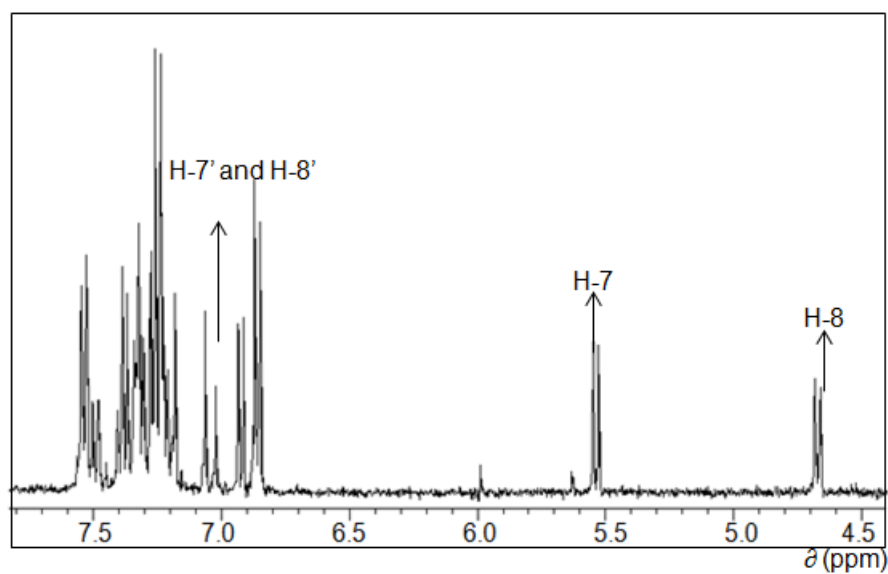


Figure 4.46 – ^1H NMR spectrum, recorded in acetone- d_6 , for dehydrodimer **14** in spectral range 7.5:4.5 ppm. Proton numbering according to figure 4.42.

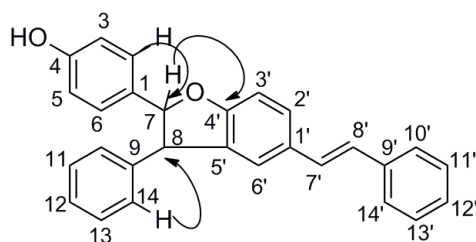


Figure 4.47 – Significant ^1H , ^{13}C long range correlations by NMR-HMBC experiments of dehydrodimer **14**, recorded in acetone- d_6 .

MS analysis carried out in negative ion mode for this synthetic product showed a pseudomolecular ion at m/z 389. In particular, MS/MS spectra indicated the same fragmentation as in the case of the dehydrodimer detected in ESI-MS/MS analysis after injection of **10** with copper(II)sulfate solution.

4.5.3 4,4'-Dihydroxy-(*E*)-stilbene

Another analogue taken into account is 4,4'-dihydroxy-(*E*)-stilbene (4,4'-DHS, **11**). It was obtained by synthesis as reported in section 3.4.3.

Replacing resveratrol with compound **11** in ESI-MS study in presence of copper(II)sulfate a different, peculiar behavior has been observed. No clusters for copper complexes, in positive ion mode detection, neither signals related to a dehydrodimer product in negative ion mode were detected. It was instead observed the oxidation product *para*-quinone **15** (Figure 4.48), responsible for the yellow color of the solution after addition of copper(II)sulfate to **11**. The structure for compound **15** was confirmed by UV-visible analysis carried out under the same solvent conditions used in MS measurement (acetonitrile/water (1:1)) which provided absorption in visible region at $\lambda_{max} = 430$ nm (Figure 4.42) [139].

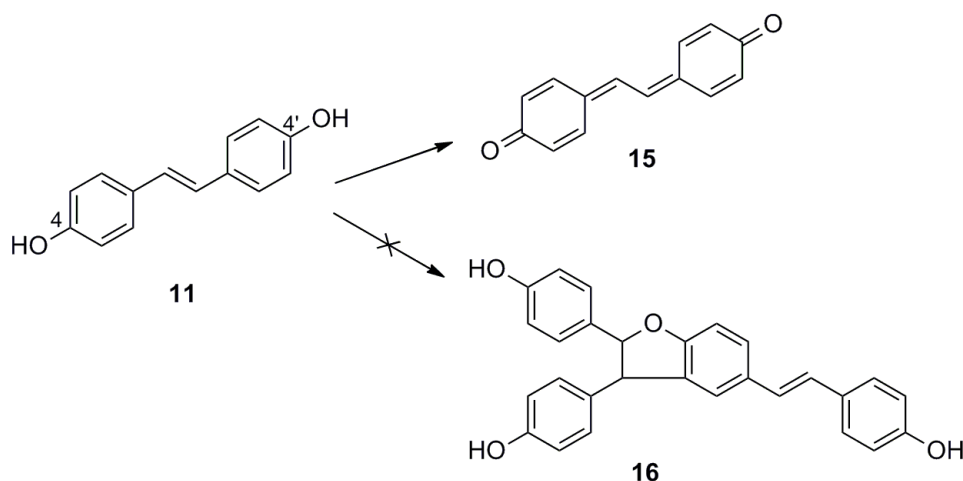


Figure 4.48 – Synthetic analogue **11** and its *para*-quinone product **15**.

In details, the UV-visible spectrum was recorded for **11** in acetonitrile/water solution (black curve), and after addition of copper(II)sulfate (red curve) solution (Section 3.2.3). These results indicated that oxidation of **11** in the presence of copper(II)sulfate was faster than in the case of resveratrol, and main product was *para*-quinone **15** and not the expected dehydrodimer **16** (Figure 4.48).

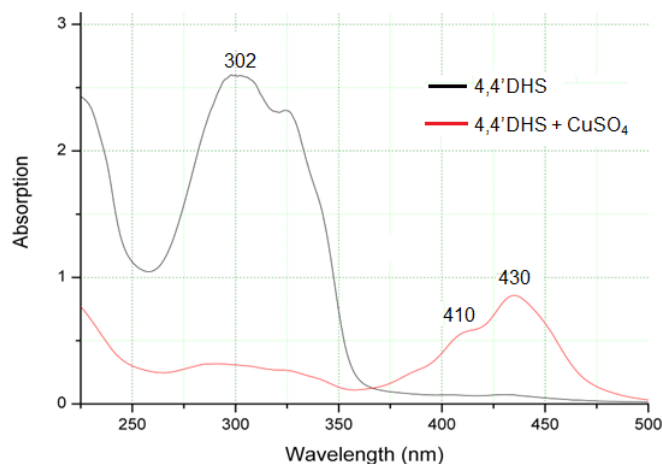


Figure 4.49 – UV-Visible spectra of pure **11** (black line) and in the presence of CuSO_4 in $\text{CH}_3\text{CN}/\text{H}_2\text{O}$ (1:1) (red line).

4.5.4 3,4-Dihydroxy-(*E*)-stilbene

Later, we studied resveratrol analogues with two OH group in *ortho* position as in compound **12**. It was synthesized (Section 3.4.4), structurally characterized by NMR and latter used for MS study.

In this case dehydrodimer **17a** and/or **17b** could be possible, together with the Diels Alder adducts **19a** and/or **19b**, the latter one reported by Shang *et al.* [21] by reaction in the presence of galvinoxyl radical, through the precursor **18** (Figure 4.50).

The negative ion mode mass spectrum of acetonitrile/water (1:1) solution of **12** with copper(II)sulfate (1:1) showed no signals attributable to dehydrodimers **17a** and/or **17b** or adducts **19a** and/or **19b**. Similarly to the behavior of **11**, a fast color change of the solution from colorless to brown was observed by addition of copper salt before injection in the ion source. Based on reported data, *ortho*-quinone **18** could be responsible for the color, but it was not detected in ESI-MS analysis.

By the reaction of **12** in the presence of copper(II)sulfate after stirring 24 hours at room temperature in dry acetonitrile solution, no any dehydrodimer was obtained but Diels Alder product was produced and it was characterized by ^1H NMR analysis and comparison with reported data [21].

Based on the evidences from this bench reaction, ESI-MS spectra of the solution of **12** with copper(II)sulfate were recorded at different time intervals (1h, 3h, 24h), but no dehydrodimers nor Diels Alder products could be detected. A probable explanation could be given by a fast production of *ortho*-quinone **18** by radical mechanism, able to convert all starting material **12**, which was not so available to react with **18** for the formation of **19a** or **19b**.

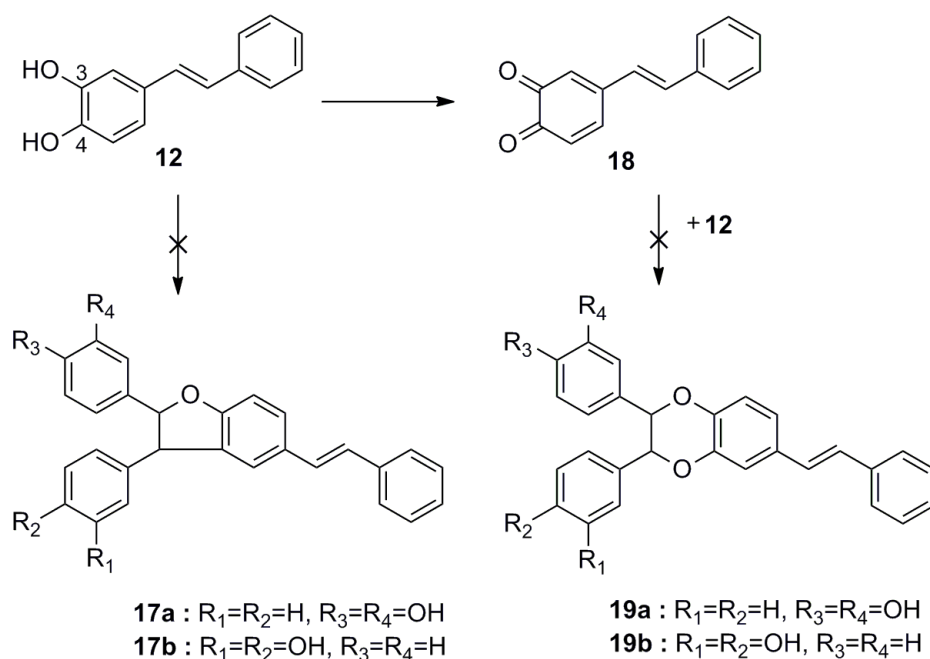


Figure 4.50 – Synthetic analogue **12** and its *ortho*-quinone product **18**, as the only product by reaction with copper(II)sulfate.

Otherwise, in the positive ion mode spectrum, an intense cluster with the most intense signal at m/z 483 was detected, attributable to a Cu(I) ion complex involving two molecules of **18**. These isotopic cluster resulted in good agreement with the simulated cluster for $[C_{28}H_{20}CuO_4]^+$, and MS/MS experiments on the selected signal at m/z 483 gave fragment at m/z 291 attributable to $[M+Cu+H_2O]^+$ ion, where M for **18**, obtained after addition of water in ion trap. This ion as a weak signal was also present in MS spectrum (Figure 4.51).

In figure 4.52 the minimized structure by molecular mechanics calculations (MM) of the ion formed by two molecules of **18** and Cu(I) ion detected at m/z 483 is shown.

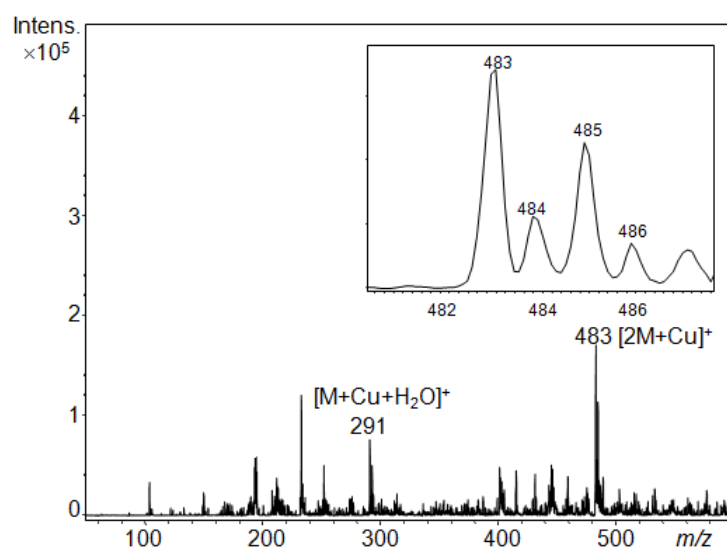


Figure 4.51 – ESI(+)-MS spectrum of **12** in the presence of CuSO_4 with expanded region of cluster at m/z 483, corresponding to the $[2\text{M}+\text{Cu}]^+$ ion, M is for **18**.

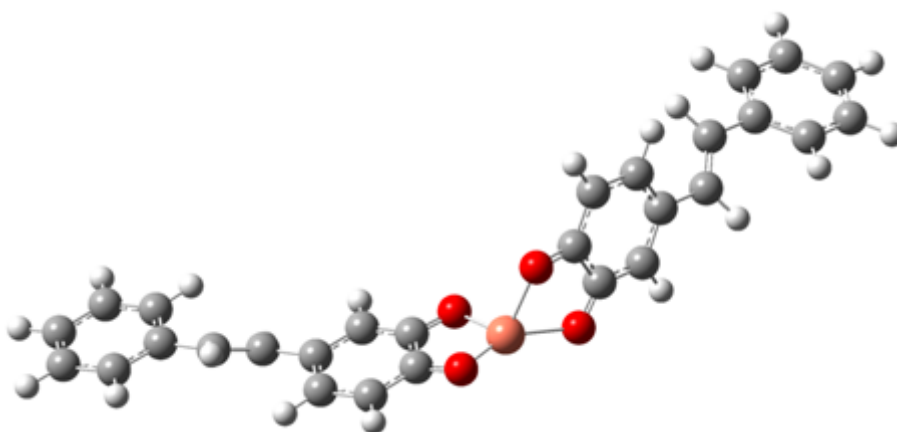


Figure 4.52 – Minimized structure by MM calculations for the $[2\text{M}+\text{Cu}]^+$ ion with M is **18** at m/z 483 in ESI(+)-MS spectrum.

4.5.5 3,5-Dihydroxy-(*E*)-stilbene

In order to define relevance of an OH group in *para*-position, we synthesized analogue **13** (Section 3.4.4) lacking of any *para* OH groups. After addition of copper(II) sulfate

to the solution of **13**, ESI(-)-MS analysis do not detect any signals corresponding to any dehydrodimers. No color changes were observed in the solution, because the position of OH groups in **13** does not allow oxidation to a quinone structure.

In ESI(+)-MS spectrum only weak signals for copper complexes were observed at m/z 487, 293 and 275 corresponding to $[2M+Cu]^+$, $[M+Cu+H_2O]^+$ and $[M+Cu]^+$ ions, respectively (Figure 4.53), where M is for **13**.

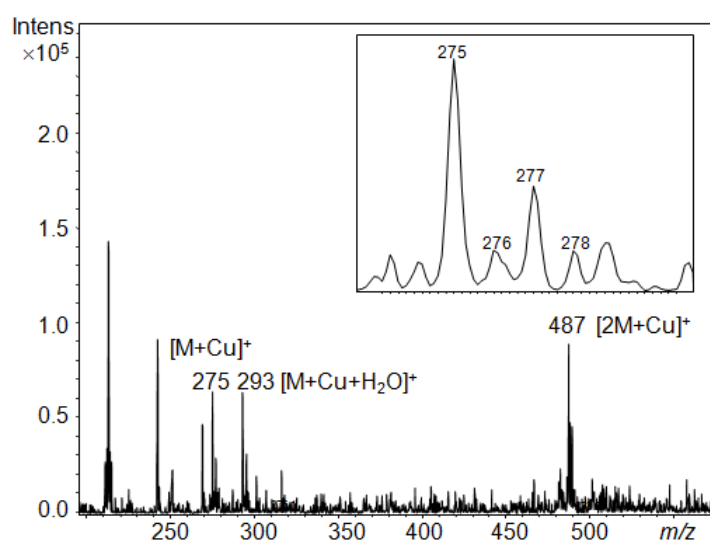


Figure 4.53 – ESI(+)-MS spectrum of **13** in the presence of $CuSO_4$ with expanded region of the cluster at m/z 275, corresponding to the $[M+Cu]^+$ ion, M is for 3,5-DHS.

In conclusion five synthetic analogues of resveratrol has been investigated in order to gain insights on the structure-reactivity relationship. The presence of a hydroxyl group in *para* position is essential for the reactivity and formation of dehydrodimers. These data support the fact that the structure of natural resveratrol is peculiar for its chemical reactivity and biological behavior.

Chapter 5

Conclusions

This gas phase reactivity of the natural product resveratrol in presence of copper(II)sulfate has been investigated by ESI-MS technique. By injecting equimolar amounts of resveratrol/CuSO₄ solutions in CH₃CN/H₂O into an ESI-MS, we have detected the formation of the complexes [Resv+Cu]⁺, [Resv+Cu+H₂O]⁺ and [2Resv+Cu]⁺. Only singly charged ions were observed, indicating that in the ESI process the reduction of Cu(II) species occurs. B3LYP/6-311G(d) calculations have been carried out for the detected complexes, with the aim to establish their geometries and energies. The most stable structures are characterized by interactions between the copper ion and the carbon atoms in the aromatic ring and/or in the alkenyl group. Resveratrol has been compared with the synthetic analogue dihydroresveratrol, which lacks of the alkenyl group between the two aromatic rings. For the latter compound only the [DHResv+Cu]⁺ complex has been detected, whose geometry corresponds to an intramolecular sandwich structure, containing the metal ion between the two aromatic rings.

Preliminary infrared multiphoton dissociation spectroscopy (IRMPD) experiments has been performed, which allow to successfully characterize the complexes. This study is in progress.

ESI-MS spectrum of resveratrol/copper(II)sulfate solution showed additional signals for a dehydrodimer, whose structure was established by the bench reaction, NMR analysis and comparison of MS fragmentation spectrum. Dehydrodimer resulted to be the same product as the one formed in the biological reaction proposed for natural resveratrol, where copper ions present in living organisms are involved in a prooxidant process.

Results by time dependent ESI-MS studies indicated that the dehydrodimer formation occurs in gas phase. In addition, the increasing formation of another oxidative product was detected.

By replacing Cu(II) with Fe(III) ions, iron complexes were not formed, but an isomeric dehydrodimer was obtained, whose structure was defined by NMR and MS comparison with product from the bench reaction. It is noteworthy that Cu- and Fe-induced dehydrodimers show the same planar structure as the natural products isolated from grapewine leaves, δ -viniferin and ε -viniferin respectively.

Computational results supported that the two isomeric dehydrodimers were formed by coupling reactions involving two different phenoxide radicals produced in the reaction with Cu(II) and Fe(III) ions.

In addition, some synthetic analogues of resveratrol have been studied in similar ESI-MS experiments in the presence of copper(II)sulfate, in order to gain insights on the structure-reactivity relationship, useful for designing new antitumor agents. The results indicate that the presence of a hydroxyl group in *para*-position is essential for the formation of dehydrodimers, supporting the peculiarity of the resveratrol structure for its chemical reactivity and biological behavior.

Abbreviations

APCI	Atmospheric Pressure Chemical Ionization
CE	Capillary Electrophoresis
CI	Chemical Ionization
CRM	Charge Residue Model
CID	Collision Induced Dissociation
EI	Electron Ionization
ESI	Electrospray Ionization
ECP	Effective Core-Potential
EDESI-MS	Energy-Dependent Electrospray Ionization Mass Spectrometry
FT-ICR	Fourier Transform Ion Cyclotron Resonance
GC	Gas Chromatography
HPLC	High Performance Liquid Chromatography
HSAB	Hard and Soft Acids and Bases
HMBC	Heteronuclear Multiple Bond Correlation
HOMO	Highest Occupied Molecular Orbital
IEM	Ion Evaporation Model
IRMPD	Infrared Multiple Photodissociation Spectroscopy
LCMS	Liquid Chromatography Mass Spectrometry
LUMO	Lowest Unoccupied Molecular Orbital

MS/MS	Tandem mass spectrometry
MS	Mass Spectrometry
MALDI	Matrix Assisted Laser Desorption/Ionization
MM	Molecular Mechanics
MW	Microwave
NMR	Nuclear Magnetic Resonance
NOESY	Bidimensional Nuclear Overhauser Effect
PDB	Protein Data Bank
PB	Poisson-Boltzmann
PAH	Polyaromatic Hydrocarbons
PCB	Polychlorinated Biphenyls
QIT	Quadrupole Ion Trap
RF	Radio frequency
ROS/RNS	Reactive Oxygen Species/ Reactive Nitrogen Species
SPE	Solid Phase Extraction
THF	Tetrahydrofuran
TOF	Time of Flight
TLC	Thin Layer Chromatography
UV	Ultraviolet-visible
ZPE	Zero-Point Energy

List of Figures

1.1	Chemical structure of resveratrol.	1
1.2	Health benefits of resveratrol [11].	2
1.3	Annual count of resveratrol articles indexed on PubMed. The results include articles with the term “resveratrol” in found in the title, abstract, or keywords [12].	3
1.4	Proposed antioxidant and prooxidant mechanisms of resveratrol, X [•] = Free radicals.	4
2.1	Schematic diagram of a mass spectrometer.	8
2.2	A schematic figure of an APCI interface.	12
2.3	Schematic of electrospray ionization. Ionization and nebulisation occurs at the tip of the capillary, which is at a potential of several kilo volts.	14
2.4	Droplet evolution scheme due to solvent evaporation at constant charge and Coulomb fissions at the Rayleigh limit. Figure in inset at the top right, illustrates the fission of one such droplet.	15
2.5	Schematic diagram of a quadrupole mass filter.	18
2.6	Schematic diagram of a triple quadrupole system. The first (Q1) and third (Q3) are mass spectrometers and the center (Q2) is a collision cell.	19
2.7	Schematic diagram of a typical ion trap mass spectrometer.	20
2.8	Stability diagram in (a _z , q _z) space for the region of stability in both r- and z-directions near the origin for the three-dimensional quadrupole ion trap.	21
2.9	Schematic representation of a cylindrical FT-ICR analyzer cell.	23
3.1	Conversion of resveratrol (1) into dihydro-resveratrol (2). Reagent and conditions: (i) H ₂ , Pd/C, ethanol, 1 h.	28
3.2	Isomerization of natural (<i>E</i>)-resveratrol to (<i>Z</i>)-isomer 9 . conditions: (i) hv, 350 nm, ethanol.	29
3.3	Synthesis of 4,4'-DHS (11). Reagents and conditions: (i) chloral hydrate, acetic acid, H ₂ SO ₄ ; (ii) Zn, ethanol, reflux, 4 h; (iii) MW irradiation, 2 h.	30

LIST OF FIGURES

3.4	Synthesis of stilbene analogues 10 , 12 , and 13 . Reagents and conditions: (i) tert-butyltrimethylsilyl chloride, 1,8-diazabicycloundec-7-ene, dichloromethane, (ii) benzyl triphenyl phosphonium bromide, K ₂ CO ₃ , iso-propanol, reflux, 4 h; (ii) tert-butyl ammonium fluoride (1M in THF), THF, 1 h.	31
3.5	Synthesis of dehydrodimer 3 . Reagent and condition (i) anhydrous CuSO ₄ , anhydrous acetonitrile, rt, 24h, Numbering is for convenience.	33
3.6	Synthesis of dehydrodimer 4 . Reagent and condition: (i) FeCl ₃ , MeOH/H ₂ O (1:1), rt, 49h.	35
3.7	Synthesis of dehydrodimer 14 . Reagent and conditions: (i) anhydrous CuSO ₄ , dry acetonitrile, rt, 24h, Numbering is for convenience.	36
3.8	Synthesis of 17a/17b and 19a/19b . Reagent and condition: (i) anhydrous CuSO ₄ , dry acetonitrile, rt, 24h.	37
4.1	ESI (+) MS spectrum obtained by injection of a 1:1 resveratrol/CuSO ₄ solution in CH ₃ CN/H ₂ O (1:1).	40
4.2	Expanded region of the ESI(+)MS spectrum obtained by injection of a 1:1 resveratrol/CuSO ₄ solution in CH ₃ CN/H ₂ O (1:1) corresponding to cluster at $m/z = 519$ for [2Resv+Cu] ⁺ in the experimental (left) and simulated (right) cases.	40
4.3	Positive-ion MS/MS fragmentation on: (a) $m/z 520 \pm 2$ corresponding to the selection of the whole cluster ascribed to [2Resv+Cu] ⁺ ion and (b) $m/z 519$ corresponding to the most intense peak of the cluster due to the contribution of ⁶³ Cu isotope.	41
4.4	MS ³ experiment on the signal selected at $m/z 309$, corresponding to [Resv + Cu + H ₂ O] ⁺ ion.	42
4.5	MS ³ experiment on the signal selected at $m/z 291$, corresponding to [Resv+Cu] ⁺ ion.	43
4.6	¹ H NMR spectrum recorded in D ₂ O in presence of CD ₃ CN, for resveratrol (a) and in the presence of anhydrous CuSO ₄ after 1h (b) in spectral range 7.7:6.2 ppm.	43
4.7	ESI(+)MS spectrum obtained by injection of 1:1 dihydro-resveratrol /CuSO ₄ solution in MeOH/H ₂ O (1:1) with a zoom on the isotopic cluster at $m/z 293/295$	44
4.8	MS/MS experiment on : (a) $m/z 294 \pm 2$, corresponding to the selection of the whole cluster ascribed to [DHResv+Cu] ⁺ ion, and (b) on the signal selected at $m/z 295$, due to the contribution of ⁶⁵ Cu isotope.	45

4.9	Energy minimized structure of the [Resv+Cu] ⁺ complex at B3LYP/6-311G(d) level of theory.	46
4.10	Energy minimized structure of the [Resv+Cu+H ₂ O] ⁺ complex at B3LYP/6-311G(d) level of theory.	47
4.11	Energy minimized structure of the [2Resv+Cu] ⁺ complex at B3LYP/6-311G(d) level of theory.	48
4.12	HOMO map of resveratrol at B3LYP/6-311G(d) level of theory. Colors near blue represent large positive values of the highest-occupied molecular orbital.	48
4.13	Energy minimized structure of the [DHResv+Cu] ⁺ complex at B3LYP/6-311G(d) level of theory.	49
4.14	IRMPD spectra recorded in -OH stretch range for [Resv+Cu] ⁺ ion; experimental (black line) and calculated IR frequencies (red line) of most stable isomer.	50
4.15	(a)ESI(+)-MS spectrum obtained by injection of a 1:1 resveratrol/CuSO ₄ solution in CH ₃ CN/H ₂ O (1:1); (b) MS/MS spectrum on [M+H] ⁺ ion at <i>m/z</i> 455; M is for the dehydrodimer 3	51
4.16	(a) ESI(-)-MS spectrum obtained by injection of a 1:1 resveratrol/CuSO ₄ solution in CH ₃ CN/H ₂ O (1:1); (b) MS/MS spectrum on [M-H] ⁻ ion at <i>m/z</i> 453, M is for the dehydrodimer 3	52
4.17	MS ³ experiment on the signal selected at <i>m/z</i> 369. M is for dehydrodimer 3	53
4.18	Fragmentation pathway proposed for [M-H] ⁻ ion at <i>m/z</i> 453 of dehydrodimer 3	54
4.19	Chemical structure of dehydrodimer 3 with indication of numbering adopted for ¹ H NMR assignment (above) and ¹ H NMR spectrum, recorded in acetone-d ₆ , for dehydrodimer 3 in spectral range 7.5:4.5 ppm (below).	55
4.20	Significant ¹ H, ¹³ C long range correlations by HMBC experiments of synthetic dehydrodimer 3 , recorded in acetone-d ₆	56
4.21	APCI(+) (left) and ESI(+) (right) mass spectrum obtained by injection of a 1:1 resveratrol/CuSO ₄ solution in CH ₃ CN/H ₂ O (1:1).	57
4.22	Abundance of i) resveratrol, ii) resveratrol-copper complexes and iii) dehydrodimer 3 and all Cu-complexes by ESI(+)-MS spectra recorded in time range by injection of 1:1 resveratrol/CuSO ₄ solution in CH ₃ CN/H ₂ O (1:1).	59
4.23	Abundance of resveratrol and oxidation products by ESI(-)-MS spectra recorded in time range by injection of 1:1 resveratrol/CuSO ₄ solution in CH ₃ CN/H ₂ O (1:1).	60

LIST OF FIGURES

4.24	ESI(-)-MS chromatography comparison spectra obtained by injection of 1:1 resveratrol /CuSO ₄ solution in CH ₃ CN/H ₂ O (1:1).	60
4.25	ESI(-)-MS spectrum showing the signal at m/z 471 obtained by injection of 1:1 resveratrol/CuSO ₄ solution in CH ₃ CN/H ₂ O (1:1) after 125 minutes from the mixing of the solution.	61
4.26	ESI(-) MS/MS spectrum on [M-H] ⁻ ion at m/z 471, obtained by injection of 1:1 resveratrol/CuSO ₄ solution in CH ₃ CN/H ₂ O (1:1) after 125 minutes from the mixing; M is for the new oxidized product.	61
4.27	Chemical structure of the natural products retrisol A and B.	62
4.28	Crystal structure of laccase from <i>Trametes versicolor</i> , as reported in Protein Data Bank (PDB ID 3KW7) Four Cu ions present in the active site are indicated in red.	63
4.29	(a) ESI(+)-MS spectrum obtained by injection of a 1:1 resveratrol/FeCl ₃ solution in CH ₃ CN/H ₂ O (1:1) ; (b) MS/MS spectrum on [M+H] ⁺ ion at m/z 455, M is for a dehydrodimer.	64
4.30	MS ³ experiment on the signal selected at m/z 349. M is for a dehydrodimer.	65
4.31	ESI (-) MS/MS spectrum by fragmentation experiment on the ion at m/z 453, obtained by injection of 1:1 resveratrol/FeCl ₃ solution in CH ₃ CN/H ₂ O (1:1); M is for the dehydrodimer.	66
4.32	MS ³ experiment on the signal selected at m/z 359. M is for dehydrodimer.	66
4.33	Structure of the dehydrodimer 4 obtained from resveratrol in the presence of FeCl ₃	67
4.34	Natural δ -viniferin (left) and (-) ϵ -viniferin (right) with indication of absolute configuration.	68
4.35	Mass spectra from fragmentation experiments of natural δ -viniferin and ϵ -viniferin obtained by HPLC-MS of <i>P.viticola</i> [132].	68
4.36	Formation of two possible phenoxide radicals A and B	70
4.37	Spin densities calculated for the two possible phenoxide radicals, A ₁ (left) and B ₁ (right).	71
4.38	Proposed reaction paths leading to the dehydrodimers 3 and 4	72
4.39	Possible alternative initial reaction paths: (i) the attack of the A ₂ radical to the ethylene unit of a neutral resveratrol molecule, (ii) the coupling of two radicals A ₂ and (iii) the coupling of two radicals A ₅	74
4.40	Considered complexes between the oxidized phenoxo radical and the reduced copper and iron metal ions.	75
4.41	Synthetic hydroxystilbene analogues 9-13 . Numbering is for convenience.	76

4.42	Dehydrodimer 14 detected by ESI-MS spectrum obtained by injection of 1:1 4-HS (10)/CuSO ₄ solution in CH ₃ CN/H ₂ O (1:1). Numbering is for convenience.	77
4.43	ESI(+)-MS spectrum obtained by injection of a 1:1 4-HS (10)/CuSO ₄ solution in CH ₃ CN/H ₂ O (1:1). M is for dehydrodimer 14	78
4.44	ESI (+) MS/MS spectrum by fragmentation of <i>m/z</i> 390 ion, obtained for a 1:1 4-HS(10)/CuSO ₄ solution in CH ₃ CN/H ₂ O (1:1); M is for the dehydrodimer 14	78
4.45	ESI(-)MS spectrum by fragmentation experiment on [M-H] ⁻ ion at <i>m/z</i> 389, obtained by injection of 1:1 4-HS(10)/CuSO ₄ solution in CH ₃ CN/H ₂ O (1:1); M is for the dehydrodimer 14	79
4.46	¹ H NMR spectrum, recorded in acetone-d ₆ , for dehydrodimer 14 in spectral range 7.5:4.5 ppm. Proton numbering according to figure 4.42.	80
4.47	Significant ¹ H , ¹³ C long range correlations by NMR-HMBC experiments of dehydrodimer 14 , recorded in acetone-d ₆	80
4.48	Synthetic analogue 11 and its <i>para</i> -quinone product 15	81
4.49	UV-Visible spectra of pure 11 (black line) and in the presence of CuSO ₄ in CH ₃ CN/H ₂ O (1:1) (red line).	82
4.50	Synthetic analogue 12 and its <i>ortho</i> -quinone product 18 , as the only product by reaction with copper(II)sulfate.	83
4.51	ESI(+)-MS spectrum of 12 in the presence of CuSO ₄ with expanded region of cluster at <i>m/z</i> 483, corresponding to the [2M+Cu] ⁺ ion, M is for 18	84
4.52	Minimized structure by MM calculations for the [2M+Cu] ⁺ ion with M is 18 at <i>m/z</i> 483 in ESI(+)-MS spectrum.	84
4.53	ESI(+)-MS spectrum of 13 in the presence of CuSO ₄ with expanded region of the cluster at <i>m/z</i> 275, corresponding to the [M+Cu] ⁺ ion, M is for 3,5-DHS.	85

References

- [1] MJ Takaoka. Of the phenolic substances of white hellebore (*Veratrum grandiflorum* Loes fil.). *J.Faculty Sci. Hokkaido Imperial University*, 3:1–16, 1940.
- [2] S Nanomura, H Kanagawa, and A Makimoto. Chemical constituents of polygonaceous plants. I. Studies on the components of Ko-jo-kon.(*Polygonum cuspidatum* SIEB et ZUCC. *Yakugaku Zasshi*, 83:988–990, 1963.
- [3] M Kubo, Y Kimura, H Shin, T Haneda, T Tani, and K Namba. Studies on the antifungal substance of crude drug (II). I. On the roots of *Polygonum cuspidatum* Sieb et Zucc(Polygonacea). *Shoyakugaku Zasshi*, 35:58–61, 1981.
- [4] M Jang, L Cai, G Udeani, K Slowing, C Thomas, C Beecher, S Fong, N Farnsworth, A Kinghorn, R Mehta, R Moon, and J Pezzuto. Cancer Chemoprevention Activity of Resveratrol, a Natural Product Derived from Grapes. *Science*, 275:218–220, 1997.
- [5] J Baur and D Sinclair. Therapeutic potential of resveratrol:the *in vivo* evidence. *Nat.Rev.*, 5:493–506, 2006.
- [6] S Renaud and R Gueguen. The French paradox and wine drinking. *Novartis Found.Symp.*, 216:208–217,discussion 152–158,217–222, 1998.
- [7] S Renaud and M de Lorgeril. Wine, alcohol, platelets, and the french paradox for coronary heart disease. *Lancet*, 339:1523–1526, 1992.
- [8] B Fuhrman, A Lavy, and M Aviram. Consumption of red wine with meals reduces the susceptibility of human plasma and low-density lipoprotein to lipid peroxidation. *Am.J.Clin.Nutr.*, 61:549–554, 1995.
- [9] A Holme and S Pervaiz. Resveratrol in cell fate decision. *J.Bioenerg.Biomembr.*, 39:59–63, 2007.

REFERENCES

- [10] CA De la Lastra and I Villegas. Resveratrol as an anti-inflammatory and anti-aging agent: Mechanisms and clinical implications. *Mol.Nutr.Food Res.*, 49:405–430, 2005.
- [11] B Aggarwal and S Shishodia. Resveratrol in Health Diseases. *CRC Press*, page Taylor and Francis group, 2006.
- [12] JM Smoliga, JA Baur, and HA Hausenblas. Resveratrol and health - a comprehensive review of human clinical trials. *Mol.Nutr. Food Res.*, 55:1129–1141, 2011.
- [13] C De la Lastra and I Villegas. Resveratrol as an antioxidant and pro-oxidant agent: mechanism and clinical implications. *Biochem.Soc.Trans.*, 35:1156–1160, 2007.
- [14] S Quideau, D Deffieux, C Douat-Casassus, and L Pouysegu. Plant Polyphenols: Chemical Properties, Biological Activities, and Synthesis. *Angew.Chem.Int.Ed.*, 50:586–621, 2011.
- [15] L Fremont. Biological effect of resveratrol. *Life.Sci.*, 66:663–673, 2000.
- [16] M Leopoldini, N Russo, and M Toscano. The molecular basis of working mechanism of natural polyphenolic antioxidants. *Food Chem.*, 125:288–306, 2011.
- [17] A Queiroz, BAQ Gomes, Moraes W Jr., and R Borges. A theoretical antioxidant pharmacophore for resveratrol. *Eur.J.Med.Chem.*, 44:1644–1649, 2009.
- [18] H Cao, X Pan, C Li, C Zhou, F Deng, and T Li. Density functional theory calculations for resveratrol. *Bioorg.Med.Chem.Lett.*, 13:1869–1871, 2003.
- [19] D Mikulski, R Gorniak, and M Molski. A theoretical study of the structural radical scavenging activity of *trans*-resveratrol analogues and *cis*-resveratrol in gas phase and water environment. *Eur.J.Med.Chem.*, 45:1015–1027, 2010.
- [20] D Mikulski, M Szelag, M Molski, and R Gorniak. Quantum-chemical study on the antioxidation mechanisms of *trans*-resveratrol reactions with free radicals in the gas phase, water and ethanol environment. *J.Mol.Struc.: THEOCHEM*, 951:37–48, 2010.

- [21] Y Shang, Y Qian, X Liu, F Dai, F Shang, W Jia, Q Liu, J Fang, and B Zhou. Radical-Scavenging Activity and Mechanism of Resveratrol-Oriented Analogues: Influence of the Solvent, Radical, and Substitution. *J.Org.Chem.*, 74:5025–5031, 2009.
- [22] L Gianelli, V Amendola, L Fabbrizzi, P Pallavicini, and G Mellerio. Investigation of reduction of Cu(II) complexes in positive-ion mode electrospray mass spectrometry. *Rapid Commun.Mass Spectrom.*, 15:2347–2353, 2001.
- [23] F Tisato, F Refosco, M Porchia, M Tegoni, V Gandin, C Marzano, M Pellei, G Papini, L Grazia, R Seraglia, and P Traldi. The relationship between the electrospray ionization behaviour and biological activity of some phosphino Cu(I) complexes. *Rapid Commun.Mass Spectrom.*, 24:1610–1616, 2010.
- [24] Y Takaya, K Terashima, J Ito, YH He, M Tateoka, N Yamaguchi, and M Niwa. Biomimic transformation of resveratrol. *Tetrahedron*, 61:10285–10290, 2005.
- [25] SS Velu, I Buniyamin, LK Ching, F Feroz, I Noorbachta, LC Gee, K Awang, I Abd. Wahab, and JF Faizal Weber. Regio- and Stereoselective Biomimetic Synthesis of Oligostilbenoid Dimers from Resveratrol Analogues: Influence of the Solvent, Oxidant, and Substitution. *Chem.Eur.J.*, 14:11376–11384, 2008.
- [26] A Rahman, Shahabuddin, SM Hadi, and JH Parish. Complexes involving quercetin, DNA and Cu(II). *Carcinogenesis*, 11:2001–2003, 1990.
- [27] Singh S, SF Asad, A Ahmad, NU Khan, and SM Hadi. Oxidative DNA damage by capsaicin and dihydrocapsaicin in the presence of Cu(II). *Cancer Letters*, 169:139–146, 2001.
- [28] H Ahsan and SM Hadi. Strand scission in DNA induced by curcumin in the presence of Cu(II). *Cancer Letters*, 124:23–30, 1998.
- [29] K Fukuhara, M Nagakawa, I Nakanishi, K Ohkubo, K Imai, S Urano, S Fukuzumi, T Ozawa, N Ikota, M Mochizuki, N Miyata, and H Okuda. Structural basis for DNA-cleaving activity of resveratrol in the presence of Cu(II). *Bioorg.Med.Chem.*, 14:1437–1443, 2006.
- [30] A Ahmad, FA Syed, S Singh, and SM Hadi. Prooxidant activity of resveratrol in the presence of copper ions: Mutagenicity in plasmid DNA. *Toxicol.Lett.*, 159:1–12, 2005.

REFERENCES

- [31] A Ahmad, FA Syed, S Singh, and SM Hadi. DNA breakage by resveratrol and Cu(II):reaction mechanism and bacteriophage inactivation. *Cancer Lett.*, 154:29–37, 2000.
- [32] P Langcake and JR Pryce. Oxidative Dimerisation of 4-Hydroxystilbene in vitro:Production of a Grapevine Phytoalexin Mimic. *J.C.S.Chem.Comm.*, 1412:208–210, 1977.
- [33] R Gonzalez-Barrio, D Beltran, E Cantos, M Gil, J Espin, and F Tomas-Barberan. Comparison of Ozone and UV-C Treatments on the Postharvest Stilbenoid Monomer, Dimer, and Trimer Induction in Var. 'Superior' White Table Grapes. *J.Agric.Food Chem.*, 54:4222–4228, 2006.
- [34] X Vitrac, A Bornet, R Vanderlinde, J Valls, T Richard, J Delaunay, J Merillon, and P Teissedre. Determination of Stilbenes (δ -viniferin, *trans*-astringin, *trans*-piceid, *cis*- and *trans*-resveratrol, ϵ -viniferin) in Brazilian Wines. *J.Agric.Food Chem.*, 53:5664–5669, 2005.
- [35] AL Waterhouse and RM Lamuela-Raventos. The occurrence of piceid, s stilbene glucoside, in grape berries. *Phytochemistry*, 37:571–573, 1994.
- [36] KCR Ascia, SE Hahn, EP Diamandis, G Soleas, and DN Goldberg. The red wine phenolic*trans*-resveratrol and quercetin block human platelet aggregation and eicosanoid synthesis:implications for protection against coronary heart disease. *Clin.chim.Acta.*, 235:207–219, 1995.
- [37] M Tereza Fernandez, M Lurdes Mira, M Helena Florancio, and KR Jennings. Iron and copper chelation by flavonoids: an electrospray mass spectrometry study. *J.Inorg.Biochem.*, 92:105–111, 2002.
- [38] J Jean-Denis, R Pezet, and R Tabacchi. Rapid analysis of stilbenes and derivatives from downy mildew-infected grapevine leaves by liquid chromatography atmospheric pressure photoionisation mass spectrometry. *J.Chromatogr.A*, 1112:263–268, 2006.
- [39] L Stella, M De Rosso, A Panighel, A Vedova, R Flamini, and P Traldi. Collisionally induced fragmentation of $[M-H]^-$ species of resveratrol and piceatannol investigated by deuterium labelling and accurate mass measurements. *Rapid Commun.Mass Spectrom.*, 22:3867–3872, 2008.

-
- [40] Z Spacil, M Shariatgorji, N Amini, P Solich, and L Ilag. Matrix-less laser desorption/ionisation mass spectrometry of polyphenols in red wine. *Rapid Commun.Mass Spectrom.*, 23:1834–1840, 2009.
- [41] J Thomson. Rays of Positive Electricity and their Applications to Chemical Analysis. *Longmans, Greens and Co. London*, 1913.
- [42] W Henderson and J McIndoe. Mass Spectrometry of Inorganic and Organometallic Compounds. *John Wiley and Sons: Chichester*, 2005.
- [43] J Banoub, R Newton, E Esmans, E Ewing, and G Mackenzie. Recent developments in mass spectrometry for the characterization of nucleosides, nucleotides, oligonucleotides, and nucleic acids. *Chem. Rev.*, 105:1869–1915, 2005.
- [44] C Das. Fundamentals of contemporary mass spectrometry, ed.Desiderio. *D.M. and Nibbering, N.M. 2007, New York: Wiley-inter science*.
- [45] K Downard. Mass spectrometry:a foundation course. *London: Royal Society of Chemistry*, 2004.
- [46] J Gross. Mass Spectrometry:a textbook. *Berlin:Spinger*, 2004.
- [47] M Barrow, W Burkitt, and P Derrick. Principles of Fourier transform ion cyclotron resonance mass spectrometry and its application in structural biology. *Analyst*, 130:18–28, 2005.
- [48] K Kitson, B Larsen, and C McEwen. Gas Chromatography and Mass Spectrometry:A Practicle Guide. *Academic Press: San Diego*, 1996.
- [49] M Munson and F Field. Chemical ionization mass spectrometry. I. General introduction. *J.Am.Chem.Soc.*, 88:2621–2630, 1966.
- [50] New approach to the mass spectroscopy of non-volatile compounds. *Biochem.Biophys.Res.Comm.*, 60:616–621, 1974.
- [51] A Bruins. Mass spectrometry with ion sources operating at atmospheric pressure. *Mass Spectrom. Rev.*, 10:53–77, 1991.
- [52] R Cole. Electrospray Ionization Mass spectrometry:Fundamentals, Instrumentation and Applications. *Mass Spectrom. Rev.*, 10:53–77, 1991.

REFERENCES

- [53] K Tanaka, Y Waki, Y Ido, S Akita, Y Yoshida, and T Yoshida. Protein and polymer analysis up to m/z 100,000 by laser ionization time-of-flight mass spectrometry. *Rapid Comm. Mass Spectrom.*, 02:151–153, 1988.
- [54] C Shackleton and K Straub. Direct analysis of steroid conjugates: the use of secondary ion mass spectrometry. *Steroids*, 40:35–51, 1982.
- [55] H Beckey. Field desorption mass spectrometry: a technique for the study of thermally unstable substances of low volatility. *Int. J. Mass Spectrom. Ion Phys.*, 02:500–503, 1969.
- [56] New Picogram Detection System Based on a Mass spectrometry with an External Ionization Source at Atmospheric Pressure. *Anal. Chem.*, 45:936–943, 1973.
- [57] V Zaikin and J Halket. Derivatization in mass spectrometry- 8. Soft ionization mass spectrometry of small molecules. *Eur. J. Mass Spectrom.*, 12:79–115, 2006.
- [58] J Fenn, M Mann, C Meng, S Wong, and C Whitehouse. Electrospray ionization for mass spectrometry of large biomolecules. *Science*, 246:64–71, 1989.
- [59] C Meng, M Mann, and J Fenn. Of protons or proteins. *Z. Phys. D*, 10:361–368, 1988.
- [60] M Yamashita and F Fenn. Electrospray ion source. Another variation on the free jet theme. *J. Phys. Chem.*, 88:4451–4459, 1984.
- [61] S Zhou and K Cook. A mechanistic study of electrospray mass spectrometry: charge gradients within electrospray droplets and their influence on ion response. *J. Am. Soc. Mass Spectrom.*, 12:206–214, 2001.
- [62] G Taylor. The stability of horizontal fluid interface in a vertical electric field. *J. Fluid. Mech.*, 02:01–15, 1965.
- [63] L Rayleigh. On the equilibrium of liquid conducting masses charged with electricity. *Phil. Mag. Ser.*, 14:184–186, 1882.
- [64] M Dole, L Mack, R Hines, R Mobley, L Ferguson, and M Alice. Molecular Beams of Macroions. *J. Chem. Phys.*, 49:2240–2249, 1968.
- [65] J Iribarne and B Thomson. On the evaporation of small ions from droplets. *J. Chem. Phys.*, 64:2287–2294, 1976.

- [66] B Thomson and J Iribarne. Field induced ion evaporation from liquid surface in atmospheric pressures. *J.Chem.Phys.*, 71:4451–4463, 1979.
- [67] A Shukla and J Futrell. Tandem mass spectrometry:dissociation of ions by collisional activation. *J.Mass Spectrom.*, 35:1069–1090, 2000.
- [68] J Loo. Studying noncovalent protein complexes by electrospray ionization mass spectrometry. *Mass Spectrom. Rev.*, 16:1–23, 1997.
- [69] W Paul and H Steinwedel. Ein neues massenspektrometer ohne Magnetfeld. *Zeitschrift fur Naturforschung*, 08:448–450, 1934.
- [70] R March. An Introduction to Quadrupole Ion Trap Mass Spectrometry. *J.Mass Spectrom.*, 32:351–369, 1997.
- [71] P Dawson. Quadrupole Mass Spectrometry and its Application. *Berlin: Springer*, 1995.
- [72] CS Ho, CWK Lam, MHM Chan, RCK Cheung, LK Law, LCW Lit, KF Ng, MWH Suen, and HL Tai. Electrospray Ionisation Mass Spectrometry:Principles and Clinical Applications. *Clin.Biochem.Rev.*, 24:3–12, 2003.
- [73] R March and J Todd. Practical Aspects of Ion Trap Mass Spectrometer. *Boca Raton: CRC Press*, 1995.
- [74] N Polfer. Infrared multiple photon dissociation spectroscopy of trapped ions. *Chem.Soc.Rev.*, 40:2211–2221, 2011.
- [75] A Marshall, C Hendrickson, and G Jackson. Fourier transform ion cyclotron resonance mass spectrometry:a primer. *Mass Spectrom.Rev.*, 17:1–35, 1998.
- [76] M Barrow, W Burkitt, and P Derrick. Principles of Fourier transform ion cyclotron resonance mass spectrometry and its application in structural biology. *Analyst*, 130:18–28, 2005.
- [77] J Hornak. The basics of NMR. *J.Agric.Food Chem.*, Retrieved, 2009-02-03.
- [78] DA Skoog, DM West, and HJ Holler. Fundamental of Analytical Chemistry. *Saunders College Publishing, Fort Worth, US*, 1992.
- [79] K Fukuhara and N Miyata. Resveratrol as a new type of DNA-cleaving agent. *Bioorg.Med.Chem.Lett.*, 8:3187–3192, 1998.

REFERENCES

- [80] G Montsko, MSP Nikfardjam, Z Szabo, K Boddi, T Lorand, R Ohmacht, and L Mark. Determination of products derived from *trans*-resveratrol UV photoisomerisation by means of HPLC-APCI-MS. *J.Photochem.Photobio.A:Chemistry*, 196:44–50, 2008.
- [81] B Trela and A Waterhouse. Resveratrol:Isomeric Molar Absorptivities and Stability. *J.Agric.Food Chem.*, 44:1253–1257, 1996.
- [82] JP Roggero. Study of Ultraviolet Irradiation of Resveratrol and Wine. *J.Food Composi.Ana.*, 13:93–97, 2000.
- [83] W Zhi-xin, Z Xue-jing, Z Yue, and Z Yong. A Convenient Synthesis of *Trans* and *Cis*-3,4',5-trihydroxystilbene. *J.Chinese.Pharm.Sci.*, 14:204–208, 2005.
- [84] RH Sieber. A study. *Liebigs Ana.Chem.*, 730:31–46, 1969.
- [85] JC Cheng, JG Fang, WF Chen, B Zhou, L Yang, and ZL Liu. Structure-activity relationship studies of resveratrol and its analogues by the reaction kinetics of low density lipoprotein peroxidation. *Bioorg.Chem.*, 34:142–157, 2006.
- [86] Y Le Bigot, R Elgharbi, M Delmas, and A Gaset. Reactions en milieu heterogene solide-liquide faiblement hydrate III: La reaction de wittig dans le systeme carbonates alcalins/solvant organique protique. *Tetrahedron*, 42:3813–3823, 1986.
- [87] JG Fang and B Zhou. Structure-Activity Relationship and Mechanism of the Tocopherol-Regenerating Activity of Resveratrol and its Analogues. *Bioorg.Chem.*, 56:11458–11463, 2008.
- [88] M Ahad Ali, K Kondo, and Y Tsuda. Synthesis and Nematocidal Activity of Hydroxystilbenes. *Chem.Pharm.Bull.*, 40:1130–1136, 1992.
- [89] S Nicotra, MR Cramarossa, A Mucci, UM Pagnoni, S Riva, and L Forti. Bio-transformation of resveratrol: synthesis of *trans*-dehydrodimers catalyzed by laccases from *Myceliophthora thermophyla* and from *Trametes pubescens*. *Tetrahedron*, 60:595–600, 2004.
- [90] KS Huang, M Lin, and YH Wang. Synthesis of Amurensin H, a New Resveratrol Dimer from the Roots of *Vitis Amurensis*. *Chin.Chem.Lett.*, 10:817–820, 1999.

- [91] Y Chun-Suo, L Mao, and W Ying-Hong. Synthesis of the active stilbenoids by photooxidation reaction of *trans-ε*-viniferin. *Chin.J.Chem.*, 22:1350–1355, 2004.
- [92] W Li, LS Ding, BG Li, and YZ Chen. Oligostilbenes from *Vitis Heyneana*. *Phytochemistry*, 42:1163–1165, 1996.
- [93] MJ Frisch, GW Trucks, HB Schlegel, GE Scuseria, MA Robb, JR Cheeseman, JA Montgomery, T Jr. Vreven, KN Kudin, JC Burant, JM Millam, SS Iyengar, J Tomasi, V Barone, B Mennucci, M Cossi, G Scalmani, N Rega, GA Petersson, H Nakatsuji, M Hada, M Ehara, K Toyota, R Fukuda, J Hasegawa, M Ishida, T Nakajima, Y Honda, O Kitao, H Nakai, M Klene, X Li, JE Knox, HP Hratchian, JB Cross, C Adamo, J Jaramillo, R Gomperts, RE Stratmann, O Yazyev, AJ Austin, R Cammi, C Pomelli, JW Ochterski, PY Ayala, K Morokuma, GA Voth, P Salvador, JJ Dannenberg, VG Zakrzewski, S Dapprich, AD Daniels, MC Strain, O Farkas, DK Malick, AD Rabuck, K Raghavachari, JB Foresman, JV Ortiz, Q Cui, AG Baboul, S Clifford, J Cioslowski, BB Stefanov, G Liu, A Liashenko, P Piskorz, I Komaromi, RL Martin, DJ Fox, T Keith, MA Al-Laham, CY Peng, A Nanayakkara, M Challacombe, PMW Gill, B Johnson, W Chen, MW Wong, and Pople Gonzalez, C. Gaussian revision e.01. *Inc Wallingford CT*, 2004.
- [94] AD Becke. Density functional thermochemistry.III. the role of exact exchange. *J.Chem.Phys.*, 98:5648, 1993.
- [95] C Lee, W Yang, and RG Parr. Developement of the Colle-Salvetti correlation energy formula into a functional of the electron density. *Phys.Rev.B*, 37:785–789, 1988.
- [96] EJ Bylaska, WA de Jong, K Kowalski, TP Straatsma, M Valiev, D Wang, E Apra, TL Windus, S Hirata, MT Hackler, Y Zhao, PD Fan, RJ Harrison, M Dupuis, DMA Smith, J Nieplocha, V Tipparaju, M Krishnan, AA Auer, M Nooijen, E Brown, G Cisneros, GI Fann, H Fruchtl, J Garza, K Hirao, R Kendall, JA Nichols, K Tsemekhman, K Wolinski, J Anchell, D Bernholdt, P Borowski, T Clark, D Clerc, H Dachsel, M Deegan, K Dyall, D Elwood, E Glendening, M Gutowski, A Hess, J Jaffe, B Johnson, J Ju, R Kobayashi, R Kutteh, Z Lin, R Littlefield, X Long, B Meng, T Nakajima, S Niu, L Pollack, M Rosing, G Sandrone, M Stave, H Taylor, G Thomas, J van Lenthe,

REFERENCES

- A Wong, and Z Zhang. NWChem, A Computational Chemistry Package for Parallel Computers. *Version 5.0*, Pacific Northwest National Laboratory, Richland:Washington 99352-0999,USA, 2006.
- [97] Jagaur. Version 7.5. *Schrodinger*, LLC:New York, NY, 2008.
- [98] AD Becke. Density-functional exchange-energy approximation with correct asymptotic behavior. *Phys.Rev.A*, 38:3098-3100, 1988.
- [99] PJ Hay and WR Wadt. Ab initio effective core potentials for molecular calculations.Potentials for K and Au including the outermost core orbitals. *J.Chem.Phys.*, 82:299-311, 1985.
- [100] PC Hariharan and JA Pople. The effect of d-functions on molecular orbital energies for hydrocarbons. *Chem.Phys.Lett.*, 16:217-219, 1972.
- [101] DJ Tannor, B Marten, R Murphy, R Friesner, D Sitkoff, A Nicholls, B Honig, M Ringnalda, and WA Goddard. Accurate First Principles Calculation of Molecular Charge Distributions and Solvation Energies from Ab Initio Quantum Mechanics and Continuum Dielectric Theory. *J.Am.Chem.Soc.*, 116:11875-11882, 1994.
- [102] A Rimola, M Sodupe, J Tortajada, and L Rodriguez-Santiago. Gas phase reactivity of Cu^+ aromatic amino acids:an experimental and theoretical study. *Int.J.Mass Spectrom.*, 257:60-69, 2006.
- [103] N Di Marco and G Bombi. Electrospray mass spectrometry(ESI-MS) in the study of metal ligand solution equilibria. *Mass Spectrom. Rev.*, 25:347-379, 2006.
- [104] A Tintaru, L Charles, P Milko, J Roithova, and D Schroder. Redox reactions of copper(II) upon electrospray ionization in the presence of acridine ligands with an amide side chain. *J.Phys.Org.Chem.*, 22:229-233, 2009.
- [105] R Franski. Electrospray ionization mass spectrometric study of 1,3,4-oxadiazole copper complexes. *J.Mass Spectrom.*, 39:272-276, 2004.
- [106] JC Ma and DA Dougherty. The Cation π -Interaction. *Chem.Rev.*, 97:1303-1324, 1997.

- [107] DA Dougherty. Cation π -Interaction in Chemistry and Biology: a New View of Benzene, Phe, Tyr, and Trp. *Science*, 271:163–168, 1996.
- [108] T Osako, Y Tachi, M Doe, M Shiro, K Ohkubo, S Fukuzumi, and S Itoh. Quantitative Evaluation of d- π -Interaction in Copper(I) Complexes and Control of Copper(I)-Dioxygen Reactivity. *Chem. Eur. J.*, 10:237–246, 2004.
- [109] ED Blue, TB Gunnoe, JL Petersen, and PD Boyle. Protonation of N-heterocyclic carbene ligand coordinated to copper(I): Coordination mode of imidazolium cation as a function of counterion as determined by solid-state structures. *J. Organomet. Chem.*, 691:5988–5993, 2006.
- [110] M Mascali and J Hansen. Design, synthesis and metal binding properties of a mixed-donor macrobicycle. *Chem. Commun.*, pages 355–356, 1998.
- [111] FB Xu, QS Li, LZ Wu, XB Leng, ZC Li, YL Zeng, XShand Chow, and ZZ Zhang. Formation of Group 11 Metal(I)-Arene Complexes: Bonding Mode and Molecule-Responsive Spectral Variations. *Organometallics*, 22:633–640, 2003.
- [112] P Milko, J Roithova, D Schroder, J Lemaire, H Schwarz, and MC Holthausen. The Phenoxy/Phenol/Copper Cation: a Minimalistic Model of Bonding Relations in Active Centers of Mononuclear Copper Enzymes. *Chem. Eur. J.*, 14:4318–4327, 2008.
- [113] RC Dunbar. Metal Cation Binding to Phenol DFT Comparison of the Competing Sites. *J. Phys. Chem. A*, 106:7328–7337, 2002.
- [114] A Lagutschenkova, R Sinha, P Maitre, and O Dopfer. Structure and Infrared Spectrum of the Ag^+ -Phenol Ionic Complex. *J. Phys. Chem. A*, 114:11053–11059, 2010.
- [115] C Coletti, R Nazzareno, D Scuderi, P Maitre, B Chiavarino, S Fornarini, F Lanucara, R Sinha, and M Crestoni. IRMPD spectroscopy of protonated S-nitrosocaptopril, a biologically active, synthetic amino acid. *Phys. Chem. Chem. Phys.*, 12:13455–13467, 2010.
- [116] V Tamboli, A Defant, I Mancini, and P Tosi. A study of resveratrol-copper complexes by electrospray ionization mass spectrometry and density functional theory calculations. *Rapid Commun. Mass Spectrom.*, 25:526–532, 2011.

REFERENCES

- [117] L Stella, M De Rosso, A Panighel, AD Vedova, R Flamini, and P Traldi. Collisionally induced fragmentation of $[M-H]^-$ species of resveratrol and piceatannol investigated by deuterium labelling and accurate mass measurements. *Rapid Commun.Mass Spectrom.*, 22:3867–3872, 2008.
- [118] QJ Kong, XY Ren, N Hu, CR Sun, and YJ Pan. Identification of isomers of resveratrol dimer and their analogues from wine grapes by HPLC/MSⁿ and HPLC/DAD-UV. *Food Chem.*, 127:727–734, 2011.
- [119] VF Tamboli, N Re, A Defant, I Mancini, and P Tosi. A joint experimental and theoretical investigation on the oxidative coupling of resveratrol induced by copper and iron ions. To be submitted.
- [120] N Mulinacci, M Innocenti, AR Santamaria, G la Marca, and G Pasqua. High-performance liquid chromatography/electrospray ionization tandem mass spectrometric investigation of stilbenoids in cell cultures of *Vitis vinifera* L., cv. Malvasia. *Rapid Commun.Mass Spectrom.*, 24:2065–2073, 2010.
- [121] RH Cichewicz, SA Kouzi, and MT Hamann. Dimerization of resveratrol by the grapevine pathogen *Botrytis cinerea*. *J.Nat.Prod.*, 63:29–33, 2000.
- [122] S Riva. Laccases:blue enzymes for green chemistry. *Trends in Biotech.*, 24:219–226, 2006.
- [123] M Fabbrini, C Galli, P Gentili, and D Macchitella. An oxidation of alcohols by oxygen with the enzyme laccase and mediation by TEMPO. *Tetrahedron Letters*, 42.
- [124] E Fritz-Langhals and B Kunath. Synthesis of aromatic aldehydes by laccase-mediator assisted oxidation. *Tetrahedron Letters*, 39:5955–5956, 1998.
- [125] H Agematu, T Tsuchida, K Kominato, N Shibamoto, T Yoshioka, H Nishida, R Okamoto, T Shin, and S Muraio. Enzymatic dimerization of Penicillin X. *J.Antibiot.*, 46:141–148, 1993.
- [126] S Furmeier and JO Metzger. Detection of Transient Radical Cations in Electron Transfer-Initiated Diels-Alder Reactions by Electrospray Ionization Mass Spectrometry. *J.Am.Chem.Soc.*, 126:14485–14492, 2004.

- [127] P Cheng and DK Bohme. Gas-Phase Formation of Radical Cations of Monomers and Dimers of Guanosine by Collision-Induced Dissociation of Cu(II)-Guanosine Complexes. *J.Phys.Chem.B*, 111:11075–11082, 2007.
- [128] S Ozgova, J Hermanek, and I Gut. Different antioxidant effects of polyphenols on lipid peroxidation and hydroxyl radicals in the NADPH⁻, Fe-ascorbate-and Fe-microsomal systems. *Biochem.Pharmacol.*, 66:1127–1137, 2003.
- [129] L Belguendouz, L Fremont, and A Linard. Resveratrol inhibits metal ion-dependent and independent peroxidation of porcine low-density lipoproteins. *Biochem.Pharmacol.*, 53:1347–1355, 1997.
- [130] Y Zhang, B Jayaprakasam, NP Seeram, LK Olson, D DeWitt, and MG Nair. Insulin Secretion and Cyclooxygenase Enzyme Inhibition by Cabernet Sauvignon Grape Skin Compounds. *J.Agric.Food Chem.*, 52:228–233, 2004.
- [131] H Kurihara, J Kawabata, S Ichikawa, and J Mizutani. (-)ε-Viniferin and Related Oligo-stilbenes from *Carex pumila* Thunb. (Cyperaceae). *Agric.Bio.Chem.*, 54:1097–1099, 1990.
- [132] R Pezet, C Perret, JB Jean-Denis, R Tabacchi, K Gindro, and O Viret. δ-Viniferin, a Resveratrol Dehydrodimer: One of the Major Stilbenes Synthesized by Stressed Grapevine Leaves. *J.Agric.Food Chem.*, 51:5488–5492, 2003.
- [133] GL Miessler and DA Tarr. Inorganic Chemistry. *2nd ed. Prentice-Hall*, pages 181–185, 1984.
- [134] WL Jolly. Modern Inorganic Chemistry. *New York: McGraw-Hill*, 1984.
- [135] I Fleming. Frontier Orbitals and organic Chemical Reactions. *Wiley, Chichester*, 1976.
- [136] CK Kim, KA Lee, CK Kim, BS Lee, and HW Lee. NBO analyses of the back-bonding in metal-olefin complexes. *Chem.Phys.Lett.*, 391:321–324, 2004.
- [137] E Alesso, R Torviso, M Erlich, L Finkielstein, B Lantano, G Moltrasio, J Aguirre, P Vazquez, L Pizzio, M Caceres, Cand Blanco, and H Thomas. Silica-supported heteropolyacids readily induce cyclodimerization of styrenes and stilbenes. *Synth.Commun.*, 32:3803–3812, 2002.

REFERENCES

- [138] M Sako, H Hosokawa, T Ito, and M Iinuma. Regioselective Oxidative Coupling of 4-Hydroxystilbenes: Synthesis of Resveratrol and ϵ -viniferin(*E*)-Dehydrodimers. *J.Org.Chem.*, 69:2598–2600, 2004.
- [139] GJ Fan, XD Liu, YP Qian, YJ Shang, XZ Li, F Dai, JG Fang, XL Jin, and B Zhou. 4,4'-Dihydroxy-*trans*-stilbene, a resveratrol analogue, exhibited enhanced antioxidant activity and cytotoxicity. *Bioorg.Med.Chem.*, 17:2360–2365, 2009.

Articles and conference contributions

Articles

1. **Vajir Tamboli**, Andrea Defant, Ines Mancini, Paolo Tosi. A study of resveratrol-copper complexes by electrospray ionization mass spectrometry and density functional theory calculations. *Rapid Commun. Mass Spectrom.* 25:526-532, 2011.
2. **Vajir Tamboli**, Nazzareno Re, Cecilia Coletti, Andrea Defant, Ines Mancini, Paolo Tosi. A joint experimental and theoretical investigation on the oxidative coupling of resveratrol induced by copper and iron ions. *To be submitted.*

Contributions to conference

1. **Vajir Tamboli**, Ines Mancini, Andrea Defant and Paolo Tosi.
“An ESI-MS/MS study on copper complexes of resveratrol and its dihydrofuran dimer”
Oral communication at the national symposium “The mass spectrometry study of biomolecules” Bari, 26 Novembre 2010.
2. **Vajir Tamboli**, Ines Mancini, Andrea Defant and Paolo Tosi.
“An ESI-MS/MS study on metal ion-catalyzed oxidative dimerization of resveratrol and its synthetic analogues”
Oral communication at the international workshop: 29th Informal Meeting on Mass Spectrometry, Fiera di Primiero Trento, 15-19 May, 2011.
3. **Vajir Tamboli**, Ines Mancini and Paolo Tosi.
“A study on the antioxidative and prooxidative mechanisms of resveratrol and its analogues by mass spectrometry”
Poster presentation at the PhD workshop in Department of Physics, University of Trento, Povo, Trento – 3-Feb-2010.

Acknowledgment

To the Almighty God “ALLAH” who has granted me all these graces to fulfill this work and who supported me and blessed me by His power and His mercy in all my life. To Him I extend my heartfelt thanks.

My thanks and appreciation goes to people without whom this work would have not been possible. I would like to thank:

My supervisor Prof. Ines Mancini for her excellent support, guidance, constant flow of ideas in this work throughout the duration of my PhD enabled me to develop an understanding of the subject, moreover, thoughtful guidance that make me successfully complete this research study.

My supervisor Prof. Poalo Tosi to whom I am grateful for his enthusiasm, guidance in this work and for the personal help, especially when it was required the most.

Prof. Simonetta Fornarini for her collaboration and allow me to do work in her laboratory in Rome.

Dr Daniela Ascenzi for her guidance in the study of gas phase reaction using mass spectrometer.

Dr Andrea Defant for his guidance in the synthetic chemistry work.

Mr Adreano Sterni for his advice and assistance with the mass spectrometry instruments and software that has helped me sort out the technical details of my work.

Mr Damiano Avi for his technical support, and being there every time with me in laboratory, he has also been a wonderful friend.

Past and present members of Atomic Molecular Physics and Bio-organic Chemistry Laboratory, Giorgina Scarduelli, Julia Aysina, Luca, Vikas Hegde, Mario, Sandro, Alberto, Petro, for their friendship and making this duration a good experience.

My parents and family especially my sisters and brother for taking a great confidence in me by giving me the opportunity to pursue my education in abroad.

I would especially like to thank Ahamad Mohiddon, Rohan Fernandes, Anshu Gaur, Trupti Warang for their constant support, guidance and encouragement especially during the tough times of write up. Last but not the least, Dattatray, Yasin,

REFERENCES

Mahesh, Abrar Kumthe, Dhananjay, Abrar Shaikh, Sachin Aiwale, Lalaso for their encouragement and support. I would like to thank all my close friends in Trento for all their support and being there every time I needed them.